12-10-2021

Torque vectoring to maximize straight-line efficiency in an all-electric vehicle with independent rear motor control

William Blake Brown
wbbrown8101@gmail.com

Torque vectoring to maximize straight-line efficiency in an all-electric vehicle with independent rear motor control

By

William Blake Brown

Approved by:

Wilburn Whittington (Major Professor)
Yucheng Liu
Tonya W. Stone
Alta Knizley
Tonya W. Stone (Graduate Coordinator)
Jason M. Keith (Dean, Bagley College of Engineering)

A Dissertation
Submitted to the Faculty of
Mississippi State University
in Partial Fulfillment of the Requirements
for the Degree of Doctor of Philosophy
in Mechanical Engineering
in the Department of Mechanical Engineering

Mississippi State, Mississippi

December 2021

Name: William Blake Brown

Date of Degree: December 10, 2021

Institution: Mississippi State University

Major Field: Mechanical Engineering

Major Professor: Wilburn Whittington

Title of Study: Torque vectoring to maximize straight-line efficiency in an all-electric vehicle with independent rear motor control

Pages in Study: 104

Candidate for Degree of Doctor of Philosophy

BEVs are a critical pathway towards achieving energy independence and meeting greenhouse and pollutant gas reduction goals in the current and future transportation sector [1]. Automotive manufacturers are increasingly investing in the refinement of electric vehicles as they are becoming an increasingly popular response to the global need for reduced transportation emissions. Therefore, there is a desire to extract the most fuel economy from a vehicle as possible. Some areas that manufacturers spend much effort on include minimizing the vehicle's mass, body drag coefficient, and drag within the powertrain. When these values are defined or unchangeable, interest is driven to other areas such as investigating the control strategy of the powertrain.

If two or more electric motors are present in an electric vehicle, Torque Vectoring (TV) strategies are an option to further increase the fuel economy of electric vehicles. Most of the torque vectoring strategies in literature focus exclusively on enhancing the vehicle stability and dynamics with few approaches that consider efficiency or energy consumption. The limited research on TV that addresses system efficiency have been done on a small number of vehicle

architectures, such as four independent motors, and are distributing torque front/rear instead of left/right which would not induce any yaw moment.

The proposed research aims to address these deficiencies in the current literature. First, by implementing an efficiency-optimized TV strategy for a rear-wheel drive, dual-motor vehicle under straight-line driving as would be experienced in during the EPA drive cycle tests. Second, by characterizing the yaw moment and implementing strategies to mitigate any undesired yaw motion.

The application of the proposed research directly impacts dual-motor architectures in a way that improves overall efficiency which also drives an increase in fuel economy. Increased fuel economy increases the range of electric vehicles and reduces the energy demand from an electrical source that may be of non-renewable origin such as coal.

DEDICATION

Firstly, I would like to dedicate this dissertation to my wife, Anna, who deserved this degree as much as I did. I would never have finished this degree had it not been for her encouragement to see this to completion. Anna has been the source of inspiration and I cannot thank her enough for everything she has done. I would also like dedicate this dissertation to my parents, Candice and William, for their unconditional love and support. They both taught me so much growing up and I am forever grateful for everything they have done and sacrificed to get me here. Finally, I would like to dedicate this dissertation to my family and friends for always being there and playing a part in shaping me into the person that I am.

ACKNOWLEDGEMENTS

I would like to express my deepest gratitude to my advisors Dr. Whittington and Dr. Liu for their guidance, feedback, and encouragements throughout this research. I would also like to thank the Center for Advanced Vehicular Systems and its staff for providing facilities and expertise to the EcoCar and Car of the Future projects. I would also like to recognize and thank Dr. Molen for his devotion and love for the students that came through the EcoCar project. Finally, I would like to thank my committee and those who helped bring this research and dissertation together.

TABLE OF CONTENTS

LIST OF TABLES

LIST OF FIGURES

LIST OF ABBREVIATIONS

Abbreviation	**Name**
BEV	Battery Electric Vehicle
CAN	Controller Area Network
CAVS	Center for Advanced Vehicular Systems
COTF	Car of the Future
DC	Direct Current
DOF	Degrees of Freedom
E-Axle	Electric Axle
EPA	Environmental Protection Agency
ESS	Energy Storage System
EV	Electric Vehicle
FWD	Front-Wheel Drive
GCAPS	Global Center for Automotive Performance Simulations
HEV	Hybrid Electric Vehicle
HV	High Voltage
HWFET	Highway Fuel Economy Test
ICE	Internal Combustion Engine
MPG	Miles Per Gallon
MPGe	Miles Per Gallon Equivalent
MSU	Mississippi State University
RPM	Revolutions Per Minute
RWD	Rear-Wheel Drive
TV	Torque Vectoring

UDDS	Urban Dynamometer Driving Schedule
US	United States
VTS	Vehicle Technical Specification
ZEV	Zero Emission Vehicle

NOMENCLATURE

Symbol	Name	Value/Units
a	Vehicle acceleration	m/s^2
A_f	Vehicle frontal area	1.9695 m^2
C_D	Coefficient of aerodynamic drag	0.28
E_{total}	Drive cycle total energy consumed	W·h
F_{aero}	Aerodynamic resistive force	N
$F_{E\text{-}Axle}$	Driving force provided by the E-Axle	N
F_{grade}	Grade resistive force	N
F_R	Resistive force	N
f_r	Coefficient of rolling resistance	0.011
F_{roll}	Rolling resistive force	N
g	Gravitational acceleration	9.8 m/s^2
g_r	Gear ratio	8.46
m	Vehicle mass	1500 kg
mi	Drive cycle total mileage	miles
$MPGe$	Miles Per Gallon Equivalent	none
$P_{E\text{-}Axle\_Out}$	Instantaneous power required by the vehicle	W
$P_{E\text{-}Axle\_In}$	Instantaneous power consumed by the E-Axle	W
r_{tire}	Tire radius	0.313 m
$R_{torque\ split}$	Torque split ratio	none
t_1	Initial time	sec
t_2	Final time	sec
t_a	Desired acceleration time for acceleration event when starting from rest	sec

U_{gas}	Amount of energy in one gallon of gasoline	33,440 W·hr/gal
V	Vehicle velocity	m/s
V_1	Initial vehicle velocity	m/s
V_2	Final vehicle velocity	m/s
V_b	Base speed of the electric machine observed at the wheels	15.4 m/s
V_f	Final vehicle speed for acceleration event when starting from rest	m/s
V_{f1}	Initial vehicle speed for acceleration event when not starting from rest	m/s
V_{f2}	Final vehicle speed for acceleration event when not starting from rest	m/s
V_g	Vehicle speed at grade	m/s
x	Longitudinal axis	m
y	Lateral axis	m

Greek

α	Road slope angle	rad
Δt_a	Desired acceleration time for acceleration event when not starting from rest	sec
η	EPA lumped efficiency of electricity generation	0.303
$\eta_{E\text{-}Axle}$	E-Axle system efficiency	none
η_{left}	Left motor efficiency	none
η_{right}	Right motor efficiency	none
η_{mech}	E-Axle mechanical efficiency	none
ρ_a	Air density	1.20 kg/m^3
θ	Angle of grade	rad
τ_{motor}	Motor torque	N·m
ω_{motor}	Motor speed	rad/s

CHAPTER I

INTRODUCTION

1.1 Background and motivation

The “Car of the Future” (COTF) program is a privately funded prototype vehicle project carried out at Mississippi State University (MSU)’s Center for Advanced Vehicular Systems (CAVS). The project’s purpose is to demonstrate how improved energy systems can make vehicles more affordable and more efficient [2]. The COTF project converted a production 2015 Rear-Wheel Drive (RWD) Subaru BRZ vehicle into a series Hybrid Electric Vehicle (HEV) with an intermediate milestone of a Battery Electric Vehicle (BEV).

This intermediate BEV step provided a point at which the vehicle could be evaluated in its all-electric state with the absence of what were once critical components including the original powertrain and powertrain electronics. For example, electric power steering and the vacuum assisted brake booster will not function properly in the absence of the engine and its controller unless the communication for the electric power steering is maintained and a source of vacuum is provided. The electric power steering requires specific communication messages to enable its functionality. These messages are usually provided by the engine controller, but since the engine controller will not be present in the prototype vehicle, the messaging will be provided by the COTF’s onboard controller. While the vacuum required by the brake booster was provided by the engine in its conventional configuration, a vacuum pump and reservoir will take its place in the prototype vehicle. Additionally, the BEV intermediate step allows long lead items required

for the HEV to be worked in parallel with the BEV development. Long lead items include investigating different battery and capacitor configurations; procuring items such as the HEV battery, capacitors, and engine; machining parts; and creating the carbon fiber enclosure for the custom battery pack. A system engineering design approach proposed by [3-14] was followed during this design project.

BEVs are a critical pathway towards achieving energy independence and meeting greenhouse and pollutant gas reduction goals in the current and future transportation sector [1]. The United States (US) transportation yields more than 3 trillion vehicle-miles driven annually which accounts for 70% of the nation's petroleum consumption [15]. This massive amount of consumption has direct impacts to air pollution and climate change, making up more than 28% of the nation’s greenhouse gases where 59% of that comes from light-duty vehicles, 23% from medium to heavy-duty vehicles, and the remaining comes from sectors such as aircraft, rail, and ships [16].

Automotive manufacturers are increasingly investing in the refinement of electric vehicles as they are becoming an increasingly popular response to the global need for reduced transportation emissions. Therefore, there is a desire to extract the most fuel economy from a vehicle as possible. Some areas that manufacturers spend much effort on include minimizing the vehicle’s mass, body drag coefficient, and drag within the powertrain. When these values are defined or unchangeable, interest is driven to other areas such as investigating the control strategy of the powertrain.

1.2 Literature review

To form a substantial background for this study, a literature review was carried out on the following areas: status of BEVs, vehicle powertrain architecture design and component selection, vehicle modeling and simulation, and torque vectoring.

1.2.1 Status of BEVs

A BEV, also known as a pure electric vehicle or all-electric vehicle, is defined as a vehicle whose only source of energy is provided by a battery pack also known as an energy storage system (ESS) [17] [18] [19]. BEVs use electric motors and motor controllers instead of the more common Internal Combustion Engine (ICE) for propulsion.

Conventional vehicles utilize petroleum-derived fuels to provide the vehicle's desired performance and achieve long driving ranges. However, conventional vehicles suffer from the inefficient ICE and produce emissions from burning gasoline resulting in environmental pollution. Hence, there is a growing interest in Electric Vehicles (EVs), including the BEV [20]. A conventional vehicle's combustion of fuel is a very inefficient process where 60% or more is wasted to heat loss, friction, and pumping losses [21]. This is a major contributor to the lack of fuel economy when compared to BEVs.

A transition to electric vehicles from vehicles powered by ICEs is a feasible solution to reduce the dependency of oil and mitigate the negative environmental impact caused by burning oil. BEVs, therefore, play a pivotal role in the pursuit of clean and sustainable energy strategies by allowing clean electric energy to be utilized in transportation which reduces pollution in the urban environment [22]. BEVs are the only automobile group that are categorized as a Zero Emission Vehicle (ZEV), which is defined as a vehicle that emits no exhaust gas from the onboard source of power [23].

In addition to the environmental benefits of BEVs over conventional ICE vehicles, BEVs can have many technical advantages over conventional vehicles. For example, BEVs have a higher overall efficiency with smoother operation and less noise [24] [25] [26]. BEVs do not have to idle when at rest, they provide a large amount of torque at low speed, and generally have better propulsion system packaging [27] [28] [29] [30]. The cost associated with the maintenance of BEVs is also significantly less than a conventional vehicle [31] [32].

One key benefit of BEVs over conventional vehicles that will be utilized for this research is BEV's enhanced control authority over vehicle dynamics which is achieved by the electric axle(s) that are providing torque to the wheels. The electric axle's response to the controller's commands happens within milliseconds unlike a conventional vehicle that takes much more time to change transmission gears and increase/decrease engine speed. The electric axle(s) also have the advantage of providing flexibility in how the vehicle distributes torque if there are two or more electric motors.

One drawback to BEVs is the limited amount of on-board energy storage. This limited available energy combined with slow charging times and lack of charging stations are some of the main challenges associated with the acceptance of BEVs. These challenges can cause the driver to experience range anxiety which is the fear of running out of energy while driving [33]. To reduce the driver's range anxiety and make the most out of the available on-board energy, research should be conducted in the field of efficiency optimization for the electric drive train to achieve an enhanced mileage [34].

1.2.2 Vehicle powertrain architecture design and component selection

Conventional vehicle powertrains are driven by some form of ICE, such as gasoline, diesel, or natural gas engines. These vehicles are very familiar and make up most of the vehicles

on the road today. BEVs are operated exclusively from onboard electricity provided by its ESS [19] which means they must be charged from an external source such as a standard wall outlet or a charging station to restore energy into the ESS. Employing electric machines for the powertrain instead of the conventional ICE leads to BEV architectures being less complex than those of regular ICE vehicles [35]. For example, there are fewer parts in a BEV powertrain which contains an ESS and an electric axle than in an ICE powertrain which includes a complex engine, transmission, and differential. Because BEVs can provide high-output torque at low input speeds, there is no longer a need for large gear ratios that are in conventional powertrain transmissions [30].

There are two basic two-wheel-drive powertrain layouts for conventional, internal-combustion vehicles: front-wheel drive (FWD) and rear-wheel drive (RWD) [36]. In a FWD vehicle, the powertrain is coupled to the front wheels where toque is provided to propel the vehicle. FWD vehicle powertrains are typically mounted in a transverse orientation, as shown in Figure 1.1. In a RWD vehicle, the powertrain is coupled to the rear wheels where torque is provided to propel the vehicle. RWD vehicle powertrains are typically mounted in a longitudinal orientation (Figure 1.1). For these conventional architectures, the ICE applies torque to the differential and the differential then distributes the torque equally to either the two front (FWD) or rear (RWD) wheels.

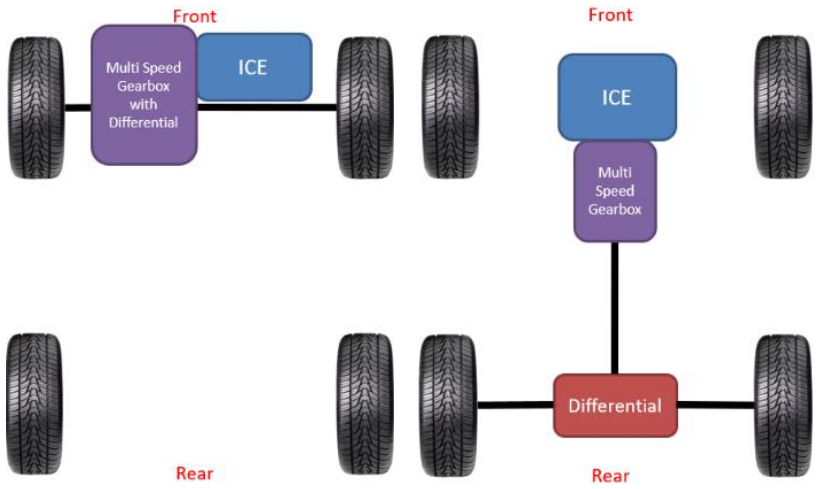

Figure 1.1 Conventional FWD (left) and RWD (right) architectures.

There are multiple BEV architectures. Some of the most common architectures include: two-wheel drive with a single motor and differential positioned with either the front or the rear wheels, as shown in Figure 1.2, and two-wheel drive with a dual motor positioned with either the front or the rear wheels, as shown in Figure 1.3 [18]. For the single-motor architecture, the electric axle applies torque to the differential which then distributes that torque to either the front (FWD) or rear wheels (RWD). Most commonly, the torque is distributed using a 50/50 split. For the dual-motor architecture, torque is usually distributed evenly during straight-line driving and while turning, the torque is distributed based on the vehicle's control strategy which is typically based on vehicle performance and stability.

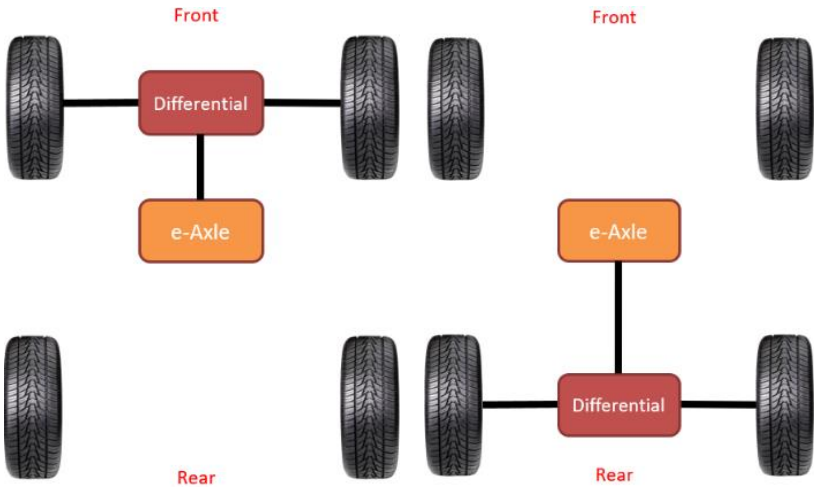

Figure 1.2 BEV single motor architecture for FWD (left) and RWD (right).

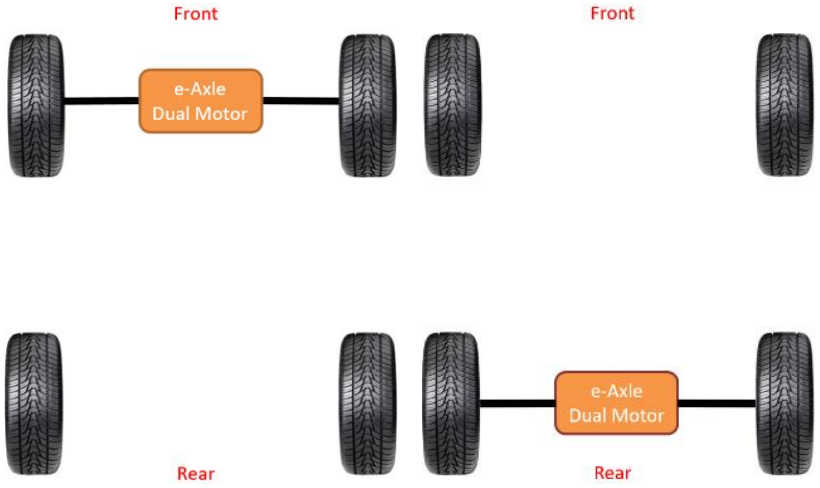

Figure 1.3 BEV dual motor FWD (left) and RWD (right).

Vehicle powertrain architecture design and component selection prior to the development of a BEV is critical since this architecture will cast a significant influence on sequential steps including implementation, control, and optimization of the vehicle [37]. Sizing of the electric machine is a significant step in the process of defining the vehicle architecture and plays an important role in meeting the desired vehicle performance requirements, which include

acceleration/deceleration, cruising, gradeability, maximum speed, cost, and drivability [38] [39]. Given vehicle characteristics, such as vehicle mass, gear ratio, frontal area, and wheel diameter, the sizing of the electric motor depends mainly on the maximum vehicle load required to meet strenuous conditions such as maximum vehicle speed, road slope, and acceleration [40]. Similarly, Weinstock [38] emphasized that the motor should be selected primarily by peak torque requirements. Other primary components, such as the battery, are dependent on the chosen electric-drive axle because the battery needs to provide the nominal high voltage required by the electric axle.

1.2.3 Vehicle modeling and simulation

BEV system architectures are often evaluated in terms of performance, efficiency, and lifetime [41]. Common stages of the engineering design process are research, design requirements, feasibility, conceptual design, preliminary design, detailed design, and production planning [42]. The conceptual design stage is the initial design phase where potential solutions are developed and evaluated against the design requirements. In the conceptual design stage for BEV system architectures, computational model and simulation is widely used as a powerful tool for development, analysis, and evaluation of various design alternatives [43] to significantly reduce the design expenses and shorten the length of the design cycle [44]. It is only after passing the evaluation that a real BEV will be built and tested on a dynamometer to evaluate its real-world performance under the same conditions applied for the computational analysis.

A drive cycle defines a vehicle target speed vs time profile that can be used in dynamic modeling and simulation along with real-world dynamometer tests. Various drive cycles are being implemented in different countries and used under different scenarios to assess vehicle performances such as fuel consumption and emissions. Useful data can be extracted from the

drive cycles, such as power required at the wheels, total energy required to complete the cycle, average power at wheels, tractive force at wheels, and percent idle time.

One important metric that is also considered by consumers is the fuel economy rated by the Environmental Protection Agency (EPA). Fuel economy can be obtained from the 2-cycle method which uses the following two EPA drive cycles: Urban Dynamometer Driving Schedule (UDDS) and Highway Fuel Economy Test (HWFET) [45]. An explanation of how the EPA drive cycles were derived was provided by Moawad et al. [46]. The UDDS cycle is used for assessing performance of a vehicle driving in a city while the HWFET cycle is for the vehicle driving on a highway [47]. The overall fuel economy of a vehicle is determined based on a weighted score of vehicle performance during these cycles.

Based on an estimate of the BEV's performance and fuel economy, a battery system can be designed to attain the desired range of the vehicle (the distance the vehicle can travel on a single charge). Drive cycle research conducted by Milligan et al. provides an estimation of the realistic range that a BEV can travel without encountering a depleted battery and resulting in a shutdown of the vehicle's electrical system [48].

1.2.4 Torque vectoring

Energy management strategies are the algorithms that are designed to make decisions to improve the fuel economy and optimize vehicle performance [49]. The preliminary objective of the control strategy is to satisfy the driver's power demand with minimum fuel consumption and optimum vehicle performance [49]. Power management strategies have impacts on fuel economy, greenhouse gasses emission, as well as effects on the durability of power-train components [50]. Therefore, different off-line and real-time optimal control approaches are being developed. The electrification of vehicles introduces an enhanced control authority over

the vehicle dynamics and provides opportunities for the development and implementation of advanced control strategies [51].

Torque Vectoring (TV), which can be present in both conventional and non-conventional vehicles, allows varying torques to be applied to the wheels independently. In conventional ICE architectures, TV requires additional hardware within the differential including an overdriven gear set, clutch packs for each output, hydraulic pumps and circuitry, and sensors. When equipped with the necessary hardware, TV is used today in conventional vehicles to improve vehicle stability and handling performance [52].

In EVs with two or more independent electric motors, TV can be achieved easily through individual adjustment of driving and braking torques to the current driving situation [53]. The precise and highly responsive torque control of individual electric motor drives can have a major impact on the vehicle's steady-state and transient handling response characteristics allowing for significant improvements in vehicle dynamics and energy management [54]. These independently controllable motors also allow for enhancement in vehicle performance [55] [56] [57] [58]. In addition, TV can help keep the vehicle on the driver's intended target path indicated by the steering wheel [59].

An energy-efficient torque distribution among the drivetrain is crucial for reducing the drivetrain power losses and extending driving range. However, most of the TV approaches in the literature focus exclusively in enhancing the vehicle stability and dynamics with few approaches that consider efficiency or energy considerations [60]. Out of the literature that does consider increasing efficiency, [61] introduces a favorable approach to formulate and solve the problem offline. This method generates lookup tables for fast, real-time implementation of the optimal control strategy for four independent motors. [61] implements a binary strategy where if the

torque is low, a single motor is used and when the torque is high, there is an equal split. [61] also confirmed that less-balanced distribution strategies can be optimal for a wide range of operating points for low torque demands.

While precise and responsive torque is highly advantageous, an unequal distribution of torque can result in unwanted vehicle motion when trying to drive in a straight line. A yaw moment is generated by assigning unequal torque demands to the left and right vehicle sides [62]. This potentially unwanted yaw moment can result in the vehicle pulling/pushing away from the driving center line. Vehicle controllers are designed to sense undesired yaw moments and implement a corrective yaw moment through actuation of powertrain components, such as the brakes, to get the vehicle back on track [63] [64] or by applying torque in either direction for each motor. These vehicle TV controllers are commonly based on a hierarchical approach, consisting of a high-level supervisory controller that evaluates a corrective yaw moment and a low-level controller that defines the individual wheel torque reference values [63].

If there exists such an operating point that allows for optimal operating efficiency and maintains vehicle stability and performance, it should be implemented and evaluated to further increase the vehicles driving range and reduce the carbon footprint that is being generated. [65] maximized the energy saving potential of an EV with four independently driven wheels by allowing a certain error in the control process of yaw rate without affecting the stability. In most cases, a slight deviation of the ideal yaw rate calculated from the 2 Degrees-of-Freedom (2DOF) linear vehicle model will not affect the driving stability of the vehicle at all, especially on the good adhesion road or at low speed [65].

The advantages of TV with respect to increased vehicle performance and stability drive BEVs to a dual-motor architecture. While increased performance may be the primary focus of

such vehicle control strategies, opportunities exist to take advantage of the torque vectoring and dual-motor architecture to increase fuel economy.

1.3 Research contribution

This research will investigate torque vectoring strategies to improve efficiency and increase vehicle fuel economy for the MSU COTF program. This research also accounts for and mitigates the yaw moment experienced by the vehicle because of TV.

Most research to date has implemented TV to improve vehicle dynamic performance while performing a maneuver other than driving in a straight line. If consideration is given to system efficiency, it is mostly a secondary objective. The limited research on TV that addresses system efficiency use a different vehicle architecture, such as four independent motors, and are distributing torque front/rear instead of left/right which would not induce any yaw moment. Additionally, very little research has been found that categorizes or addressed yaw motion as it pertains to straight-line driving with left/right TV.

The proposed research aims to address these deficiencies in the current research. First, by implementing an efficiency-optimized TV strategy for a rear-wheel drive, dual-motor vehicle under straight-line driving. Second, by characterizing the yaw moment and implementing strategies to mitigate any undesired yaw motion.

The application of the proposed research directly impacts dual-motor architectures in a way that improves overall efficiency which also drives the increase in fuel economy. Increased fuel economy reduces the energy demand from an electrical source that may be of non-renewable origin such as coal. Increased fuel economy also leads to an increase in the limited range of BEVs which increases the acceptance of BEVs. Furthermore, these improvements can be achieved by updating existing vehicle software without adding any physical equipment.

1.4 Organization of the dissertation

Chapter II outlines the electric axle selection for the COTF BEV. Chapter III presents a one-dimensional vehicle model and Chapter IV outlines the drive cycle analysis. Chapter V presents the vehicle performance using a 50/50 torque split during the drive cycles. Chapter VI and Chapter VII present the efficiency-optimized torque vectoring and vehicle performance, respectively.

Chapter VIII presents the 3 Degrees-of-Freedom (3DOF) model and Chapter IX compares the vehicle performance using the 3DOF model to the one-dimensional model. Chapter X and Chapter XI present the yaw-mitigation strategies and vehicle performance, respectively. Finally, Chapter XII presents the conclusion and future work.

CHAPTER II

COTF ELECTRIC AXLE SELECTION

2.1 COTF BEV architecture

The baseline production vehicle for the COTF is a 2015 Subaru BRZ. This vehicle was selected and donated for this project by the project sponsor. The Subaru BRZ uses a conventional longitudinally mounted gasoline engine with a conventional RWD drivetrain, as shown in Figure 2.1. A dual-motor, RWD architecture (Figure 2.1) was selected for the BEV architecture because the production vehicle was already suited for RWD and significant modifications would be needed to convert the production vehicle to FWD. The BEV architecture selected most resembles the vehicle in its production state. This allows for the possibility of reusing the existing rear subframe. If the subframe cannot be reused, the mounting points can be utilized with a custom subframe. Another advantage of this specific architecture is that the rear hubs have already been set up for independent output shafts. The location of the electric motors in the rear also allows for easy access to the spare tire compartment, which is the planned area to be used for the high-voltage (HV) bus fuse box, onboard charger, and auxiliary power module. Some disadvantages of this architecture include its limited vertical space that would reduce the ground clearance and may require the removal of the fuel tank, which could be reused in the HEV stage. The original 2.0L 4-cylinder ICE is removed for the BEV intermediate step and will not be reused. Due to its physical size, overall efficiency, and unnecessary features for an HEV (e.g., alternator, HVAC compressor, etc.), it is expected that in the final HEV configuration, the vehicle will have a series

HEV architecture employing an engine/generator combination of a Weber MPE850 ICE paired with a YASA-400 motor. The engine/generator will be placed in the original engine bay and will share this space with many of the HEV components such as part of the battery and vacuum pump for brake assist.

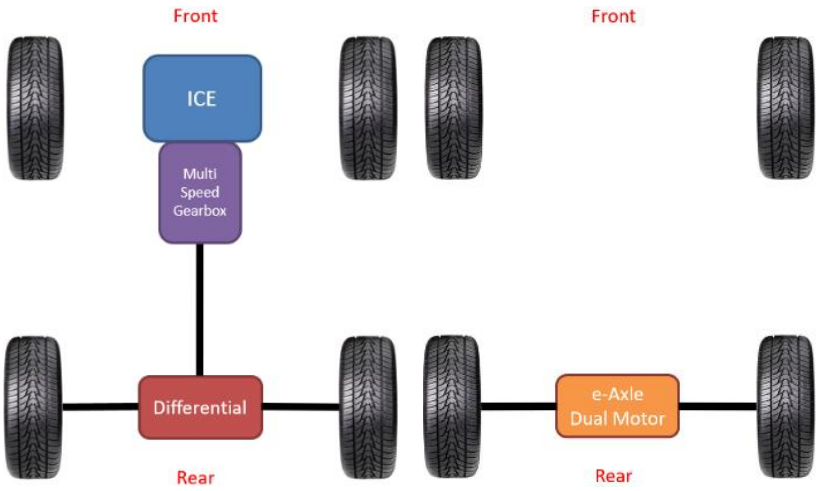

Figure 2.1 Conventional RWD architecture (left) and BEV dual-motor RWD (right).

To convert to a BEV, the ICE, transmission, driveshaft, and rear drive unit must be removed and replaced with an HV battery, HV cabling, electric axle, HV charger, DC-DC converter, and supervisory controller. Table 2.1 compares the key components for the production vehicle and the BEV. Before the electrical components can be selected, design targets or vehicle requirements must be defined.

Table 2.1 Key components of the production vehicle vs the BEV.

Production Vehicle	BEV
Engine	Electric Axle
Transmission	
Drive Shaft	
Differential	
Intake	
Exhaust	
Emissions Equipment	
Fuel/Fuel Tank	High Voltage Battery
Fuel Lines/Filler Neck	High Voltage Cable
Alternator	DC-DC Converter
	High Voltage Charger
	Supervisory Controller

2.2 Vehicle technical specifications

The Vehicle Technical Specifications (VTS) defines critical vehicle requirements such as how long it will take to accelerate from 0 to 96.5 kph for maximum vehicle weight. Requirements such as this will guide the component selection and design process. For COTF, the VTS were provided by the sponsor and adjusted to align with common requirement criteria such as acceleration and gradeability and the performance of the original production vehicle. For the selection of powertrain components, straight-line acceleration time from 0 to 96.5 kph (0 to 60 mph), acceleration from 80.5 to 112.5 kph (50 to 70 mph), and gradeability are the key performance requirements because these requirements are the most strenuous with respect to the required power. The performance of the production vehicle and the BEV VTS are provided in Table 2.2. Except for vehicle mass, the BEV should offer the same performance as the production vehicle. For the first project milestone, the BEV should maintain the same performance as the production vehicle with an increased mass of no more than 200 kg. The increased mass is mainly due to the addition of a large HV energy storage system (ESS) such as

a battery pack. Once the VTS is defined (Table 2.2), the necessary power and energy requirements for the electric drive unit, cabling, and battery can be determined.

Table 2.2 Production vehicle performance and BEV VTS.

Metric	**Production Performance** [61]	**BEV VTS**
Acceleration 0-96.5 kph (0-60 mph)	6.3 sec	6.3 sec
Acceleration 80.5-112.5 kph (50-70 mph)	10.0 sec	10.0 sec
Gradeability @ 96.5 kph (60 mph)	10+ %	10+ %
Mass	1300 kg	< = 1500 kg

2.3 Required acceleration power

The acceleration metrics, 0 kph to 96.5 kph and 80.5 kph to 112.5 kph, define the amount of time that it takes for the vehicle to accelerate from 0 kph to 96.5 kph and 80.5 kph to 112.5 kph, respectively. The acceleration metric of 0 kph to 96.5 kph is commonly published by manufactures and identifies how quickly the vehicle can accelerate from a standstill to a cruising speed. The acceleration metric of 80.5 kph to 112.5 kph is not as commonly published and is considered an on-ramp or passing metric where the driver is looking to accelerate up to speed with traffic when trying to merge into traffic or where the driver is looking to pass slower traffic. These metrics assume the vehicle is traversing across a zero-grade surface. For acceleration 0 kph to 96.5 kph the BEV VTS is 6.3 seconds. Given this target, the minimum power required for acceleration from rest, P_a, can be determined from the equation below [3]:

$$P_a = \frac{m}{2t_a}\left({V_f}^2 + {V_b}^2\right) + \frac{2}{3}mgf_r V_f + \frac{1}{5}\rho_a C_D A_f {V_f}^3 \tag{2.1}$$

where

m is the vehicle mass in kg,

t_a is the desired acceleration time in seconds,

V_b is the base speed of the electric machine observed at the wheels in m/s,

V_f is the final speed for the acceleration event in m/s,

g is the acceleration of gravity in m/s^2,

f_r is the rolling resistance coefficient,

ρ_a is the density of the air in kg/m^3,

A_f is the frontal area of the vehicle in m^2, and

C_D is the aerodynamic drag coefficient of the vehicle.

For acceleration evaluation, it must be assumed that the battery can provide the desired instantaneous power needed by the electric drive unit, i.e., the battery is assumed to behave as an ideal power source. Values of parameters and variables used for this calculation are listed in Table 2.3. In that table, the maximum allowable vehicle mass of 1500 kg was used, the McLaren E-Axle base speed of 15.4 m/s was applied (this is the speed at which the motor torque is no longer constant in its torque vs. speed graph), the rolling resistance coefficient value was 0.011, which assumed the vehicle is on a surface type between concrete and asphalt [17], the frontal area (1.9695 m^2) is the cross sectional area of the vehicle from a reference point of the front or rear end, and the drag coefficient associated with this vehicle (0.28) was adopted [19].

Table 2.3 Parametric values for calculation of the acceleration power (0 - 90.5 kph)

Variable	Value
m	1500 kg
t_a	6.3 sec
V_b	15.4 m/s
V_f (96.5 kph)	26.8 m/s
g	9.81 m/s^2
f_r	0.011
ρ_a	1.2 kg/m^3
A_f	1.9695 m^2
C_D	0.28

Substituting values from Table 2.3 into Eqn. (2.1) shows that to accelerate the BEV from 0 kph to 96.5 kph in 6.3 seconds, a minimum power of 119.9 kW is required at the wheels.

The VTS for acceleration time from 80.5 kph to 112.5 is 10.0 seconds. To calculate the power required to go from 80.5 kph to 112.5 kph, Eqn. (2.1) is first solved for time, t_a as:

$$t_a = \frac{m * \left({V_f}^2 + {V_b}^2\right)}{2\left(P_a - \frac{2}{3}mgf_r V_f - \frac{1}{5}\rho_a C_D A_f {V_f}^3\right)} \tag{2.2}$$

Then, the equation for delta time, Δt_a, to go from V_{f1} to V_{f2} is determined by subtracting Eqn. (2.2) with $V_f = V_{f1}$ from Eqn. (2.2) with $V_f = V_{f2}$, as shown below in:

$$\Delta t_a = \frac{m * {V_{f2}}^2}{2\left(P_a - \frac{2}{3}mgf_r V_{f2} - \frac{1}{5}\rho_a C_D A_f {V_{f2}}^3\right)} - \frac{m * {V_{f1}}^2}{2\left(P_a - \frac{2}{3}mgf_r V_{f1} - \frac{1}{5}\rho_a C_D A_f {V_{f1}}^3\right)} \tag{2.3}$$

where

V_{f2} is the final speed for the acceleration event in m/s,

V_{f1} is the initial speed for the acceleration event in m/s, and

Δt_a is the delta time for the acceleration event in seconds.

P_a is then determined by solving Eqn. (2.3). Using the values in Table 2.4, a minimum of 48.2 kW is required to accelerate the BEV from 80.5 kph to 112.5 kph in 10.0.

Table 2.4 Parametric values for calculation of the acceleration power (80.5 - 112.5kph)

Variable	Value
Δt_a	10 sec
V_{f1} (80.5 kph)	22.4 m/s
V_{f2} (112.5 kph)	31.3 m/s

2.4 Required gradeability power

Gradeability is the grade or angle at which the vehicle can operate at steady state speed. The BEV VTS for gradeability is to maintain 96.5 kph while on a maximum grade of 10%. To

meet this gradeability, the minimum required power for gradeability, P_g, can be determined from [20]:

$$P_g = mgsin(\theta)V_g + mgf_r \cos(\theta)\, V_g + \frac{1}{2}\rho_a C_D A_f {V_g}^3 \quad (2.4)$$

where V_g is the speed at grade in m/s, θ is the angle of grade in radians ($\theta = arctan(Percent\ Grade/100)$). Therefore, to maintain 96.5 kph on a 10% grade (5.7°), a continuous power of 50.4 kW of is needed.

2.5 Power requirements summary

Table 2.5 summarizes the power required to achieve the acceleration and gradeability VTS. The power needed to accelerate the BEV from 0 to 96.5 kph in 6.3 seconds is significantly greater than the power needed to accelerate from 80.5 to 112.5 kph in 10 seconds and the power needed to maintain at 96.5 kph a 10% grade. The 0-96.5 kph acceleration, therefore, defines the minimum power requirement for the electric axle, which is 119.9 kW.

Table 2.5 Power requirements for the electric axle.

Metrics	Power Requirements (kW)
Acceleration 0-96.5 kph (0-60 mph)	119.9
Acceleration 80.5-112.5 kph (50-70 mph)	48.2
Gradeability @ 96.5 kph (60 mph)	50.4

2.6 Electric axle selection

Based on the estimated power required to meet the VTS acceleration and gradeability, the drive unit/traction motor can be selected. After investigating available motors, an all-in-one electric package, electric axle, that includes a motor, a lubrication system, electrical connections, potentially a gearbox, power electronics, and both mechanical and electrical safety disconnect mechanisms, was desired for a more efficient vehicle integration. Available electric axles that

met the power and component requirements were then further evaluated for adaptability within the vehicle rear subframe area, production readiness, and procurement time. This led to a new partnership with McLaren Engineering, a division of Linamar, to provide a prototype E-Axle that was previously designed for their advanced development vehicles, as shown in Figure 2.2. This prototype was already designed and built so it was available immediately.

Figure 2.2 McLaren Engineering E-Axle [59].

The McLaren E-Axle includes two independent 80 kW motors, each with an 8.46 to 1 gear reduction, which met the minimum power requirement of 119.9 kW with a margin of about 40 kW. It also includes an internal lube pump, heat exchangers, and motor controllers to provide an all-in-one package unit. This E-Axle architecture was designed to be both modular and scalable to provide a solution for a wide range of applications from electric-assisted vehicles to full HEVs and BEVs. Additionally, it has the capability to provide active torque vectoring based on independent commands sent to the unit via controller area network (CAN) communication. A differential is no longer needed when such an axle is used because the E-Axle has two

independent motors. Each wheel can have an independent source of torque from its respective motor, so it is not necessary to split or distribute one source of torque to each wheel.

Some of the most relevant specifications of the E-Axle are displayed in Table 2.6. Figure 2.3 shows the simulated motor efficiency bands as a function of the motor torque and motor speed. All electrical losses associated with the E-Axle were considered in determining this efficiency.

Table 2.6 McLaren E-Axle specifications.

Criteria	**E-Axle**
Dimension (L × D x H)	705 × 446 × 314 (mm)
Total power (peak)	160 kW
Total power (continuous)	100 kW
Gear ratio, g_r	8.46
Total torque (total)	3,000 N·m
Maximum speed	136 kph
Mass	120 kg
Input voltage (minimum)	170 VDC
Input voltage (nominal)	360 VDC
Input voltage (maximum)	750 VDC

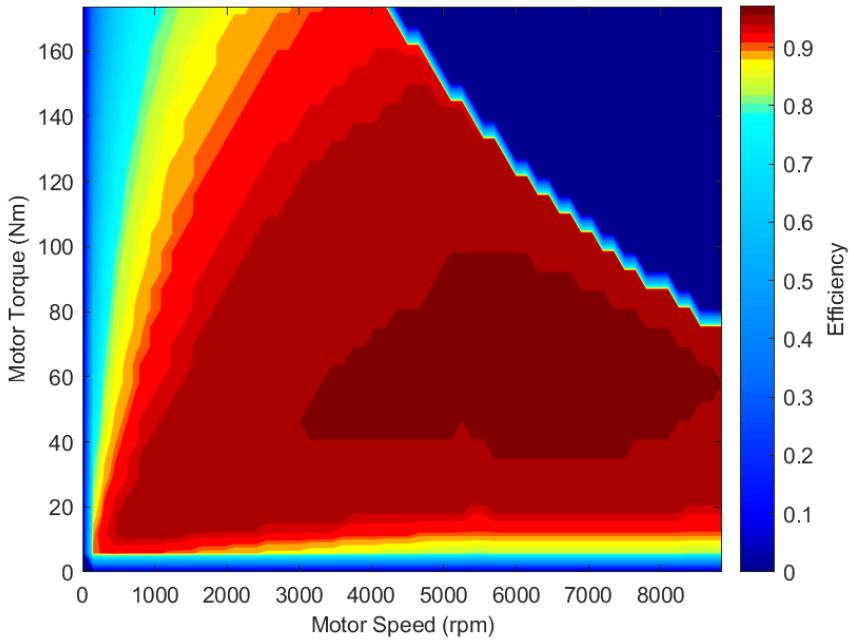

Figure 2.3 Simulated E-Axle single-motor efficiency map, provided by Parker Hannifin Corporation [62].

2.7 VTS evaluation

After the E-Axle is selected, the performance should be estimated to verify that the selection meets the required VTS. Eqn. (2.2) shows how to calculate the time to accelerate, t_a, assuming 100% axle efficiency. This equation can be modified to accommodate the effect of the axle's efficiency (η_{axle}) on t_a:

$$t_a = -\frac{M_v * \left({V_b}^2 + {V_f}^2\right)}{2\left(\frac{\rho_a C_D A_f {V_f}^3}{5} + \frac{2Mgf_r V_f}{3} - P_t * \eta_{axle}\right)} \tag{2.5}$$

The mechanical efficiency of the axle is approximately 95% and the average electrical efficiency of the axle is 80%, according to the documentation provided with the axle.

For the chosen E-Axle, the 0 - 96.5 kph (0 - 60 mph) acceleration time is expected to be 4.9 seconds, which is a large improvement compared to the target value of 6.3 seconds. The 80.5 - 112.5 kph (50 - 70 mph) acceleration time is expected to be 2.6 seconds, which is below the target value of 10.0 seconds, representing a 74% reduction from the production vehicle. Given the E-Axle power is greater than the gradeability power requirement, the gradeability criterion can be certainly met. Overall, the expected BEV with the chosen E-Axle meets the VTS. These values are summarized in Table 2.7.

Table 2.7 Expected BEV performance vs VTS.

Metric	**Production Vehicle Performance** [61]	**BEV VTS**	**BEV Model Prediction**
Acceleration 0-96.5 kph (0-60 mph)	6.3 sec	6.3 sec	4.9 sec
Acceleration 80.5-112.5 kph (50-70 mph)	10.0 sec	10.0 sec	2.6 sec
Gradeability @ 96.5 kph (60 mph)	10+ %	10+ %	10+ %
Mass	1300 kg	< = 1500 kg	1500 kg

CHAPTER III

ONE-DIMENSIONAL VEHICLE MODEL

The equation of linear motion for the vehicle can be expressed as $F_{E\text{-}Axle} - F_R = ma$, according to Newton's second law, where $F_{E\text{-}Axle}$ is the driving force provided from the E-Axle, F_R is the resistive force, m is the mass of the vehicle, and a is its acceleration. Assuming a constant acceleration, the required E-Axle force to accelerate the vehicle is:

$$F_{E-Axle} = m\frac{V_2 - V_1}{t_2 - t_1} + F_R \tag{3.1}$$

where V_1 and V_2 denote the initial and final velocity, respectively; while t_1 and t_2 denote the initial and final time, respectively.

3.1 Total resistive force

The total resistive force, F_R , is a sum of the aerodynamic resistive force (F_{aero}), rolling resistive force (F_{roll}), and the grade resistive force (F_{grade}), as described by the equation:

$$F_R = F_{aero} + F_{roll} + F_{grade} \tag{3.2}$$

Figure 3.1 shows a plot of vehicle resistance versus speed. The rolling and grade resistance are constant with speed while the aerodynamic resistance increases exponentially with speed. Therefore, the total resistance increases exponentially as the speed increases, as illustrated in Figure 3.1. It is worth mentioning that some losses and loads were not considered in this study, including electrical transmission losses from the battery to the E-Axle, accessory parasitic loads, and creature comforts such as the air conditioning and radio.

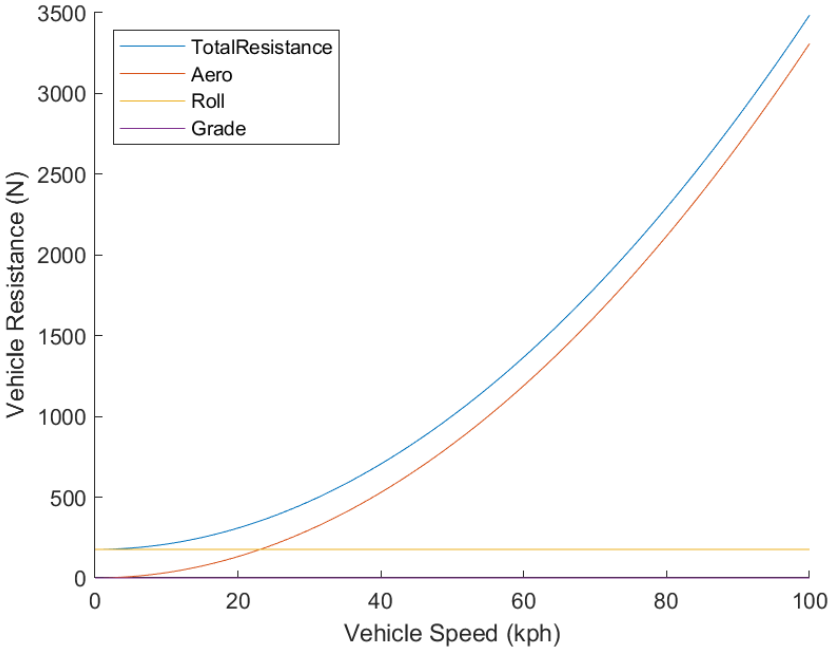

Figure 3.1 Vehicle resistive force vs speed.

3.1.2 Aerodynamic resistance

Aerodynamic resistance, F_{aero}, or aerodynamic drag, is the resistance imposed on the vehicle by the surrounding air due to the body profile and acts in the opposite direction of the vehicle motion. The aerodynamic resistive force is defined as:

$$F_{aero} = \frac{1}{2}\rho_a C_D A_f V^2 \tag{3.3}$$

where ρ_a is the air density, C_D is the coefficient of aerodynamic drag, A_f is the frontal area of the vehicle, and V is velocity of the vehicle. Factors that contribute to the aerodynamic drag coefficient include turbulent air flow around the vehicle body, friction between air and the vehicle body, and vehicle component resistance such as heat exchangers, spoilers, and air vents.

3.1.3 Rolling resistance

Rolling Resistance, F_{roll}, is the resistance imposed by the interface between tires and the road surface, which is calculated as:

$$F_{roll} = f_r mg \cos \alpha \tag{3.4}$$

where f_r is the coefficient of rolling resistance, g is gravitational acceleration, and α is the road slope angle.

Table 3.1 lists the coefficients of rolling resistance, f_r, for various road surfaces. Factors that contribute to the rolling resistance include resistance from tire deformation, tire penetration, and surface compression, as well as tire slippage and air circulation around the wheel. For this analysis, a value of 0.011 is chosen for this variable indicating a surface resembling a clean and dry road surface made of asphalt.

Table 3.1 Coefficients of rolling resistance for various road surfaces [11].

Road Surface	Coefficient of rolling resistance, f_r
Pavement	0.013
Concrete/asphalt	0.011
Rolled gravel	0.020
Unpaved road	0.050
Field	0.1 – 0.35

3.1.4 Grade resistance

Grade Resistance, F_{grade}, is the resistance applied on the vehicle that drives up a sloped road with an angle that is greater than zero degrees and is a result of gravity acting on the vehicle. Hence it can be determined as:

$$F_{grade} = mg \sin \alpha \tag{3.5}$$

3.2 Motor characteristics

Instantaneous power required by the vehicle at the wheels (E-Axle output power) can be estimated as:

$$P_{E-Axle\_Out} = F_{E-Axle}V \tag{3.6}$$

The efficiency for each motor can be determined from the motor speed, ω_{motor}, and motor torque, τ_{motor}. The motor speed can be determined from the velocity of the vehicle as:

$$\omega_{motor} = \frac{\mathrm{V}}{r_{tire}} g_r \tag{3.7}$$

where r_{tire} is the tire radius of the wheel, V is the vehicle velocity in m/s as dictated by the drive cycle, and g_r is the gear ratio of the E-Axle (Table 2.6)

The motor torque is defined as the ratio between the motor power and the motor speed, which is $\tau_{motor} = P_{motor}/\omega_{motor}$ where P_{motor} is the portion of the total power provided by the E-Axle ($P_{E\text{-}Axle\_Out}$) which is applied to the motor following a prescribed torque split ratio. Given the motor torque and motor speed, the motor efficiency is determined from Figure 2.3.

After calculating the instantaneous power required at the wheels and based on the instantaneous motor efficiencies, the instantaneous power consumed by the E-Axle (E-Axle input power) is determined from:

$$P_{E-Axle\_In} = \frac{P_{E-Axle\_out}}{\eta_{left} \times \eta_{mech}} R_{torque\ split} + \frac{P_{E-Axle\_out}}{\eta_{right} \times \eta_{mech}} (1 - R_{torque\ split}) \tag{3.8}$$

where η_{left} and η_{right} are the efficiency of the left motor and right motor, respectively; η_{mech} is the mechanical efficiency of the E-Axle, which is 95% (Table 2.6); and $R_{torque\ split}$ is the percentage of the total torque applied to the left motor.

The E-Axle system efficiency can then be determined from:

$$\eta_{E-Axle} = \frac{P_{E-Axle\_Out}}{P_{E-Axle\_In}} \tag{3.9}$$

3.3 Vehicle specifications

Table 3.2 provides the values for the physical characteristics of the vehicle, whose drive unit/traction motor is a McLaren Engineering all-in-one electric package, E-Axle [19].

Table 3.2 Vehicle characteristics for one-dimensional model.

Parameter	Value
Mass, m	1500 kg
Vehicle frontal area, A_f	1.9695 m^2
Aerodynamic drag coefficient, C_D	0.28
Tire radius, r_{tire}	0.313 m

CHAPTER IV

DRIVE CYCLE ANALYSIS

4.1 Drive cycles

The overall fuel economy of a vehicle is determined based on a weighted score of the vehicle's performance during the UDDS and HWFET drive cycles. The UDDS drive cycle shown in Figure 4.1 is approximately 12 km long; the average speed is 31.5 kph and has a duration of 1369 seconds for a vehicle to complete that cycle. The HWFET drive cycle shown in Figure 4.2 is approximately 16.5 km long and the average speed is 77.7 kph, requiring 765 seconds to complete. These characteristics are summarized in Table 4.1. It should be noted that during these tests, the vehicle should be driven on a straight road with no slope or a dynamometer that simulates resistances the vehicle would undergo on the road.

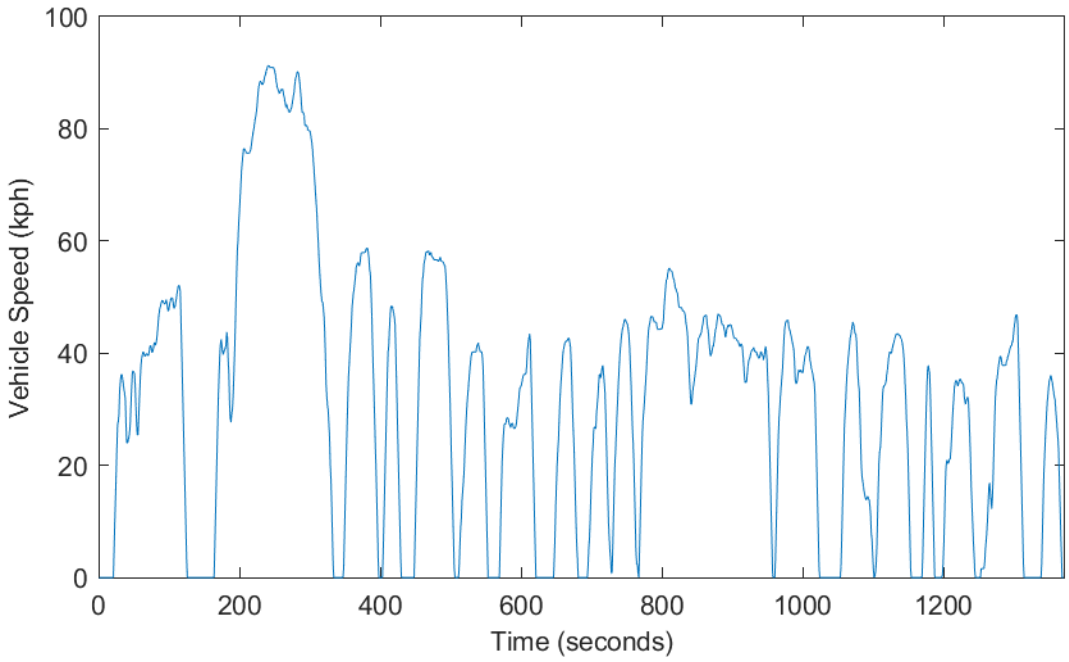

Figure 4.1 UDDS drive cycle [38].

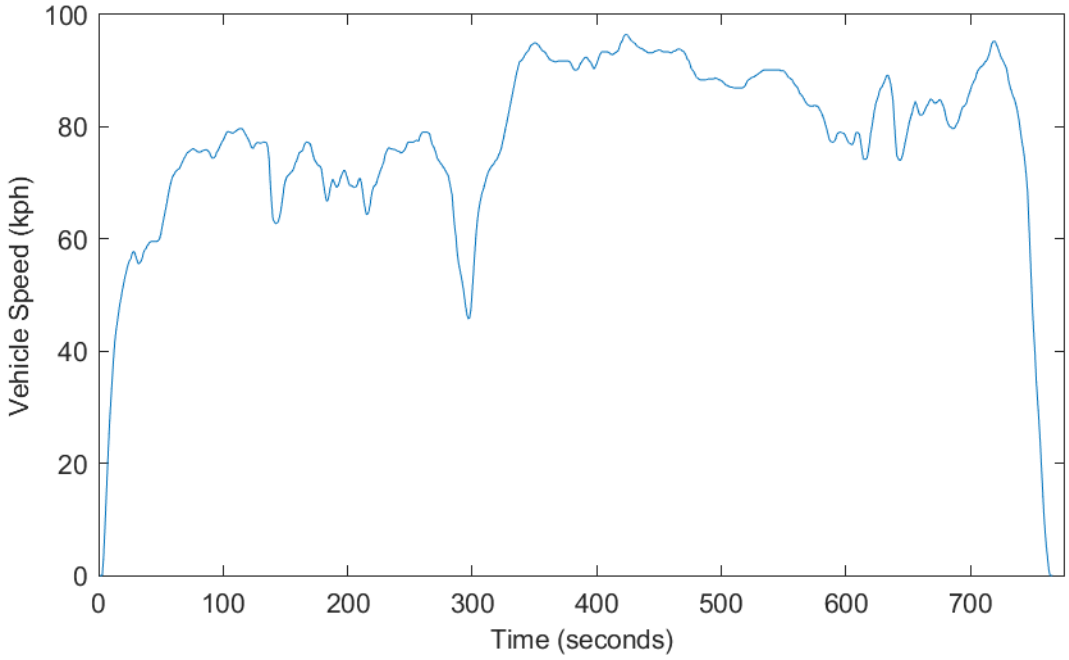

Figure 4.2 HWFET drive cycle [38].

Table 4.1 UDDS and HWFET drive cycle characteristics

Drive Cycle Metrics	UDDS	HWFET
Length (km)	12	16.5
Average Speed (kph)	31.5	77.7
Duration (sec)	1369	765
Time spent at rest (sec)	259	6

4.2 Fuel economy

The vehicle's EPA fuel economy ratings are measured with EPA's city (UDDS) and highway (HWFET) test procedures (the "2-cycle" procedure) and defined as miles per gallon (MPG) for conventional vehicles or miles per gallon equivalent (MPGe) for unconventional vehicles. After obtaining the ratings from the UDDS drive cycle and HWFET drive cycle tests, a combined city/highway value is then calculated using a 55% / 45% city-highway weighted average [69]. The MPGe, formerly referred to as miles per gallon gasoline equivalent, can be calculated for each drive cycle using the following equation:

$$MPGe = \frac{1}{E_{total}/mi} U_{gas}\eta \tag{4.1}$$

where E_{total} is the total energy consumed during the drive cycle; mi is the total mileage of the drive cycle, 7.46 miles for the UDDS drive cycle and 10.25 miles for the HWFET drive cycle; U_{gas} is the amount of energy in one gallon of gasoline, which is 33,440 W·hr/gal [70]; and η is a lumped efficiency value of 0.303 that is provided by the EPA to account for the average electricity generation efficiency (32.8%) and average transmission efficiency to the consumer (92.4%) [71]. These efficiency values are independent of the vehicle and account for all losses associated with power plants and transmission to consumer.

CHAPTER V

SIMULATED VEHICLE PERFORMANCE USING THE ONE-DIMENSIONAL MODEL WITH A 50/50 TORQUE SPLIT

A drive cycle defines a vehicle target speed vs time profile that can be used in modeling and simulation along with real-world dynamometer tests. Useful data can be extracted from the drive cycles, such as power required at the wheels, total energy required to complete the cycle, average power at wheels, and fuel economy.

Using the vehicle model, Chapter III, and the vehicle characteristics given in Table 3.2, the required power, motor efficiency, E-Axle efficiency, and fuel economy can be calculated for the UDDS and HWFET drive cycles.

The torque split ratio is controllable; however, the ratio will be assumed to be a 50/50 torque split between the two E-Axle motors. This 50/50 split is representative of a differential unit that's purpose is to allow for unequal speeds and equalize torque distribution.

5.1 E-Axle power and energy required

The instantaneous power required for the UDDS and HWFET drive cycles are plotted in Figure 5.1 and Figure 5.2, respectively. This instantaneous required power is what the vehicle requires at the wheels to meet the drive cycle's instantaneous velocity. It does not account for efficiency losses in the motor. A negative required power would be available for regeneration. Table 5.1 displays a summary of energy and power required for the vehicle to complete the UDDS and HWFET drive cycles and meet all the requirements. In that table, the total positive

energy required at the wheels was determined as the integral of power when power is greater than zero, which occurs primarily when the vehicle is accelerating. Similarly, the total negative energy required at the wheels is the integral of power when power is less than zero, which occurs primarily when the vehicle is decelerating. Average propulsion power at the wheels is an average of the positive power and peak power output at the wheels is the maximum power experienced over the drive cycle. Finally, the time spent at rest is the summation of the time when the vehicle velocity is zero. The required power predicts the loading that the vehicle will be subject to during the tests, which must be provided by the propulsion system. For this vehicle, the peak power required at the wheels, 33.88 kW, does not exceed the peak power available from the E-Axle, 160 kW.

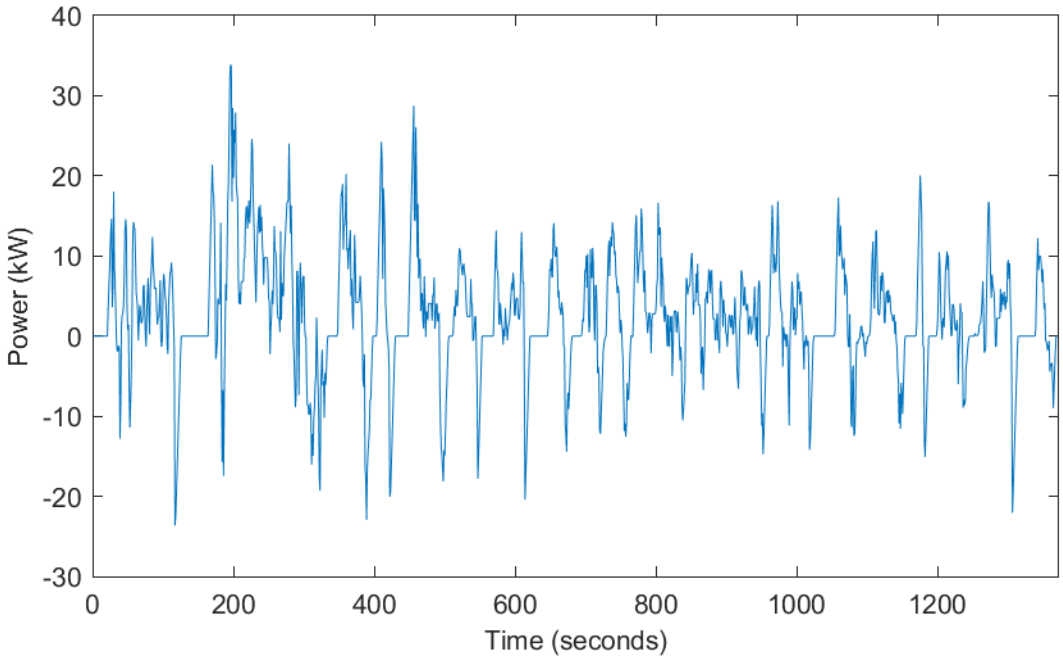

Figure 5.1 Instantaneous power required for the UDDS drive cycle.

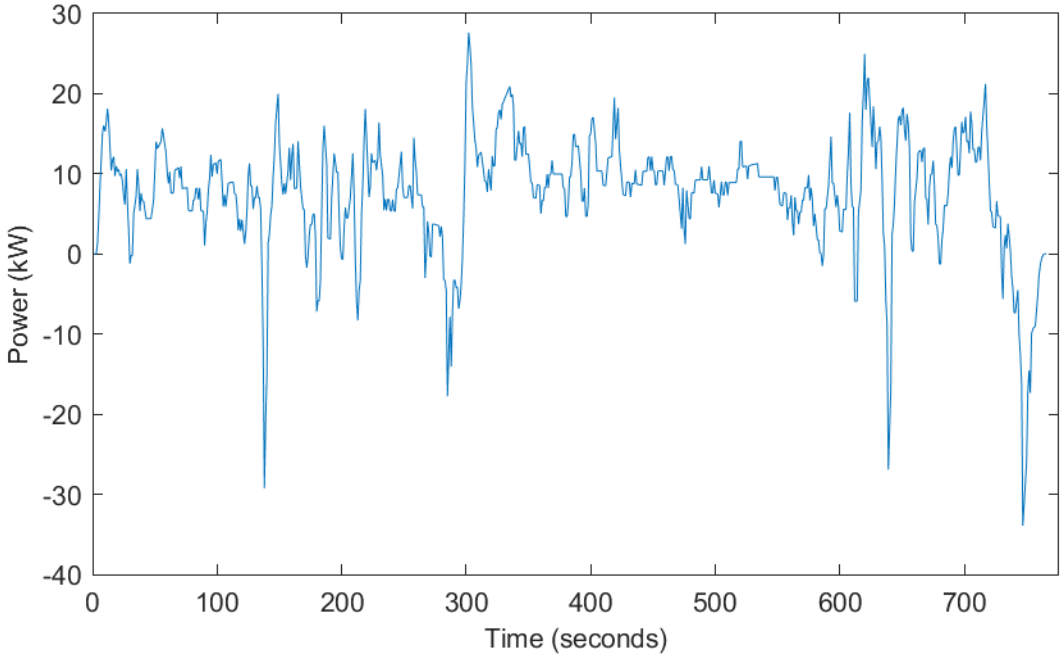

Figure 5.2 Instantaneous power required for the HWFET drive cycle.

Table 5.1 Required energy and power for the UDDS and HWFET drive cycles.

Metrics	UDDS	HWFET
Total positive (propulsion) energy required (kWh)	1.498	1.786
Total negative (regeneration) energy required (kWh)	0.556	0.178
Average positive (propulsion) power required (kW)	5.397	9.229
Peak power output required (kW)	33.88	33.90

5.2 Motor efficiency

Because the torque is split 50/50 between the two E-Axle motors, the motor efficiency is the same for both motors. Figure 5.3 and Figure 5.4 show the motor efficiency during the UDDS and HWFET drive cycles, respectively.

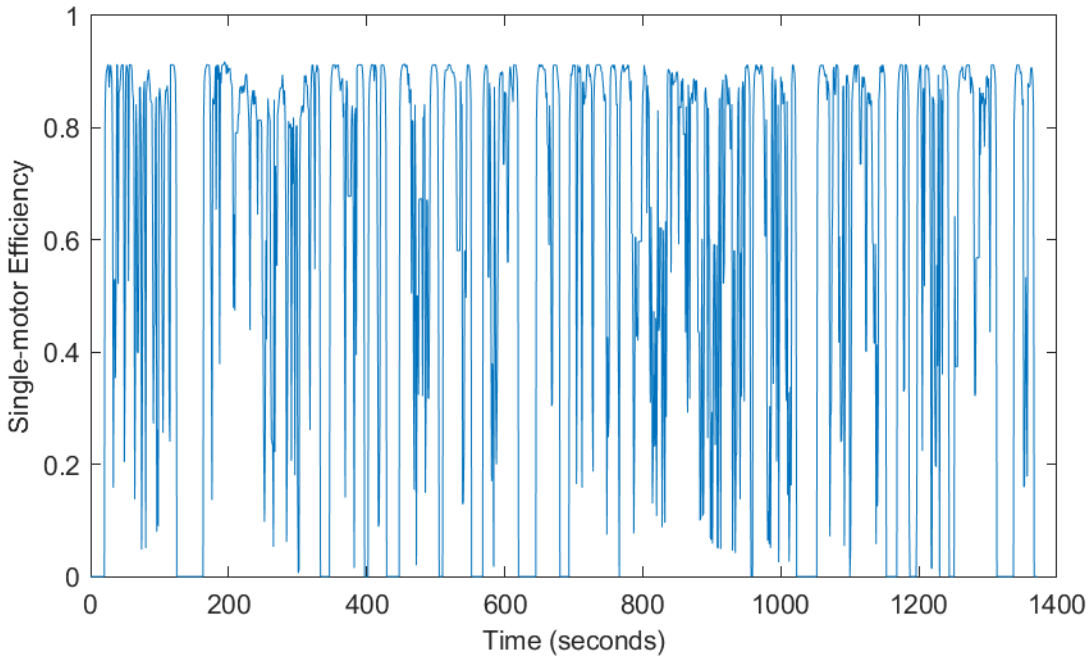

Figure 5.3 Single-motor efficiency during the UDDS drive cycle.

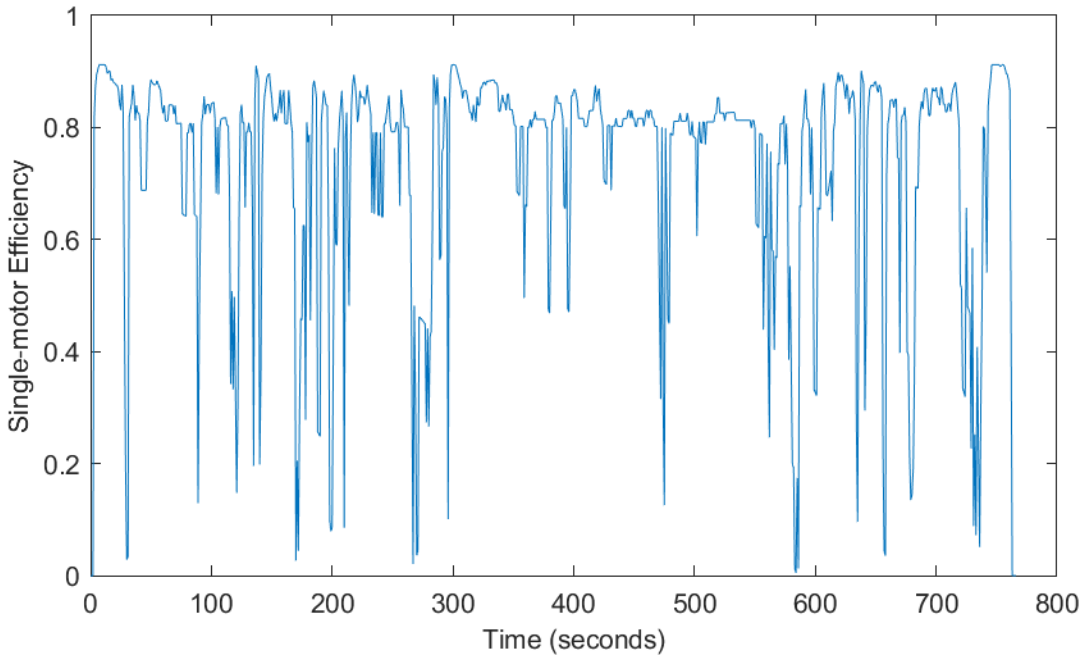

Figure 5.4 Single-motor efficiency during the HWFET drive cycle.

Figure 5.5 and Figure 5.6 overlay the motor operating points for the UDDS and HWFET drive cycles, respectively, onto the motor efficiency plot, Figure 2.3. The black operating points represent positive motor torque values, indicating that the motor is providing torque in the direction of rotation. In this case, it can be deduced that the motor force and the vehicle velocity are in the same direction. The green operating points represent negative motor torque values at which regeneration occurs while the speed is in the positive direction. When the motor torque is in the opposite direction to the vehicle speed, the motor is being pushed and acts like a generator, resulting in energy being transferred back to the battery. It should be noted that, for these drive cycles, the vehicle velocity is assumed to be positive, so the motor speed is always positive. For the UDDS city drive cycle (Figure 5.5), the motor operates on a wide range of motor torques (from 0 N·m to 90 N·m) and motor speeds (from 0 rpm to 6700 rpm). Whereas, for the HWFET highway drive cycle (Figure 5.6), each motor operates primarily on a smaller range of low motor torques (< 30 N·m) and high motor speeds (from 3000 rpm to 7000 rpm).

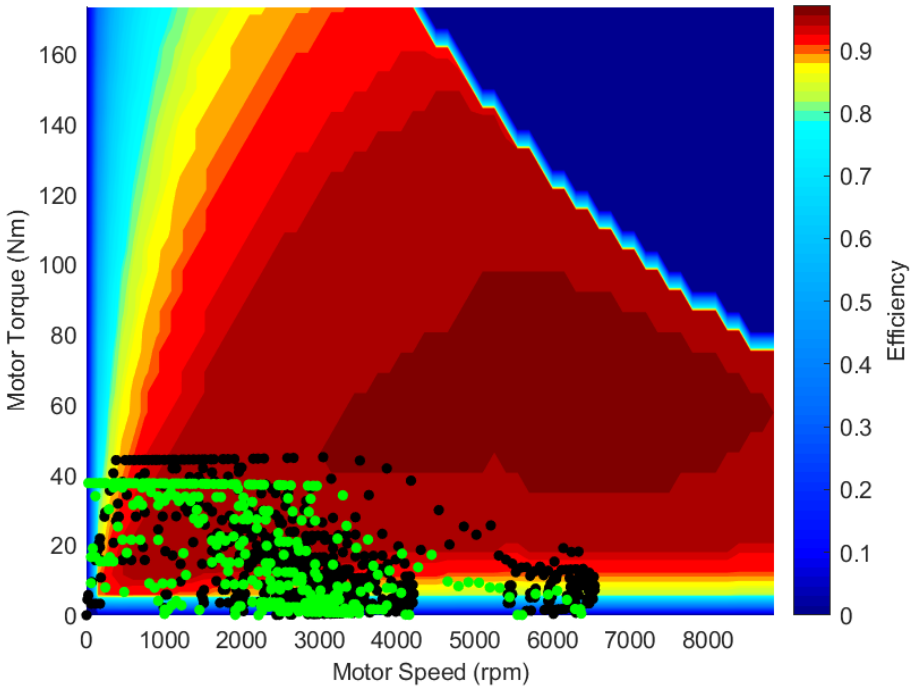

Figure 5.5 Motor efficiency for positive (black points) and negative (green points) motor torque for the UDDS drive cycle.

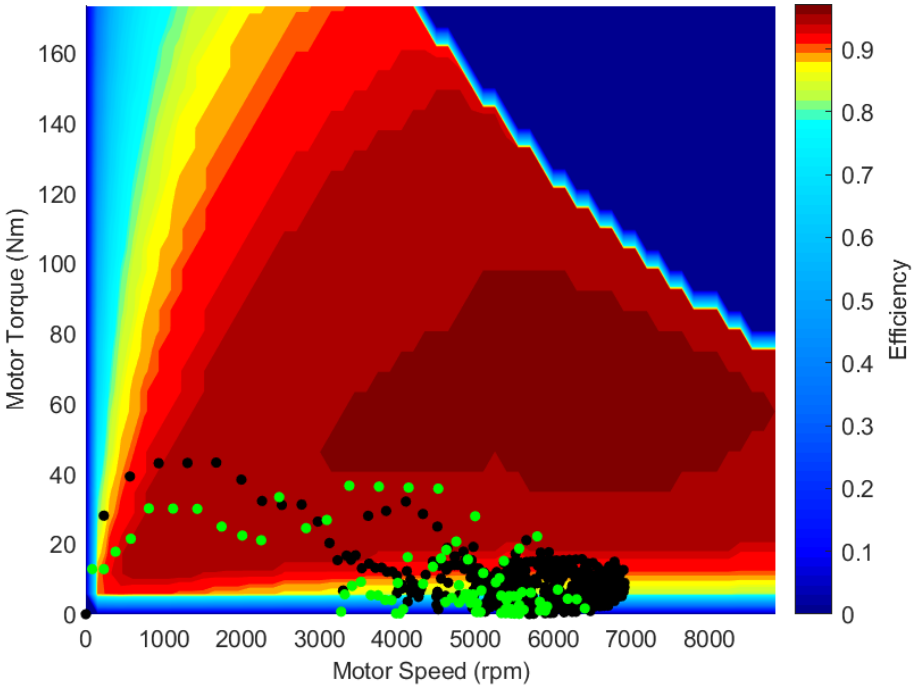

Figure 5.6 Motor efficiency for positive (black points) and negative (green points) motor torque for the HWFET drive cycle.

5.3 E-Axle power and energy consumed

Figure 5.7 and Figure 5.8 display the instantaneous power consumed at the E-Axle for the UDDS and HWFET drive cycles, respectively. Power required, Figure 5.2, is also shown in Figure 5.8 to see that the power consumed is slightly higher than the power required at the wheels. Table 5.2 lists a summary of the calculated energy and power consumed at the E-Axle for the UDDS and HWFET drive cycles. After accounting for the motor efficiency, the peak power consumed by the E-Axle, 37.055 kW, is well within the available power, 160 kW. The total positive, propulsion energy required to complete the UDDS and HWFET drive cycles was 1.855 kWh and 2.291 kWh, respectively. The total negative, regenerative energy during the drive cycles is 0.481 kWh for UDDS and 0.147 kWh for HWFET. Through regeneration within the E-Axle, this negative energy reduces the amount of energy required from the battery over the course of the drive cycle.

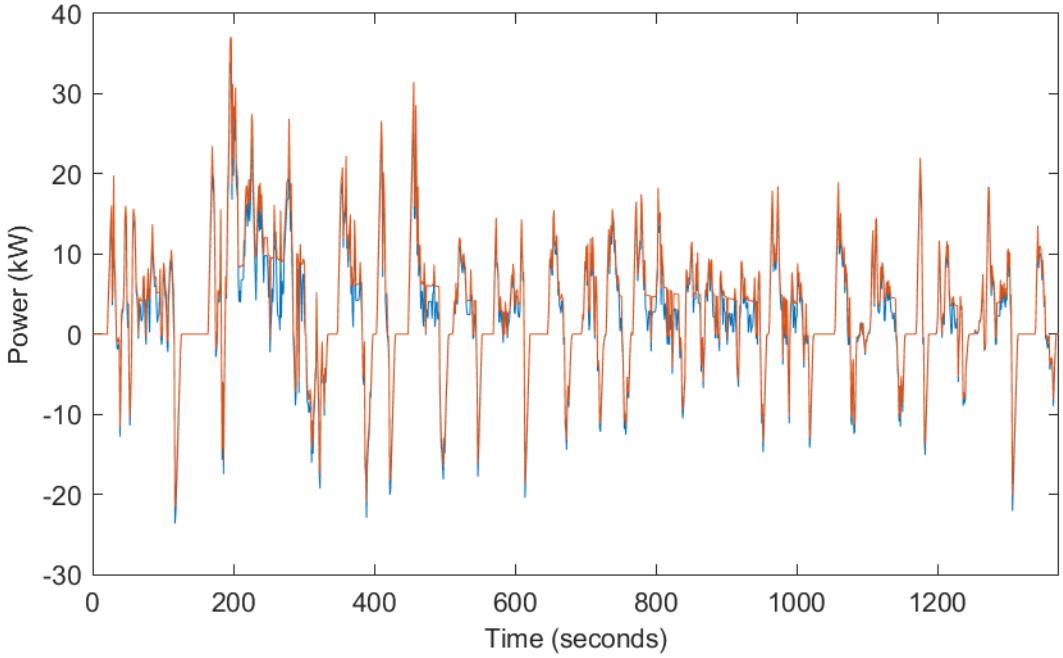

Figure 5.7 Power consumed at the E-Axle (orange) and power required at the wheels (blue) for the UDDS drive cycle.

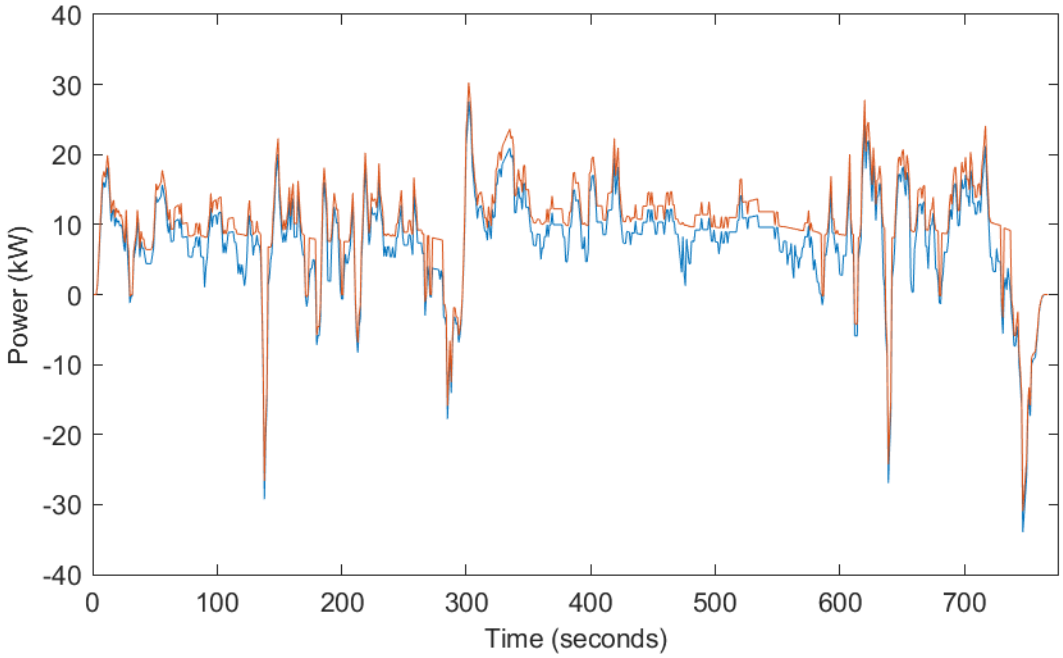

Figure 5.8 Power consumed at the E-Axle (orange) and power required at the wheels (blue) for the HWFET drive cycle.

Table 5.2 E-Axle energy and power consumed summary for the UDDS and HWFET drive cycles.

Metrics	UDDS	HWFET
Total positive (propulsion) energy consumed (kWh)	1.855	2.291
Total negative (regeneration) energy available (kWh)	0.481	0.147
Average positive (propulsion) power consumed (kW)	6.129	11.445
Peak power consumed (kW)	37.055	-30.919

5.4 Fuel economy

Figure 5.6 provides the fuel economy ratings for the UDDS drive cycle, the HWFET drive cycle, and the combined fuel economy. The MPGe values can be directly compared to the MPG ratings for conventional powertrain vehicles. When comparing the BEV MPGe to its original production MPG, the BEV is significantly higher, by 118% for the combined fuel economy, indicating the BEV can travel farther per an equivalent amount of energy and therefore is a more efficient option.

Table 5.3 Fuel economy ratings for the production vehicle and the BEV.

Fuel economy ratings	Production MPG [62]	BEV MPGe	Increase for BEV
UDDS/City	21	55.4	164%
HWFET/Highway	29	48.9	67%
Combined	24	52.4	118%

CHAPTER VI

TORQUE VECTORING TO OPTIMIZE SYSTEM EFFICIENCY

To further increase the fuel economy, one area to target is the electric axle efficiency. While the operating efficiency of each motor cannot be changed, the points at which the motors operate at can be changed based on what the controller is commanding. The E-Axle gear ratio could be adjusted for the motors to operate in a higher-efficiency region; however, this would have to be done early in the electric axle design. Another option is to optimize the torque split between the two motors. Instead of the 50/50, left/right torque split, an optimal split that will maximize E-Axle system efficiency is determined offline and then used in the simulation. A benefit to this optimization problem is that no hardware changes to the system are required as it is all accomplished purely in software.

The goal is to dynamically select the most optimal torque split between each of the independent motors in the E-Axle. This optimization can occur independent of the drive-cycle simulations allowing a desktop computer to process data and select the best solution possible by whatever TV strategy is used. For a given E-Axle torque output and motor speed (which is common to both motors when traveling in a straight line), the torque split ratio was swept. For each combination, the E-Axle efficiency was determined and the torque split ratio that yielded the maximum E-Axle efficiency was chosen and then placed in a look up table for that motor speed and E-Axle torque combination.

Figure 6.1 shows the resulting torque split ratio across E-Axle torque outputs and motor speeds. At lower torque outputs, it is more efficient to only operate a single motor rather than try to split the torque. Figure 6.2 and Figure 6.3 compares the E-Axle system efficiency for the 50/50 torque split to the optimized torque split. It demonstrates that efficiency can be improved, especially at lower torque outputs.

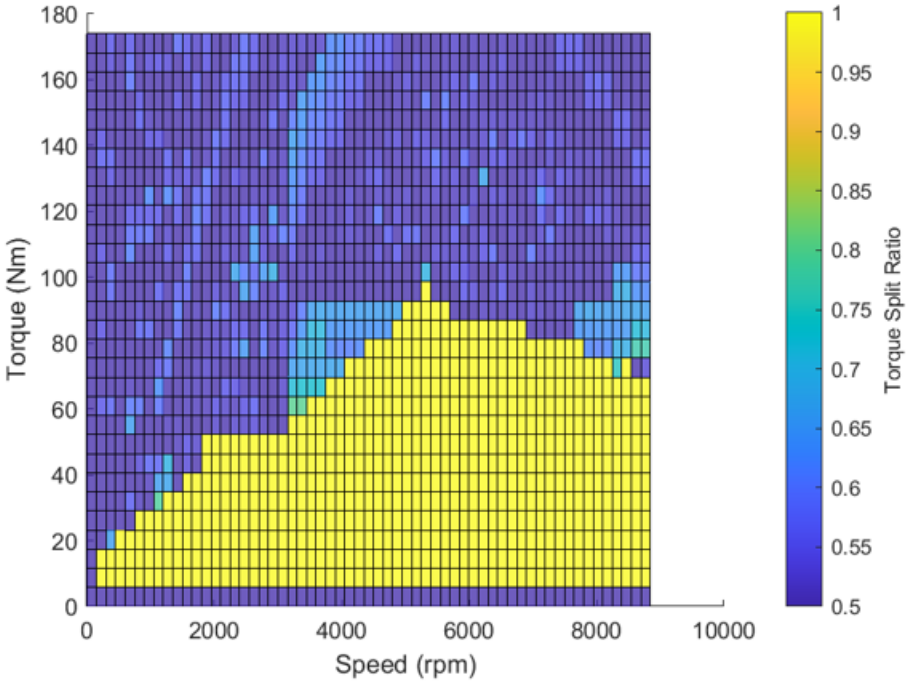

Figure 6.1 Torque split ratio for maximum E-Axle efficiency.

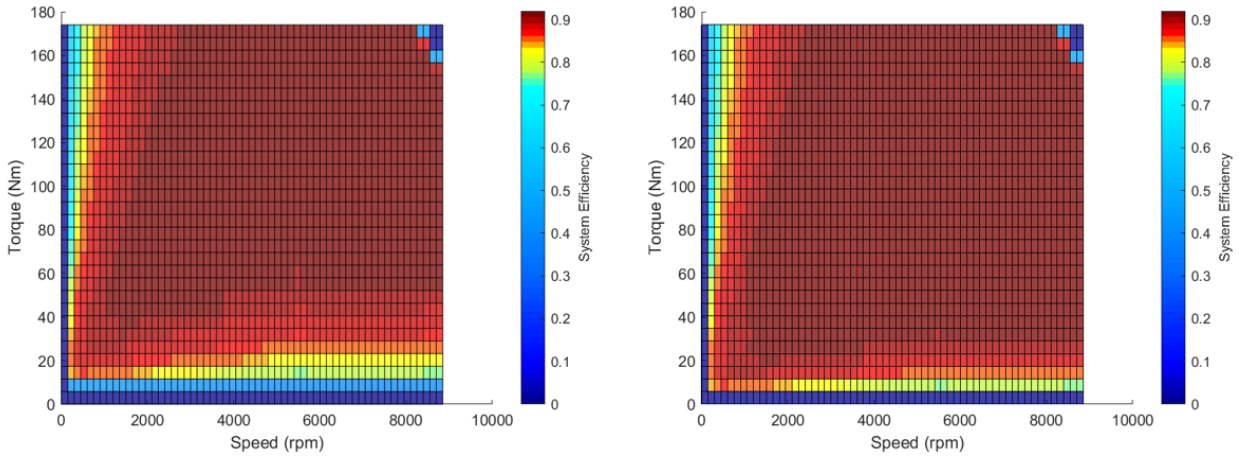

Figure 6.2 E-Axle system efficiency for a 50/50 split (left) and optimized split (right).

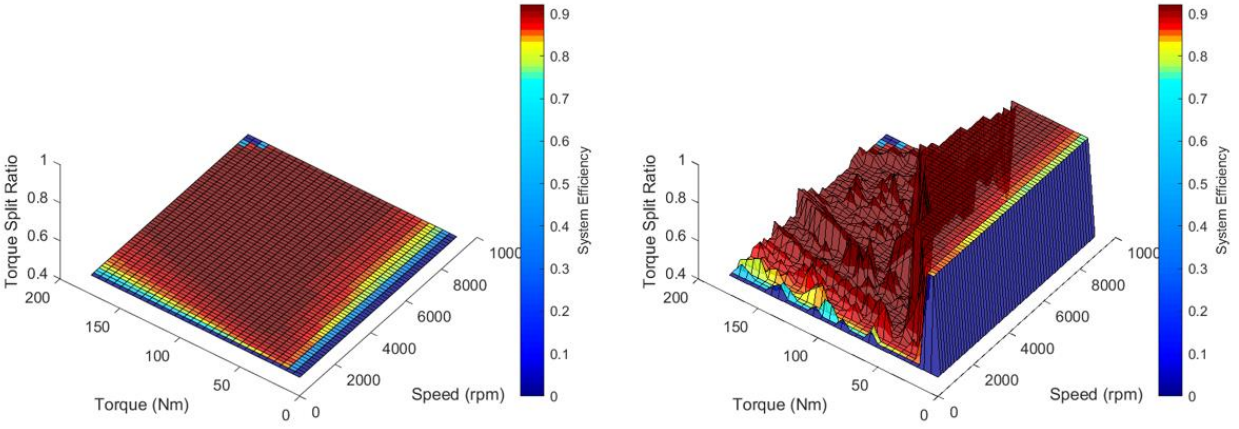

Figure 6.3 E-Axle system efficiency with torque split ratio for a 50/50 split (left) and optimized split (right).

CHAPTER VII

SIMULATED VEHICLE PERFORMANCE USING THE ONE-DIMENSIONAL MODEL WITH OPTIMIZED TORQUE VECTORING

Using the optimal torque split ratio, the drive cycle analysis was repeated. Figure 7.1 and Figure 7.2 compare the system efficiency for the 50/50 split and the Optimized split for both the UDDS and HWFET drive cycles, respectively. These plots show that Optimized split yields a higher system efficiency over the 50/50 split. This improvement is greater in the HWFET cycle due to the higher speeds and fewer acceleration events.

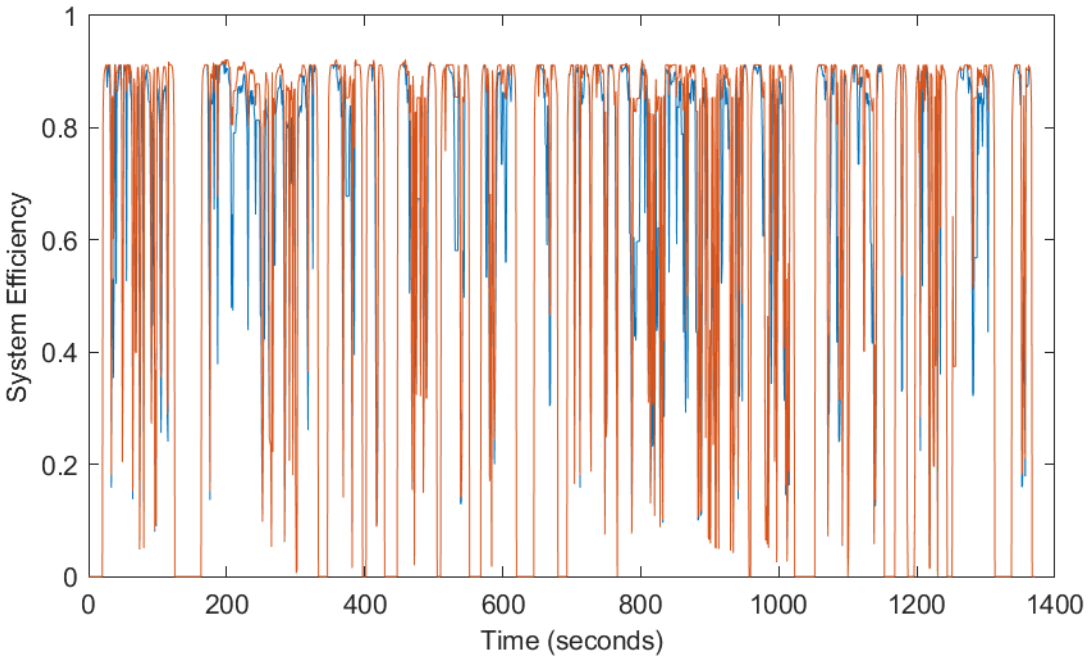

Figure 7.1 E-Axle system efficiency: optimized (orange) and 50/50 (blue) for the UDDS drive cycle.

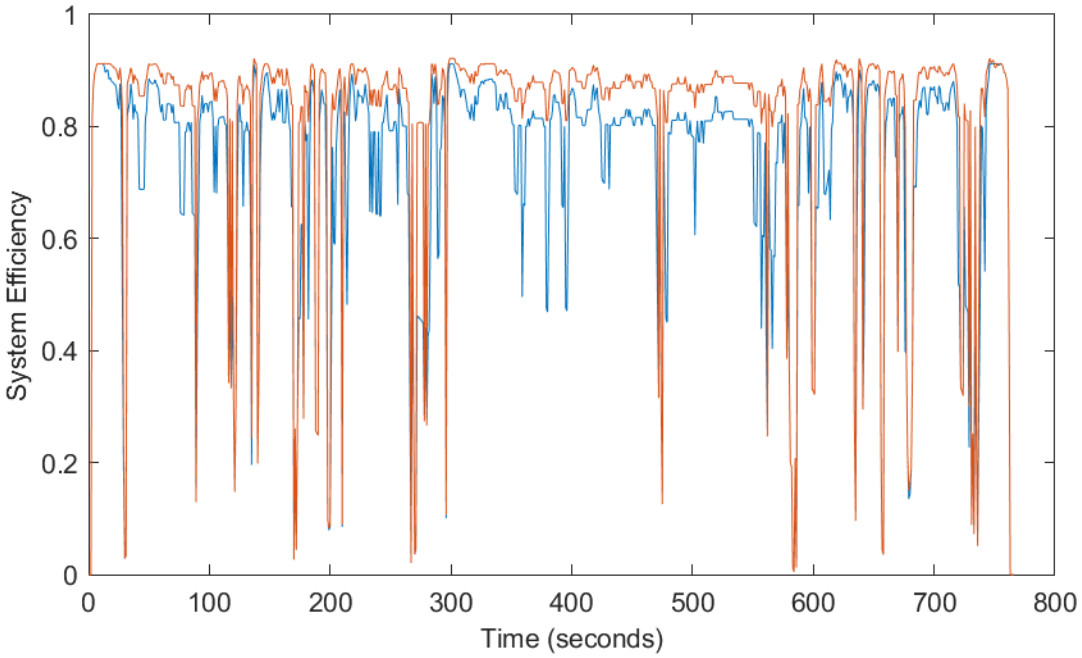

Figure 7.2 E-Axle system efficiency: optimized (orange) and 50/50 (blue) for the HWFET drive cycle.

Table 7.2 compares the E-Axle energy and power consumption across the two drive cycles. The total positive energy consumed after optimizing was reduced slightly and the negative energy captured during regeneration was increased slightly. Table 7.3 presents the fuel economy improvements for the torque vectoring which was optimized for system efficiency. For the UDDS, HWFET, and Combined fuel economy, the TV strategy yielded an increase of 9.0%, 10.0 %, and 9.5%, respectively, over the 50/50 split.

Table 7.2 E-Axle energy and power consumed for the UDDS and HWFED drive cycles: 50/50 split vs optimized.

Metrics	UDDS		HWFET	
	50/50	**Optimal**	**50/50**	**Optimal**
Total positive (propulsion) energy consumed (kWh)	1.855	1.753	2.291	2.104
Total negative (regeneration) energy available (kWh)	0.481	0.493	0.147	0.156
Average positive (propulsion) power consumed (kW)	6.129	5.893	11.445	10.605
Peak power consumed (kW)	37.055	36.903	-30.919	-31.241

Table 7.3 BEV Fuel economy ratings: 50/50 split vs optimized.

Fuel economy ratings	BEV MPGe		Increase
	50/50	**Optimized**	
UDDS/City	55.4	60.4	9.0%
HWFET/Highway	48.9	53.8	10.0%
Combined	52.4	57.4	9.5%

CHAPTER VIII

3DOF MODEL

Using a TV strategy optimized for E-Axle efficiency, it was shown that improvements could be made over the baseline 50/50 left/right split. The optimized torque split ratio improved the combined fuel economy by 9.5% over the 50/50 split. Improvements in fuel economy are critical to reducing dependency on fossil fuels and to reduce consumer's concerns about range anxiety in BEVs.

Up to this point, the vehicle model has assumed straight-line, one-dimensional motion. However, when the torque is split unevenly to one side or the other under a TV strategy, a yaw moment will be induced on the vehicle and cause the vehicle to deviate from the driver-intended, straight-line path.

To characterize this yaw moment and the degree of off-axis deviation, a dynamic, 3 degrees-of-freedom model is implemented where the three degrees of freedom are longitudinal (x), lateral (y), and yaw rotation (x-y moment). This dynamic vehicle model will make use of Simulink's Vehicle Dynamic Blockset [73] models such as the vehicle model, the tire model, and the driver model.

During implementation of the control strategies, if the driver's commanded torque was negative, a 50/50 torque split ratio was used. This was done to maintain low-speed stability within the model which allows for aggressive decelerations that are demanded from the driver while trying to meet the drive cycle profile. Due to the little time for each deceleration event and

overall small number of events, the amount of energy available for regeneration is relatively low. So, there is little motivation to optimize the torque split during these regions especially at the expense of vehicle stability.

8.1 Vehicle model

The exact vehicle model used in this study is the Vehicle Body 3DOF Dual Track which per Simulink implements a 3DOF, rigid, two-axle vehicle body model to calculate longitudinal, lateral, and yaw motion [74]. The model accounts for body mass, aerodynamic drag, and weight distribution between the axles due to acceleration and steering.

8.2 Tire model

The exact tire model used in this study is the Combined Slip Wheel 2DOF which per Simulink implements the longitudinal and lateral behavior of a wheel characterized by the Magic Formula [75] [76]. This model can be used in driveline and vehicle simulations where low frequency tire-road and braking forces are required to determine vehicle acceleration, braking, and wheel-rolling resistance. The model is suitable for applications that require combined lateral slip, for example, in lateral motion and yaw stability studies. Based on the driveline torque, brake pressure, road height, wheel camber angle, and inflation pressure, the model determines the wheel rotation rate, vertical motion, forces, and moments in all six degrees of freedom [77].

This tire model requires many variables to accurately model a specific tire. A leader in the simulation industry, Global Center for Automotive Performance Simulations (GCAPS) [78], was contacted and they provided the input files (.tir files) needed to accurately model the tires.

8.3 Driver model

The exact driver model used in this study is the Predictive Driver which per Simulink implements a controller that generates normalized steering, acceleration, and braking commands to track longitudinal velocity and a lateral reference displacement [79]. For the drive cycle analysis, the target longitudinal velocity is the drive cycle velocity, and the target lateral reference displacement is zero.

CHAPTER IX

SIMULATED VEHICLE PERFORMANCE USING THE 3DOF MODEL

Using the 3DOF model, the drive cycle analysis was repeated for the 50/50 torque split and the optimized torque split. These results were then compared back to the one-dimensional model to verify the model. With the 3DOF model, the vehicle's off-axis deviation from straight line driving can now be characterized when operating under the efficiency-optimized torque vectoring control strategy.

9.1 50/50 torque split

Table 9.1 compares the energy and power consumed results from the 3DOF model vs the one-dimensional (1DOF) model when using a 50/50 torque split. The energy and power predicted by 3DOF model closely match that of the one-dimensional model. The 3DOF model predicted slightly less total energy consumed and slightly more total energy regenerated, which indicates the one-dimensional model was conservative when predicting energy consumption. Table 9.2 compares the predicted fuel economy ratings between the two models. Using the 3DOF model, the combined fuel economy is 59.1 vs 52.4 when using the one-dimensional model and 24 for the production vehicle.

Table 9.1 E-Axle energy and power consumed summary for the UDDS and HWFET drive cycles for a 50/50 torque split, 3DOF vs one-dimensional.

Metrics	UDDS		HWFET	
	1DOF	3DOF	1DOF	3DOF
Total positive (propulsion) energy consumed (kWh)	1.855	1.698	2.291	2.156
Total negative (regeneration) energy available (kWh)	0.481	0.521	0.147	0.156
Average positive (propulsion) power consumed (kW)	8.517	7.927	12.166	11.551
Peak positive (propulsion) power consumed (kW)	37.055	35.025	30.287	28.452
Peak negative (regeneration) power available (kW)	21.549	22.123	30.919	30.719

Table 9.2 Fuel economy ratings for a 50/50 torque split, 3DOF vs one-dimensional.

Fuel economy ratings	1DOF	3DOF
UDDS/City	55.4	64.6
HWFET/Highway	48.9	52.4
Combined	52.4	59.1

9.2 Optimized torque split

Table 9.3 compares the energy and power consumed for the UDDS and HWFET drive cycles when using the optimized torque split and Table 9.4 compares the fuel economy ratings between the two models. Using the 3DOF model, the combined fuel economy is 64.5 vs 57.4 when using the one-dimensional model and 24 for the production vehicle.

Table 9.3 E-Axle energy and power consumed summary for the UDDS and HWFET drive cycles for an optimized torque split, 3DOF vs one-dimensional.

Metrics	UDDS		HWFET	
	1DOF	3DOF	1DOF	3DOF
Total positive (propulsion) energy consumed (kWh)	1.753	1.609	2.104	1.967
Total negative (regeneration) energy available (kWh)	0.493	0.521	0.156	0.156
Average positive (propulsion) power consumed (kW)	8.05	7.193	11.170	10.521
Peak positive (propulsion) power consumed (kW)	36.903	36.052	29.975	28.599
Peak negative (regeneration) power available (kW)	21.685	22.123	31.241	30.718

Table 9.4 Fuel economy ratings for an optimized torque split, 3DOF vs one-dimensional.

Fuel economy ratings	1DOF	3DOF
UDDS/City	60.4	69.9
HWFET/Highway	53.8	57.9
Combined	57.4	64.5

9.3 Deviation from straight-line driving

Figure 9.1 and Figure 9.2 show the deviation from straight-line driving for the UDDS and HWFET drive cycles, respectively, when using the optimized torque split ratio. Due to the unequal torque applied to the wheels, the vehicle, which starts at x=0, y=0, traverses circularly. It is apparent from these plots that the one-dimensional (longitudinal (x)) model is insufficient and the yaw movement needs to be accounted for.

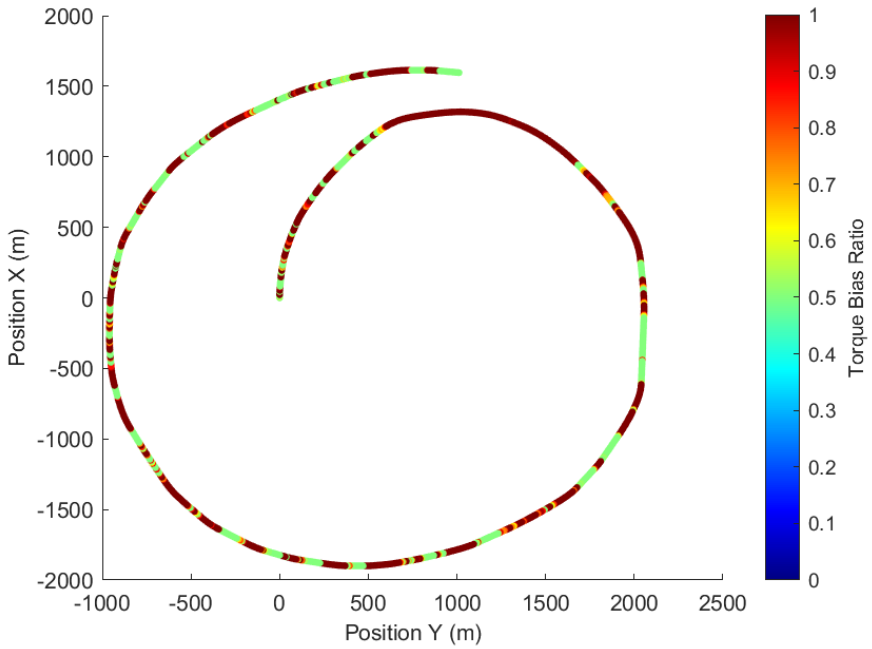

Figure 9.1 Vehicle position using optimized torque split and no yaw mitigation strategy during UDDS.

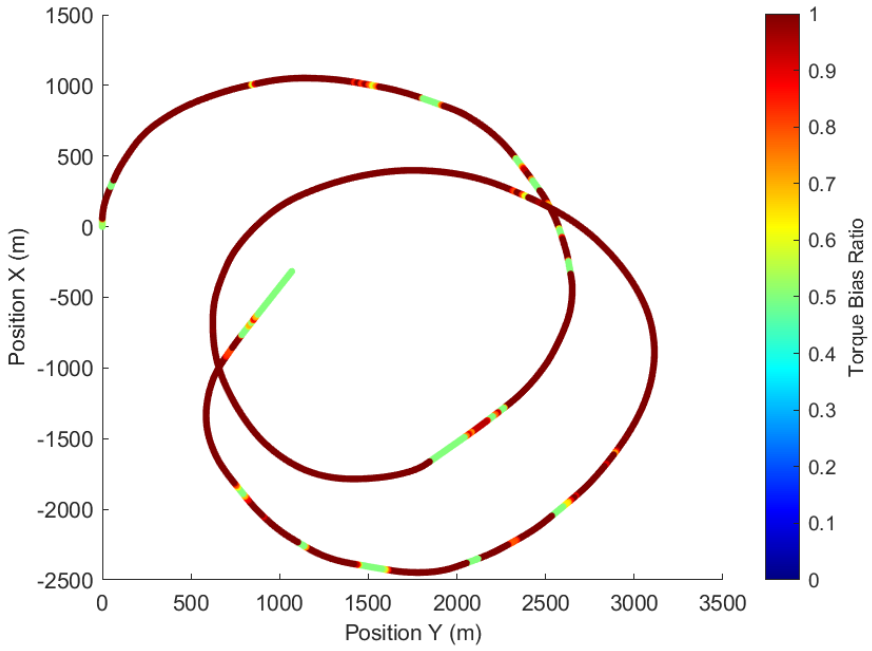

Figure 9.2 Vehicle position using optimized torque split and no yaw mitigation strategy during HWFET.

CHAPTER X

YAW MITIGATION STRATEGIES

Several strategies were investigated to mitigate this potentially undesired yaw motion:

1. Allow yaw corrections using the steering wheel.
2. Limit the degree of drift from center by switching the dominant torque from one side to the other.
3. Limit yaw motion by trading system efficiency.
4. Consider a physical update to the E-Axle: Couple the motor output shafts to allow equal torque distribution.

10.1 Correct yaw through driver steering

The first control method implemented to mitigate undesired yaw motion was to allow steering corrections with a simulated driver that would react to deviations from the intended straight-line path. This method utilized the built in Simulink driver model mentioned in Section 8.3. The driver's outputs for the steering command were limited to +/- 8 degrees of steering wheel movement. This value was selected subjectively and deemed appropriate as it allows the driver to stay on the intended path without being too extreme of a correction and could be seen as an equivalent amount of correction a driver might normally apply, for example, if on an embanked road. Because we are allowing the driver to correct the vehicle's trajectory, the optimal efficiency torque bias ratio was applied for the duration of the drive cycles. Driver steering is not enabled for any other method.

10.2 Switch dominant torque from side to side

The second control method implemented to mitigate undesired yaw motion was to rapidly switch the dominant torque from side to side. The first attempt was switched at a rate of 0.01 seconds or 100 hertz. This resulted in the vehicle not staying on its intended straight-line path. The rate/frequency was increased to 0.001 seconds or 1000 hertz and resulted in the vehicle traveling in a straight line. The optimal efficiency torque bias ratio was applied for the duration of the drive cycles and switched from left to right at a rate of 1000 hertz. This method assumes that the E-Axle can receive and respond to torque commands in intervals of 1000 hertz. It also assumes there are not any additional losses with operating the motor in this fashion.

10.3 Trade system efficiency to reduce yaw motion

The third control method implemented to mitigate undesired yaw motion was to limit the difference between the left and right torque while still trying to apply a torque split ratio that is more efficient that the 50/50 split. This strategy limited the optimal efficiency torque bias ratio such that the difference between the left and right torque was not greater than 1% of the total torque. This extremely low percentage still resulted in the vehicle not following a straight path. Any benefits seen from this method are marginal and will require some driver interaction or other method to correct the vehicle's intended path.

10.4 Couple the motor output shafts

The fourth control method implemented to mitigate undesired yaw motion was to physically couple the outputs of each motor to each other, resulting in equal torque being applied to each of the rear wheels. This would allow for the optimal efficiency torque split ratio to be used while still applying an equal amount of torque to each side of the vehicle. An equal torque

split will result in the vehicle staying on its intended straight-line path. A drawback to this method is the fact that it requires a physical modification of the E-Axle.

CHAPTER XI

SIMULATED VEHICLE PERFORMANCE OF THE YAW MITIGATION STRATEGIES

For each torque vectoring strategy, E-Axle power required and consumed, left and right motor efficiency, left and right motor torque, torque bias ratio, yaw rate, and longitudinal vs lateral position are presented. Then, a summary of the total power and energy across all the strategies is presented along with the fuel economy.

11.1 Baseline 50/50 torque split

As a point of comparison, the results for a 50/50 torque split using the 3DOF model are provided for the UDDS and HWFET drive cycles.

11.1.1 UDDS

For the UDDS drive cycle while operating under a 50/50 torque split, Figure 11.1 shows the E-Axle power required and power consumed. Figure 11.2. provides the motor efficiency overlayed with operating points for each motor. For the 50/50 split, the left and right motors are operating at the same torque/speed points, so the efficiency plots will be the same. This is also demonstrated by Figure 11.3 which shows the left and right motor torques are the same and the torque bias ratio is 0.5.

Figure 11.4 shows the vehicle yaw rate during the drive cycle. As expected for the 50/50 torque split, the vehicle yaw rate is 0 deg/s because the left and right motor torques are the same. Figure 11.5 shows vehicle deviation from straight-line driving where X is the longitudinal

direction (intended driving path), and Y is the off-axis deviation. As expected for the 50/50 torque split, the vehicle does not deviate from the straight-line driving path.

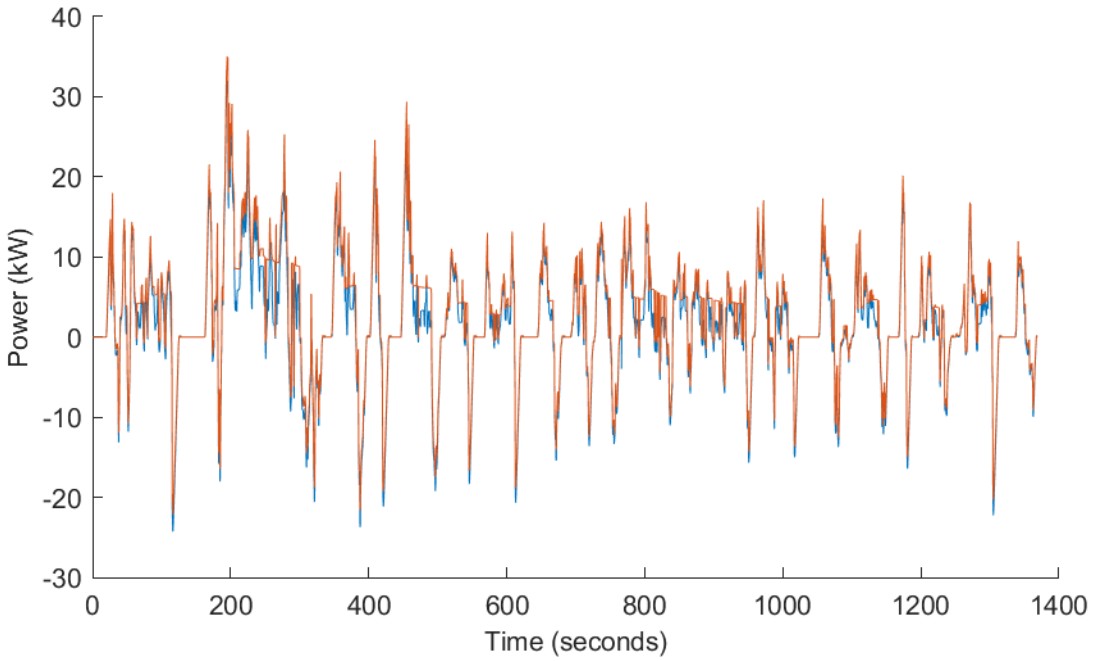

Figure 11.1 50/50 torque split during UDDS: power required (blue) and power consumed (orange).

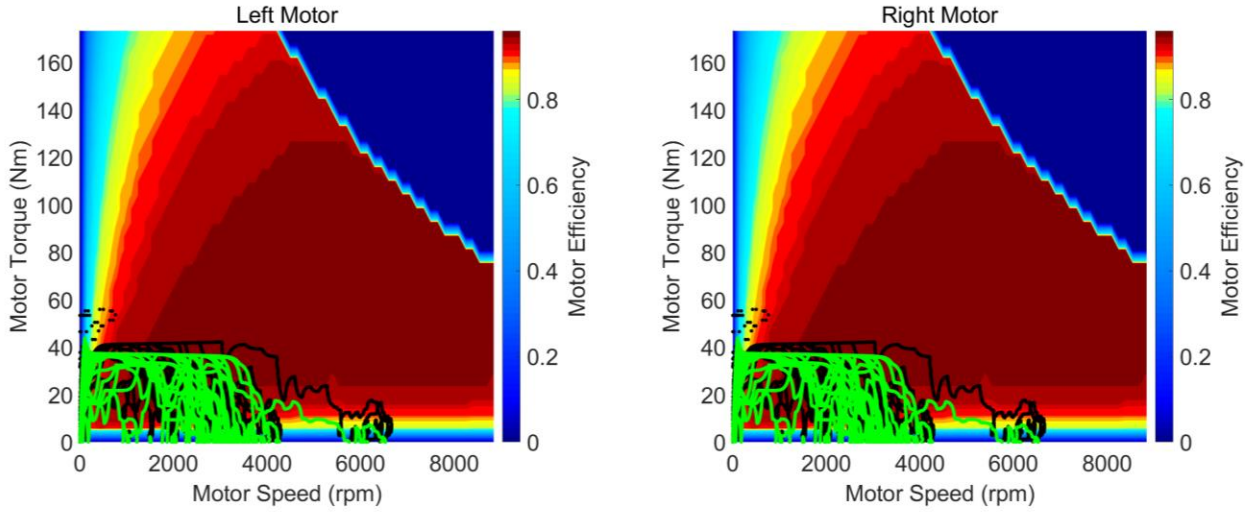

Figure 11.2 50/50 torque split during UDDS: efficiency map with operating points for the left motor (left) and the right motor (right).

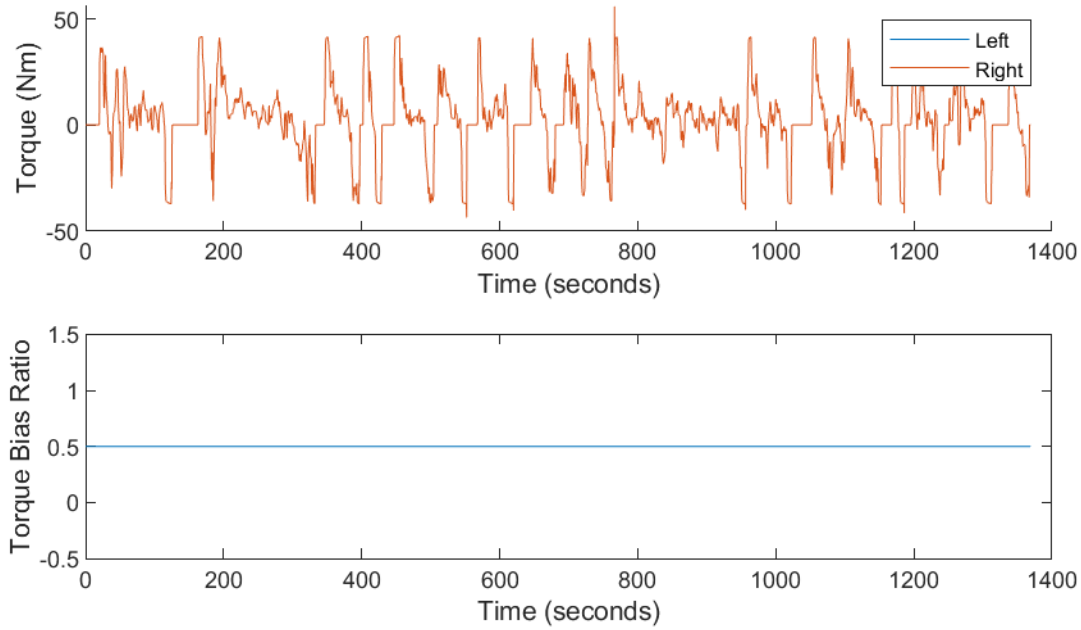

Figure 11.3 50/50 torque split during UDDS: left and right motor torque (top) and torque bias ratio (bottom).

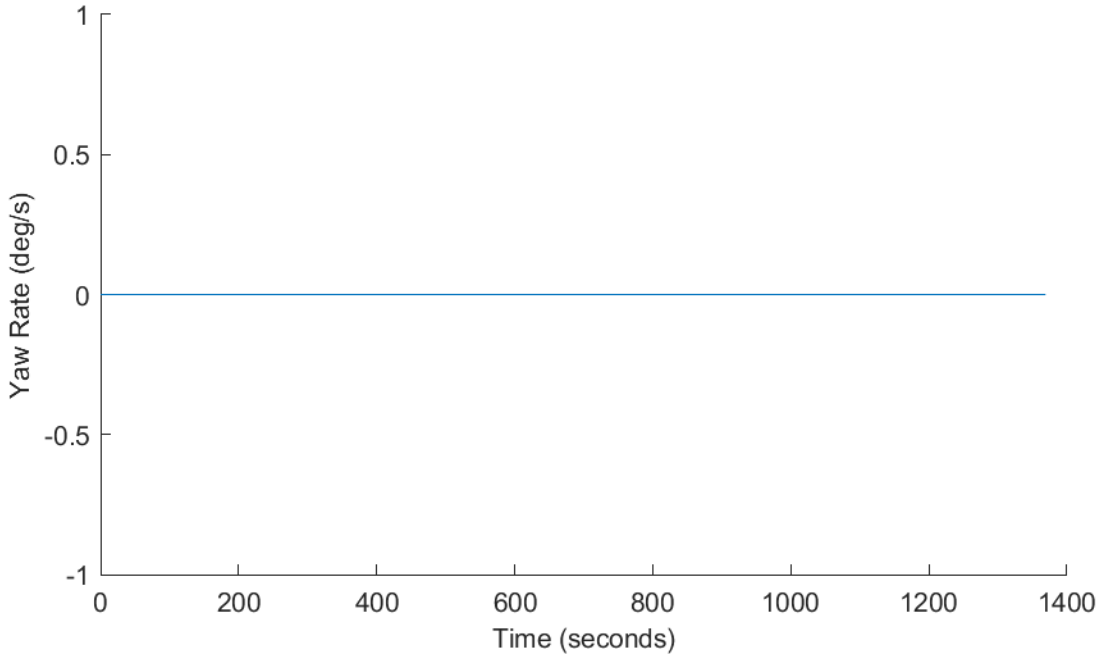

Figure 11.4 50/50 torque split during UDDS: vehicle yaw rate.

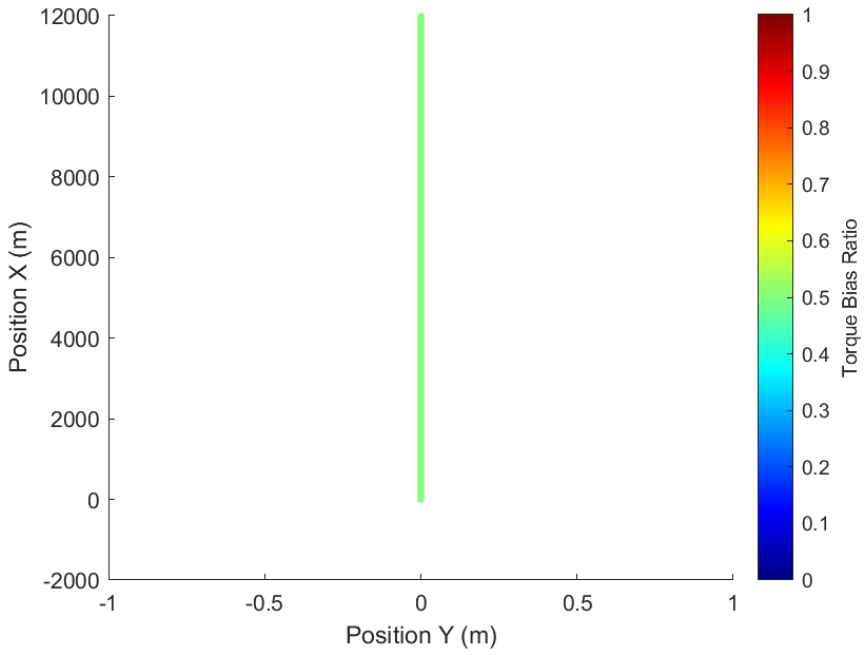

Figure 11.5 50/50 torque split during UDDS: deviation form straight-line driving.

11.1.2 HWFET

For the HWFET drive cycle while operating under a 50/50 torque split, Figure 11.6 shows the E-Axle power required and power consumed. Figure 11.7 provides the motor efficiency overlayed with operating points for each motor. For the 50/50 split, the left and right motors are operating at the same torque/speed points, so the efficiency plots will be the same. This is also demonstrated by Figure 11.8 which shows the left and right motor torques are the same and the torque bias ratio is 0.5.

Figure 11.9 shows the vehicle yaw rate during the drive cycle. As expected for the 50/50 torque split, the vehicle yaw rate is 0 deg/s because the left and right motor torques are the same. Figure 11.10 shows vehicle deviation from straight-line driving where X is the longitudinal direction (intended driving path), and Y is the off-axis deviation. As expected for the 50/50 torque split, the vehicle does not deviate from the straight-line driving path.

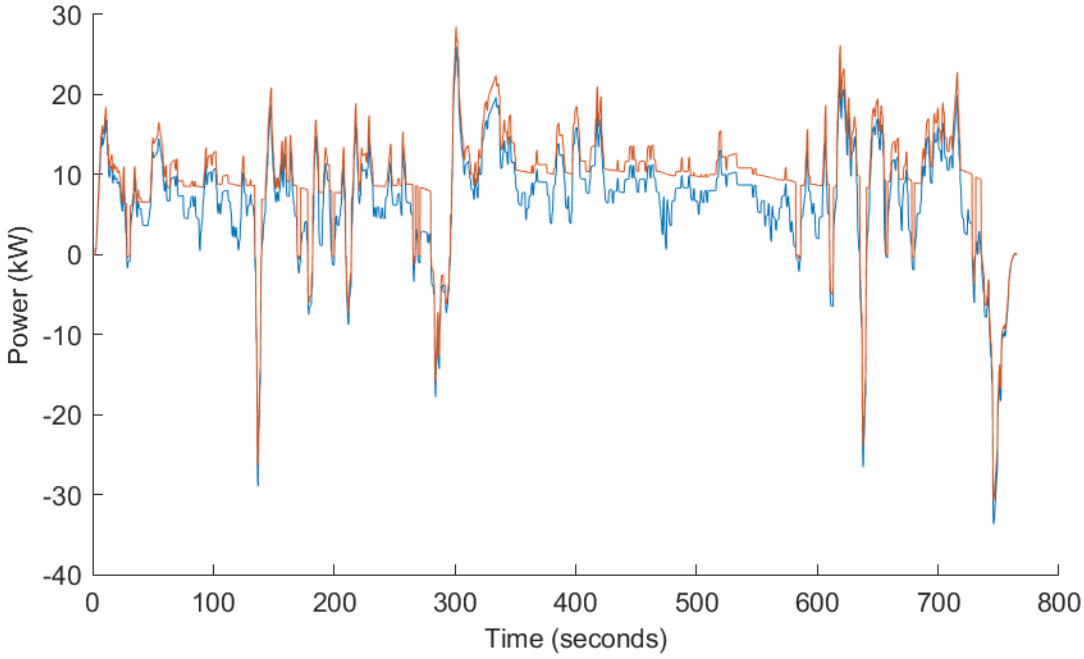

Figure 11.6 50/50 torque split during HWFET: power required (blue) and power consumed (orange).

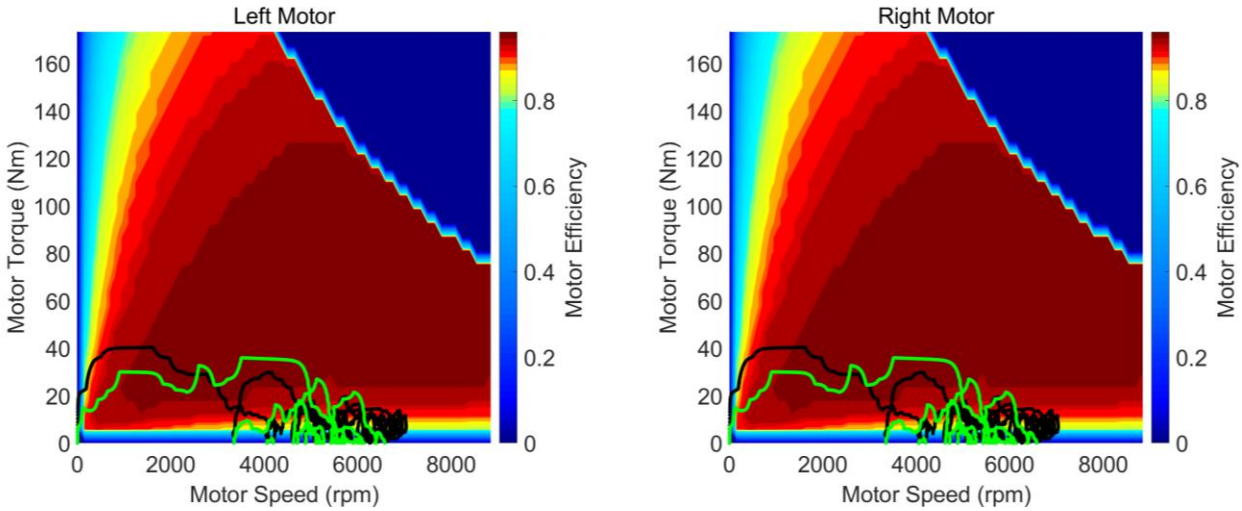

Figure 11.7 50/50 torque split during HWFET: efficiency map with operating points for the left motor (left) and the right motor (right).

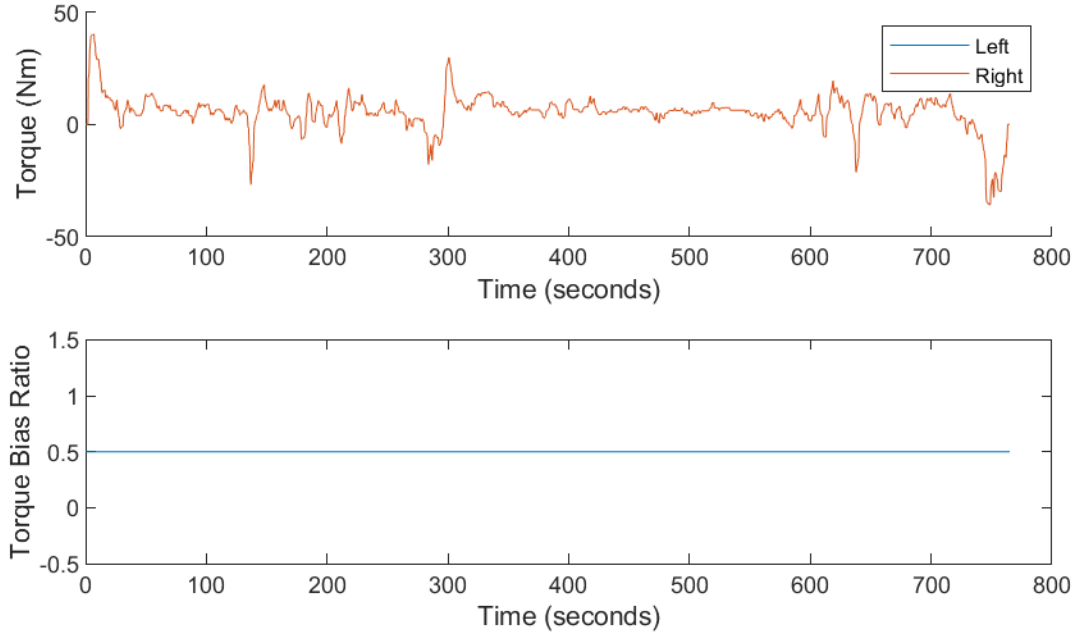

Figure 11.8 50/50 torque split during HWFET: left and right motor torque (top) and torque bias ratio (bottom).

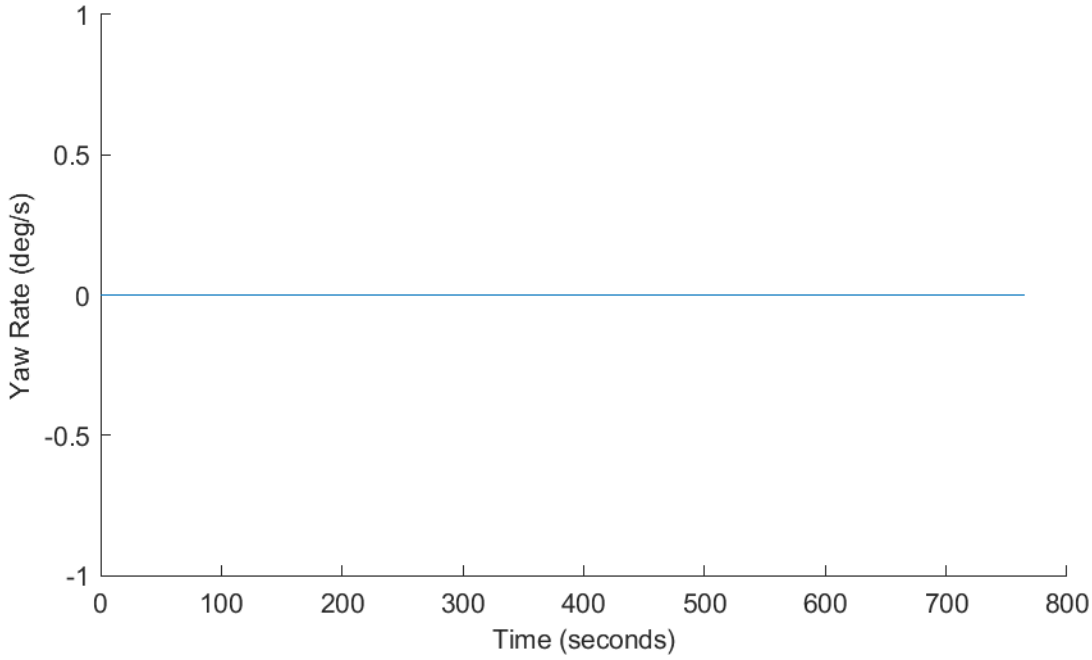

Figure 11.9 50/50 torque split during HWFET: vehicle yaw rate.

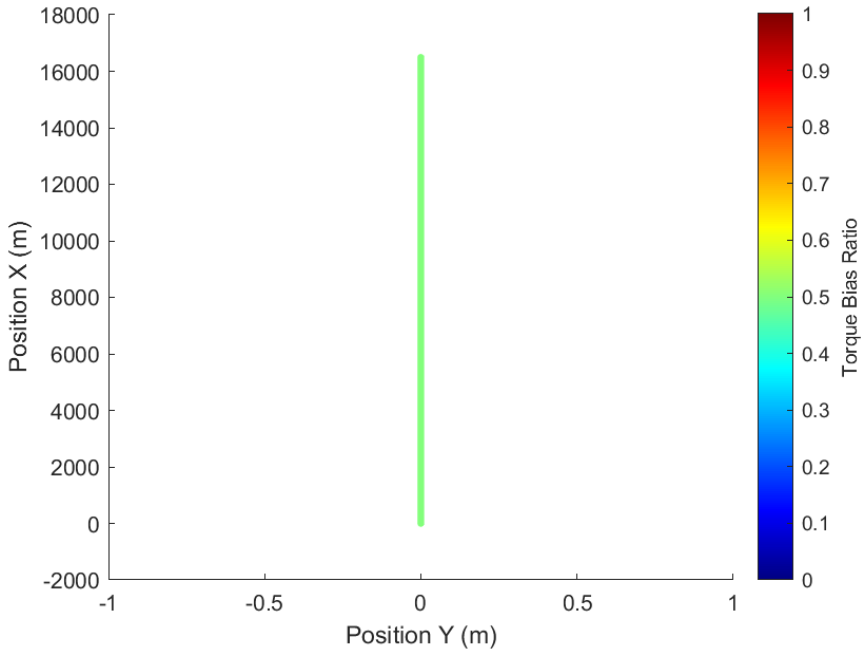

Figure 11.10 50/50 torque split during HWFET: deviation form straight-line driving.

11.2 Driver steering strategy

11.2.1 UDDS

For the UDDS drive cycle while operating under the Driver Steering Strategy, Figure 11.11 shows the power required and power consumed. Figure 11.12 shows the left motor supplies most of the torque, when torque is positive, and is supplemented by the right motor when additional torque is needed. The motor efficiency plot, Figure 11.13, shows for positive motor torque, the right motor is only used when the motor speed is less than about 4000 rpm.

Figure 11.14 shows the vehicle yaw rate during the drive cycle primarily stays within 0.2 deg/s; however, there are frequent spikes up to 1 deg/s. Figure 11.15 shows the vehicle maintains straight-line driving, which is a result of the driver compensating for the vehicle's yaw rate.

Figure 11.16 shows the driver's steering wheel angle during the drive cycle which averages -0.82 deg and peaks at -7.4 deg.

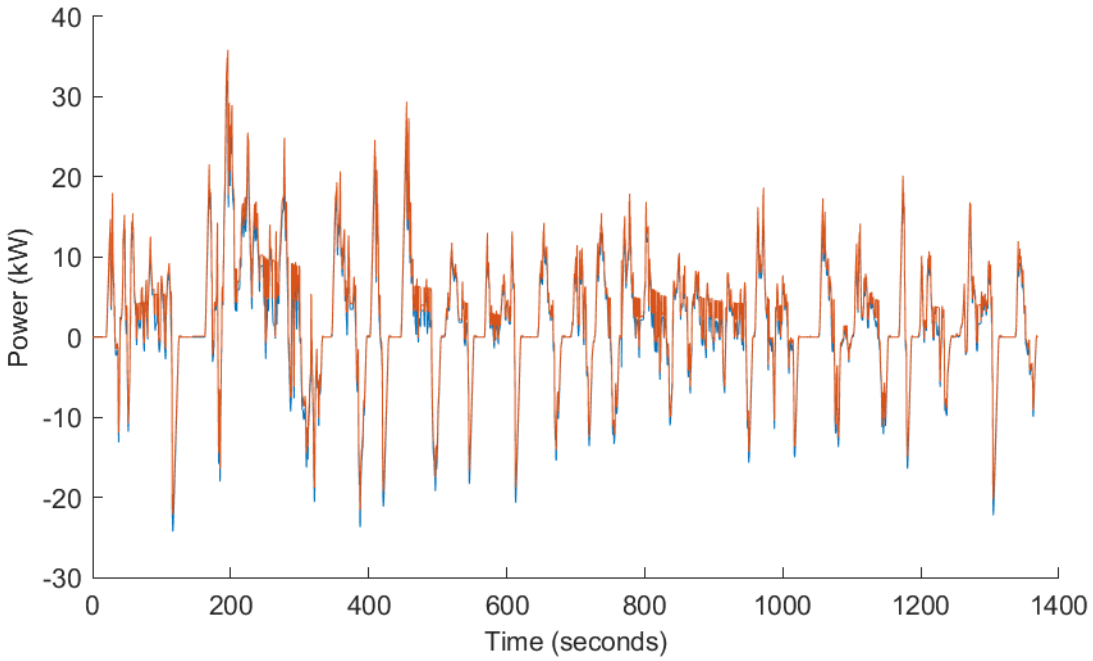

Figure 11.11 Driver steering during UDDS: power required (blue) and power consumed (orange).

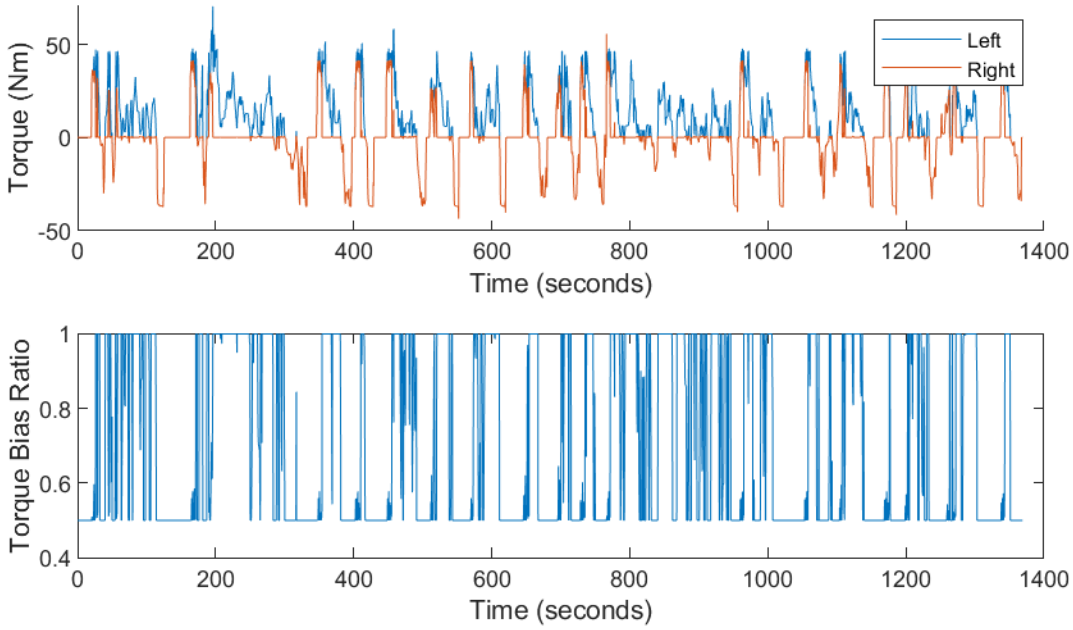

Figure 11.12 Driver steering during UDDS: left and right motor torque (top) and torque bias ratio (bottom).

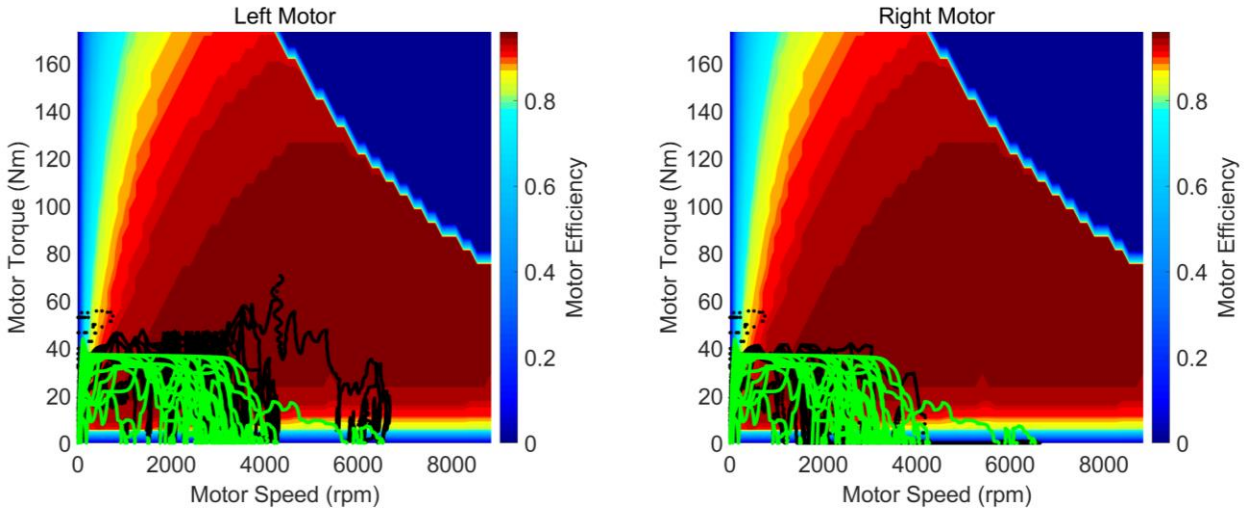

Figure 11.13 Driver steering during UDDS: efficiency map with operating points for the left motor (left) and the right motor (right).

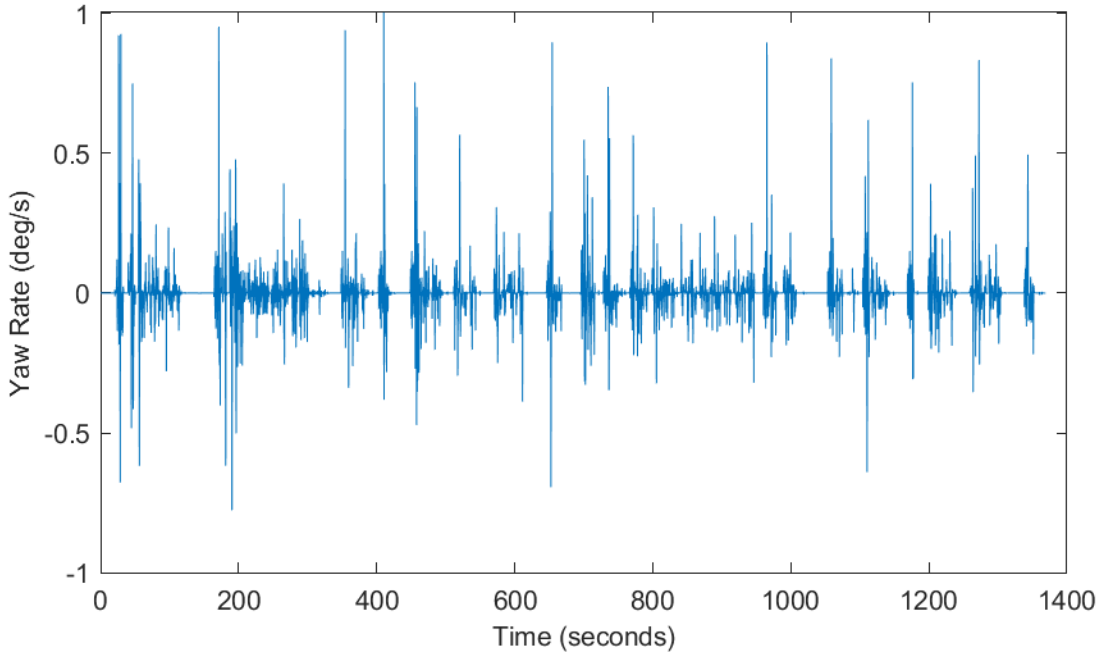

Figure 11.14 Driver steering during UDDS: vehicle yaw rate.

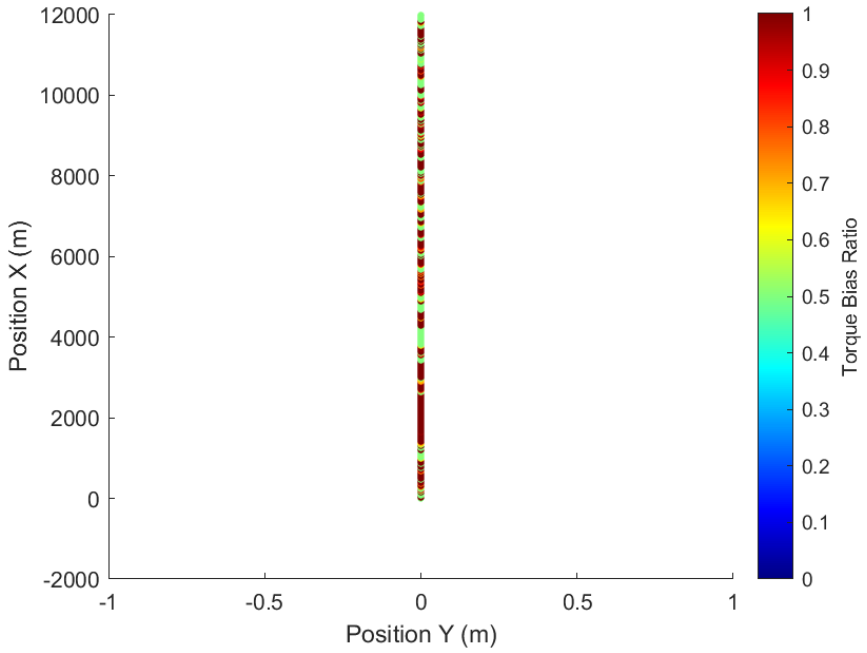

Figure 11.15 Driver steering during UDDS: deviation form straight-line driving.

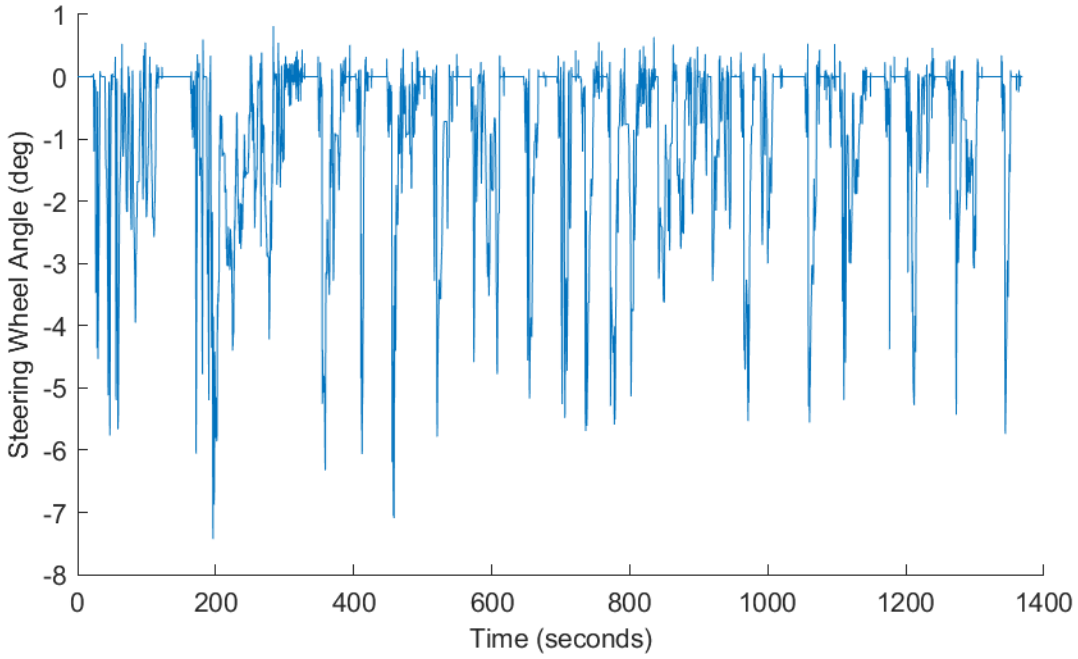

Figure 11.16 Driver steering during UDDS: steering wheel angle.

11.2.2 HWFET

For the HWFET drive cycle while operating under the Driver Steering Strategy, Figure 11.17 shows the E-Axle power required and power consumed. Figure 11.18 shows the left motor supplies most of the torque, when torque is positive, and is supplemented by the right motor when additional torque is needed. The motor efficiency plot, Figure 11.19, shows for positive motor torque, the right motor is only used when the motor speed is less than about 3000 rpm.

Figure 11.20 shows the vehicle yaw rate during the drive cycle primarily stays within 0.1 deg/s; however, there are spikes up to 0.37deg/s. Figure 11.21 shows vehicle maintains straight-line driving, which is a result of the driver compensating for the vehicle's yaw rate. Figure 11.22 shows the driver's steering wheel angle during the drive cycle which averages -1.4 deg and peaks at -7.4 deg.

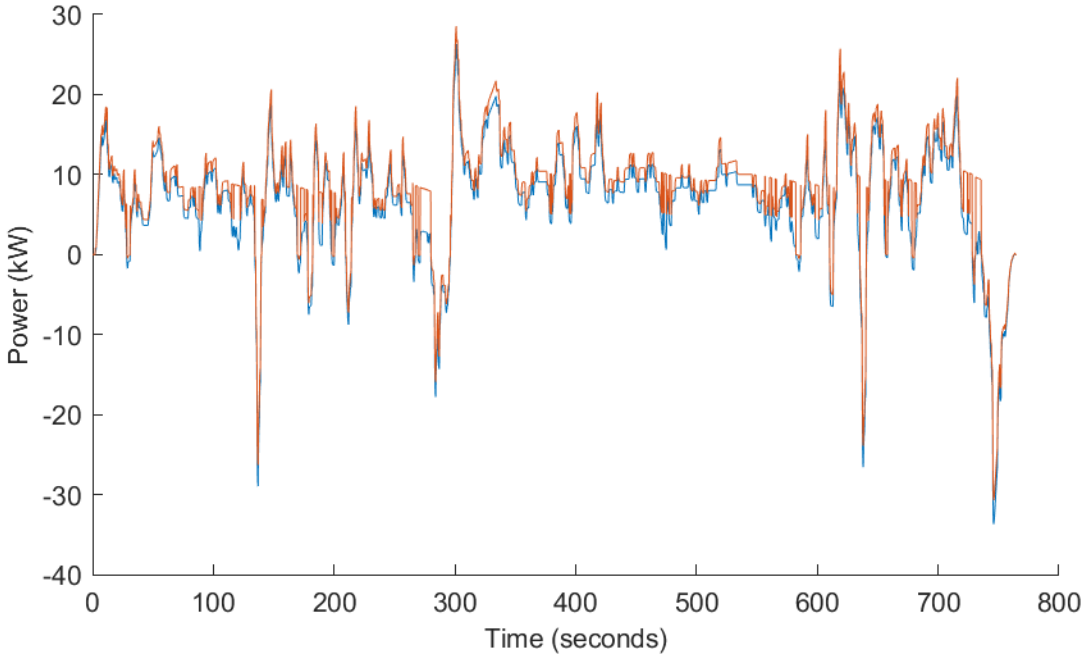

Figure 11.17 Driver steering during HWFET: power required (blue) and power consumed (orange).

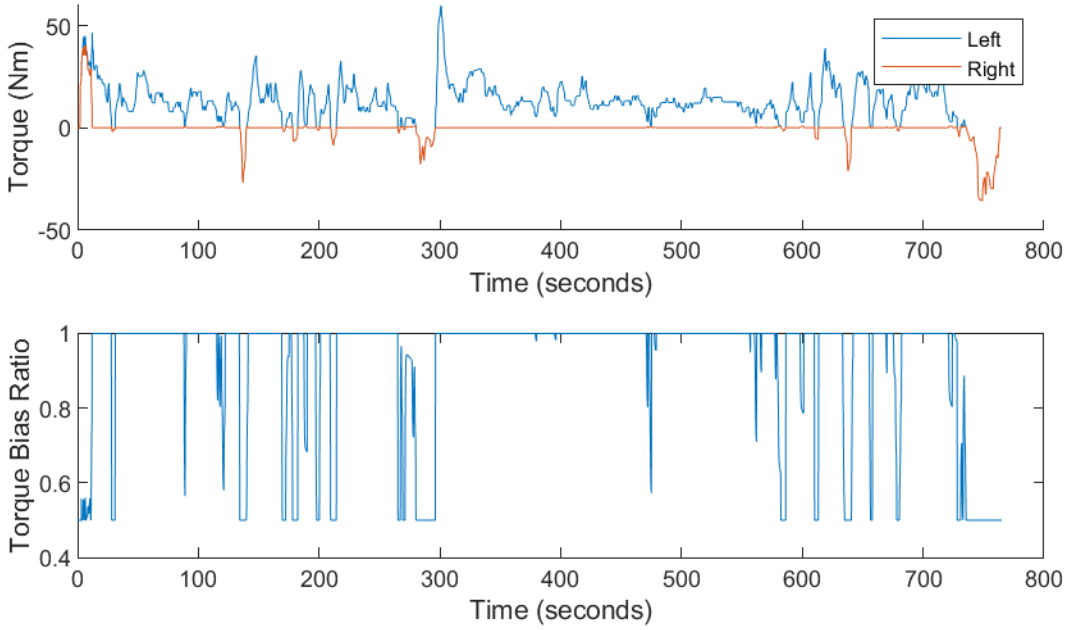

Figure 11.18 Driver steering during HWFET: left and right motor torque (top) and torque bias ratio (bottom).

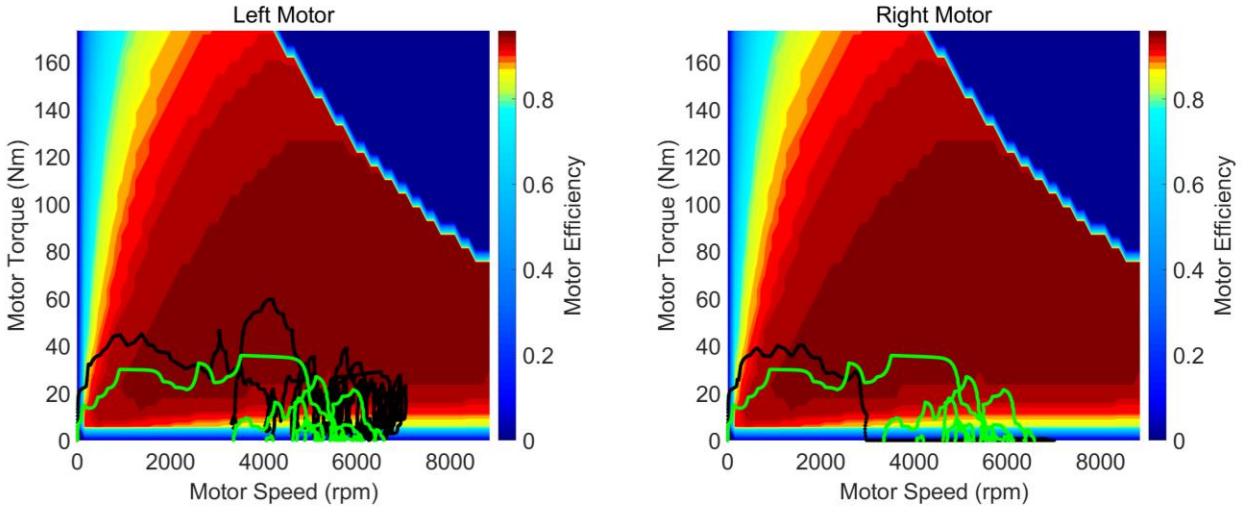

Figure 11.19 Driver steering during HWFET: efficiency map with operating points for the left motor (left) and the right motor (right).

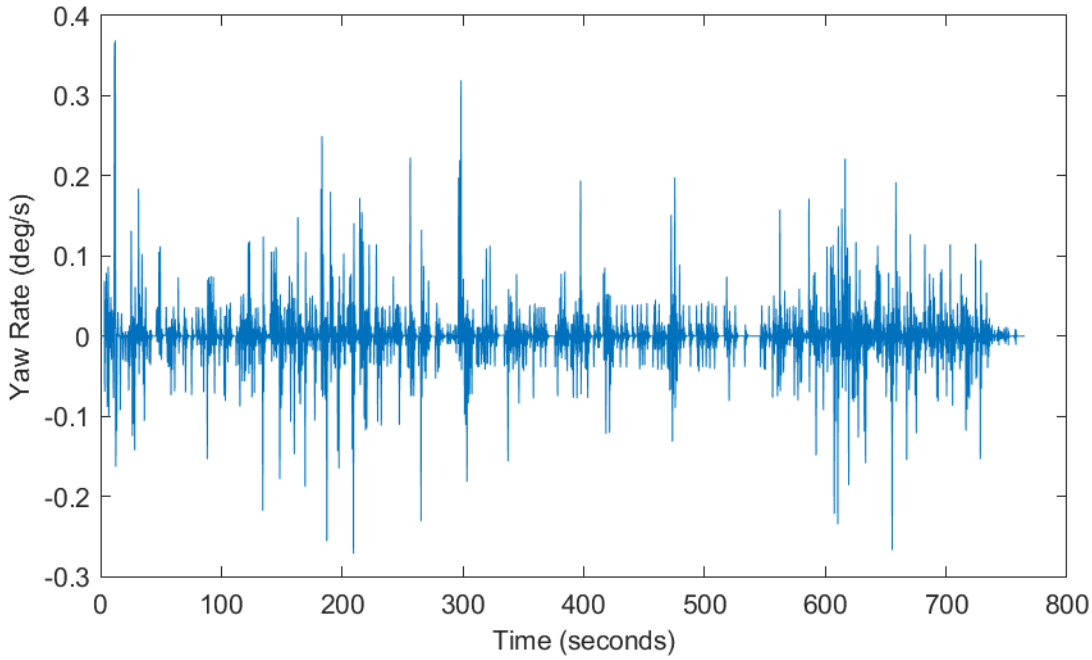

Figure 11.20 Driver steering during HWFET: vehicle yaw rate.

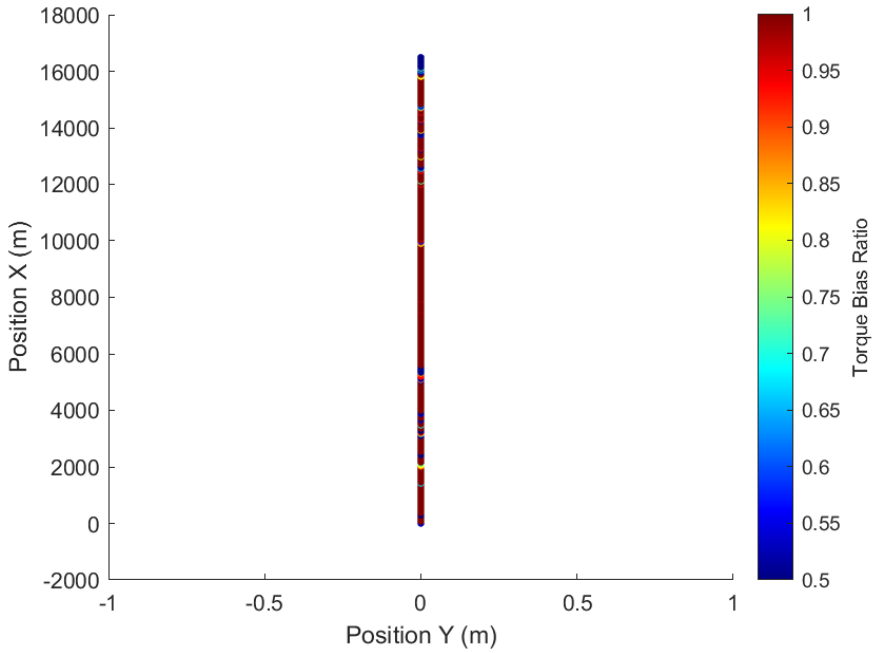

Figure 11.21 Driver steering during HWFET: deviation form straight-line driving.

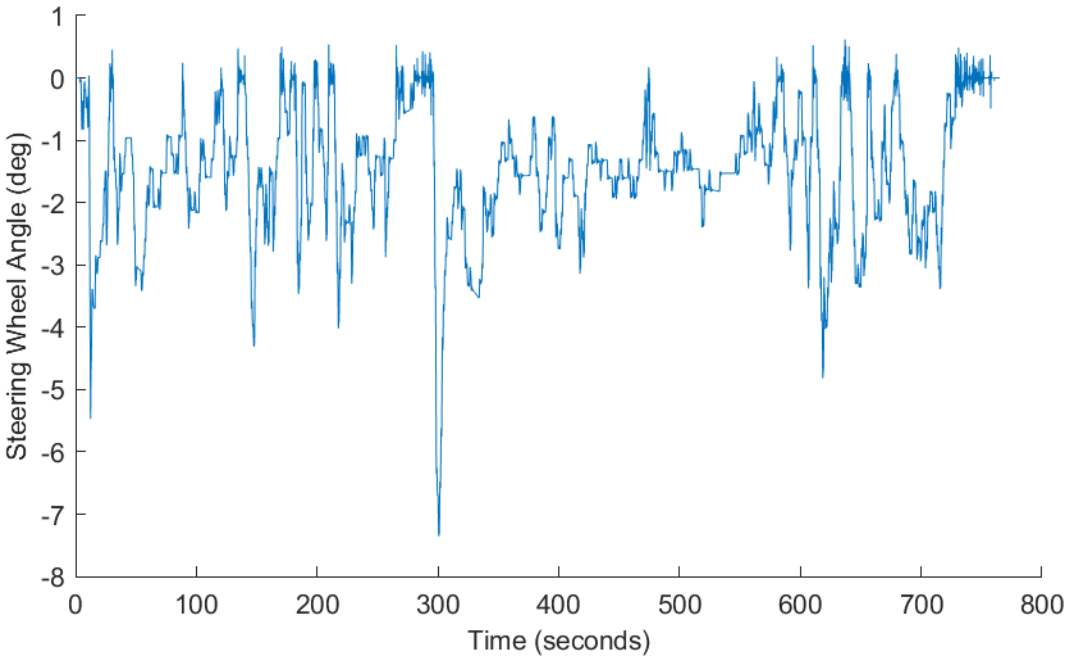

Figure 11.22 Driver steering during HWFET: steering wheel angle.

11.3 Dominant switching strategy

11.3.1 UDDS

For the UDDS drive cycle while operating under the Dominant Switching Strategy, Figure 11.23 shows the E-Axle power required and power consumed. Figure 11.24 shows nearly equal torque being applied to the left and right motors. This is also demonstrated by the motor efficiency plot, Figure 11.25. Given the dominant torque is switching side-to-side at a 1000 Hz rate, these plots will be nearly identical.

Figure 11.26 shows this strategy produces minimal vehicle yaw rates that are primarily less than 0.005 deg/s with occasional spikes up to 0.03 deg/s. This translates into near straight-line driving. Figure 11.27 shows the vehicle maintains straight-line driving for about 1800 meters (time = 216 sec) and then starts to deviate. A second noticeable deviation occurs at about 5000 meters (time = 420 sec). At the end of the drive cycle, the vehicle deviated 1.2 m.

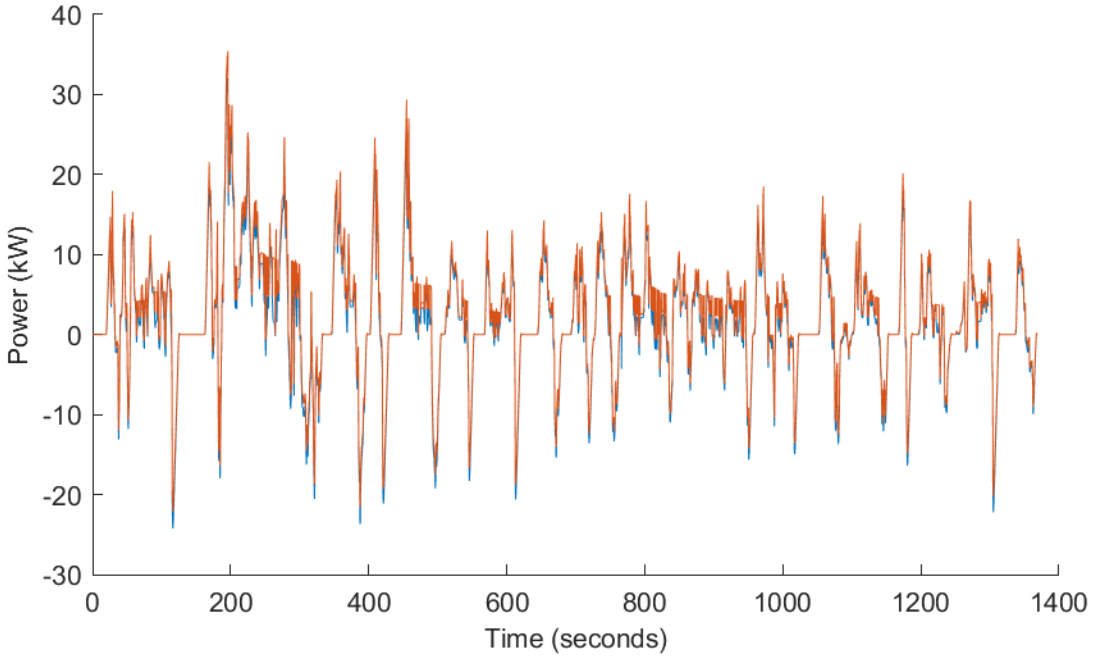

Figure 11.23 Dominant switching during UDDS: power required (blue) and power consumed (orange).

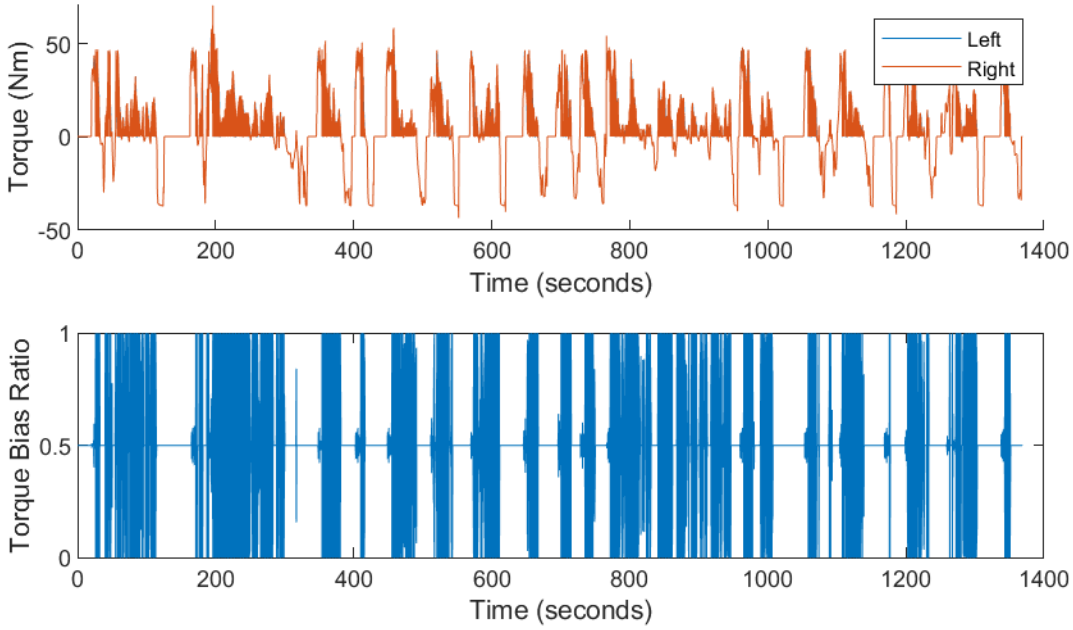

Figure 11.24 Dominant switching during UDDS: left and right motor torque (top) and torque bias ratio (bottom).

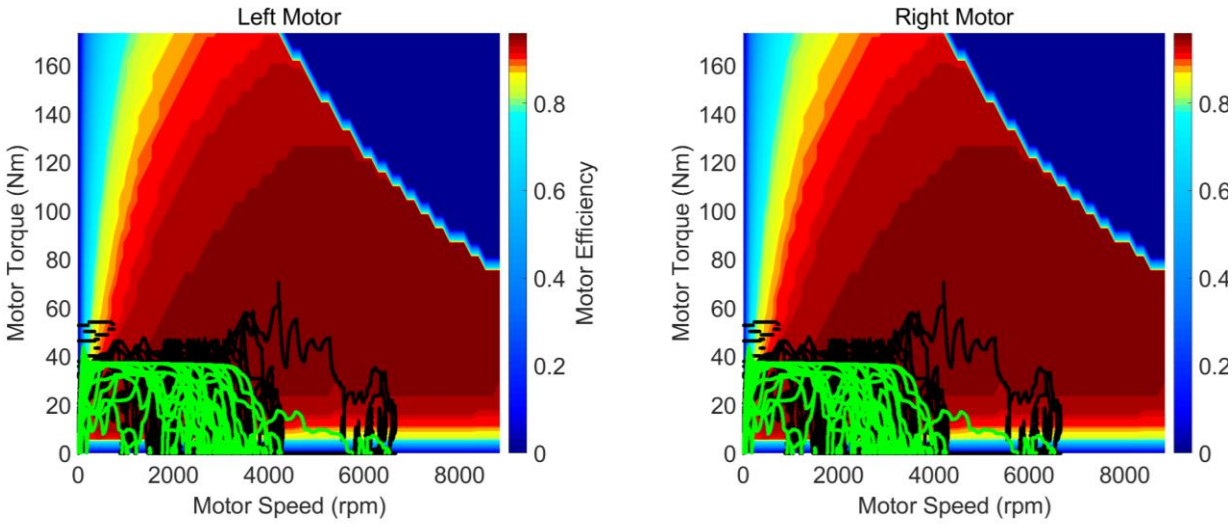

Figure 11.25 Dominant switching during UDDS: efficiency map with operating points for the left motor (left) and the right motor (right).

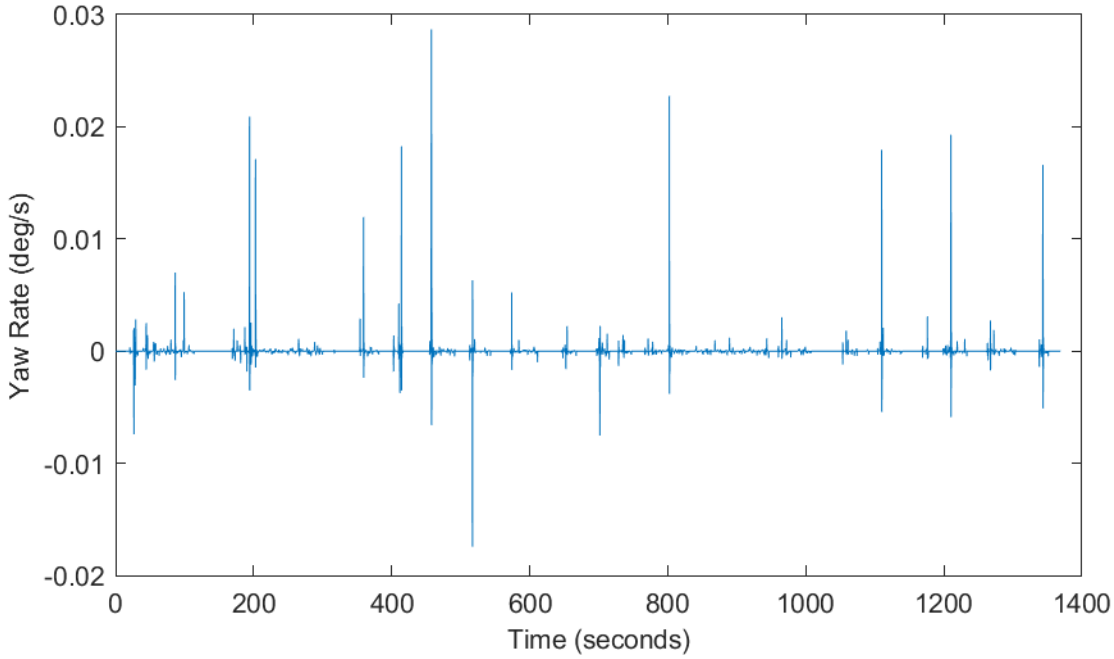

Figure 11.26 Dominant switching during UDDS: vehicle yaw rate.

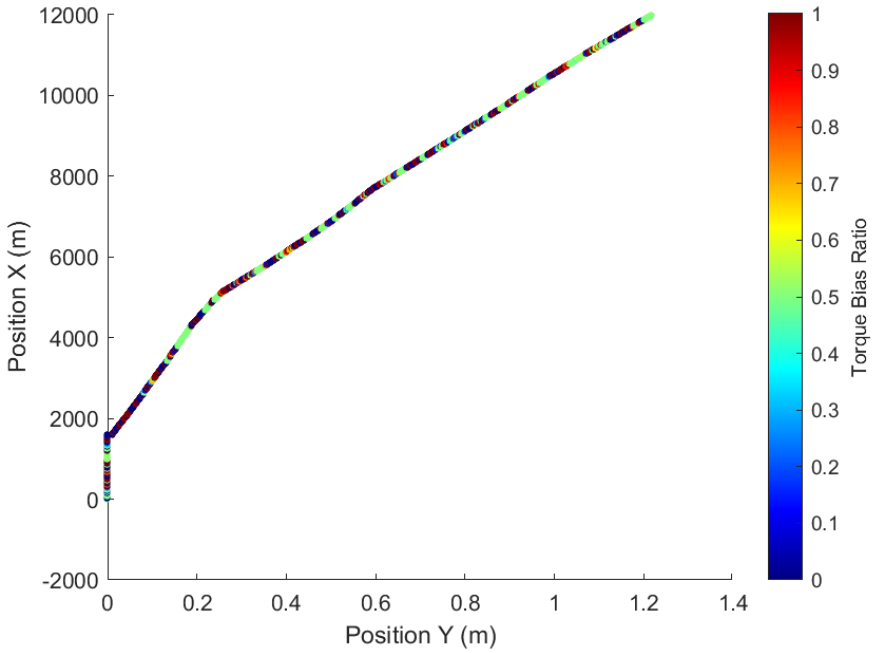

Figure 11.27 Dominant switching during UDDS: deviation form straight-line driving.

11.3.2 HWFET

For the HWFET drive cycle while operating under the Dominant Switching Strategy, Figure 11.28 shows the E-Axle power required and power consumed. Figure 11.29 shows nearly equal torque being applied to the left and right motors. This is also demonstrated by the motor efficiency plot, Figure 11.30. Given the dominant torque is switching side-to-side at a 1000 Hz rate, these plots will be nearly identical.

Figure 11.31 shows this strategy produces minimal vehicle yaw rates that are primarily less than 0.005 deg/s with two spikes of 0.01 deg/s and 0.02 deg/s. This translates into near straight-line driving. Figure 11.32 shows the vehicle maintains straight-line driving for about 1800 meters (time = 106 sec) and then starts to deviate slightly. A second noticeable deviation

occurs at about 5000 meters (time = 263 sec). At the end of the drive cycle, the vehicle deviated 0.54 m.

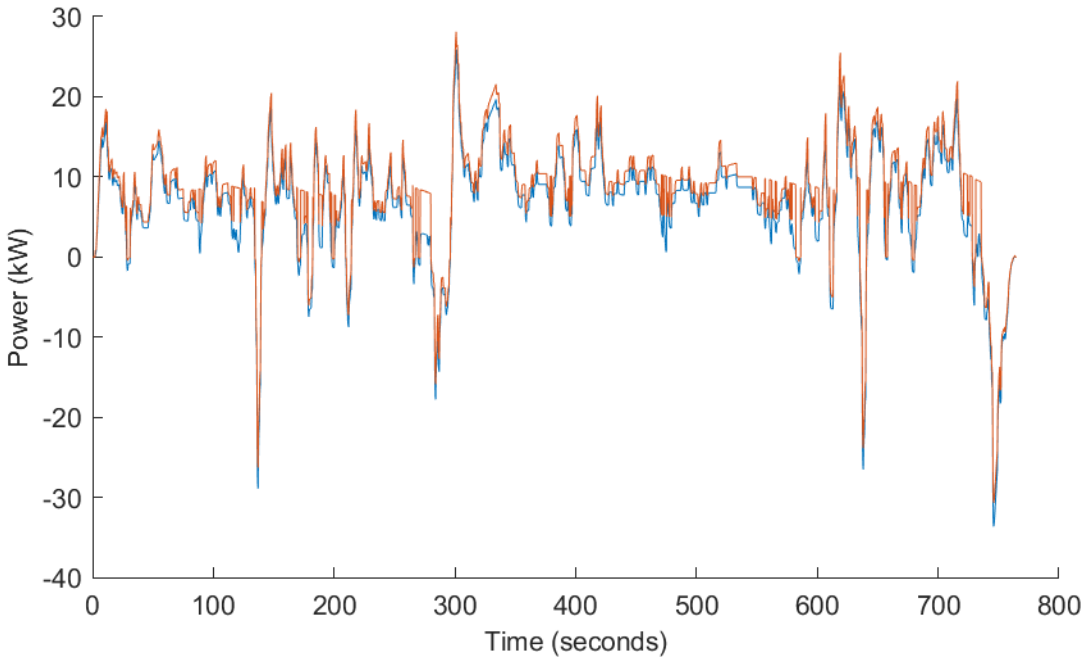

Figure 11.28 Dominant switching during HWFET: power required (blue) and power consumed (orange).

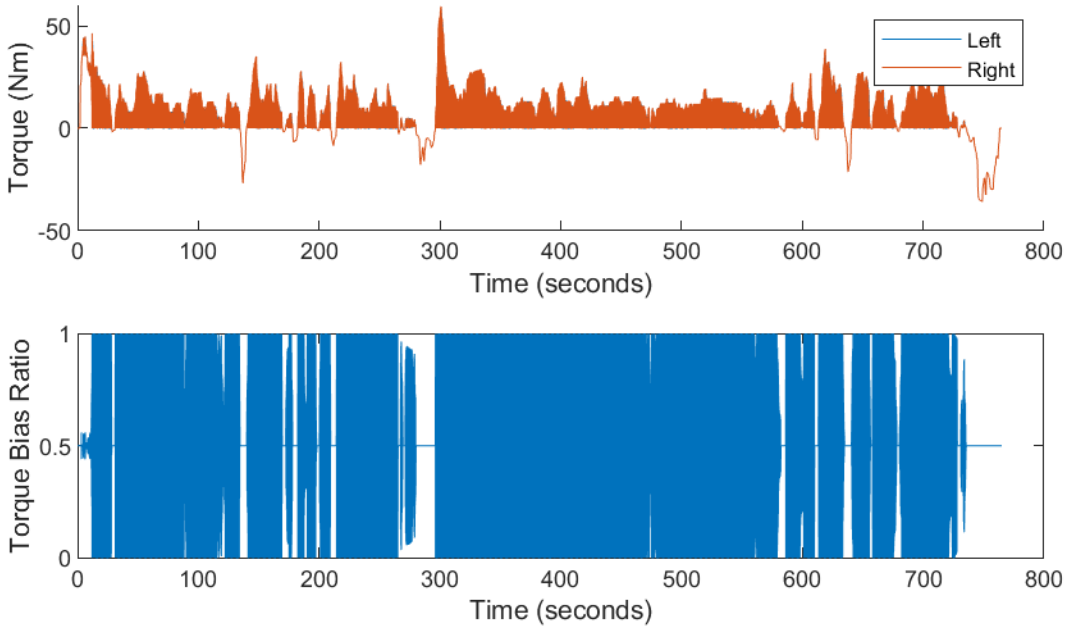

Figure 11.29 Dominant switching during HWFET: left and right motor torque (top) and torque bias ratio (bottom).

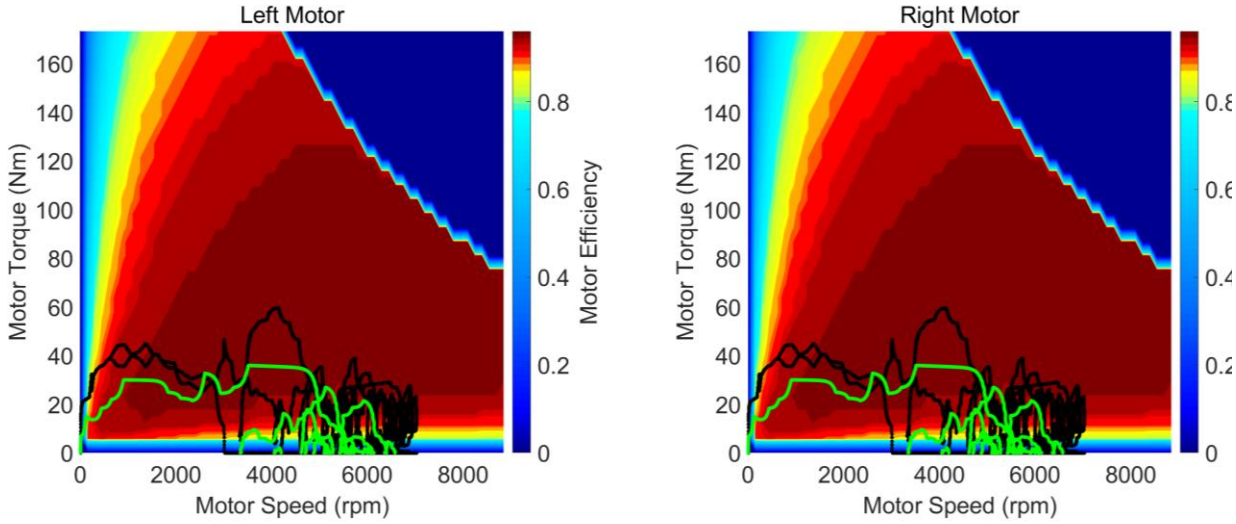

Figure 11.30 Dominant switching during HWFET: efficiency map with operating points for the left motor (left) and the right motor (right).

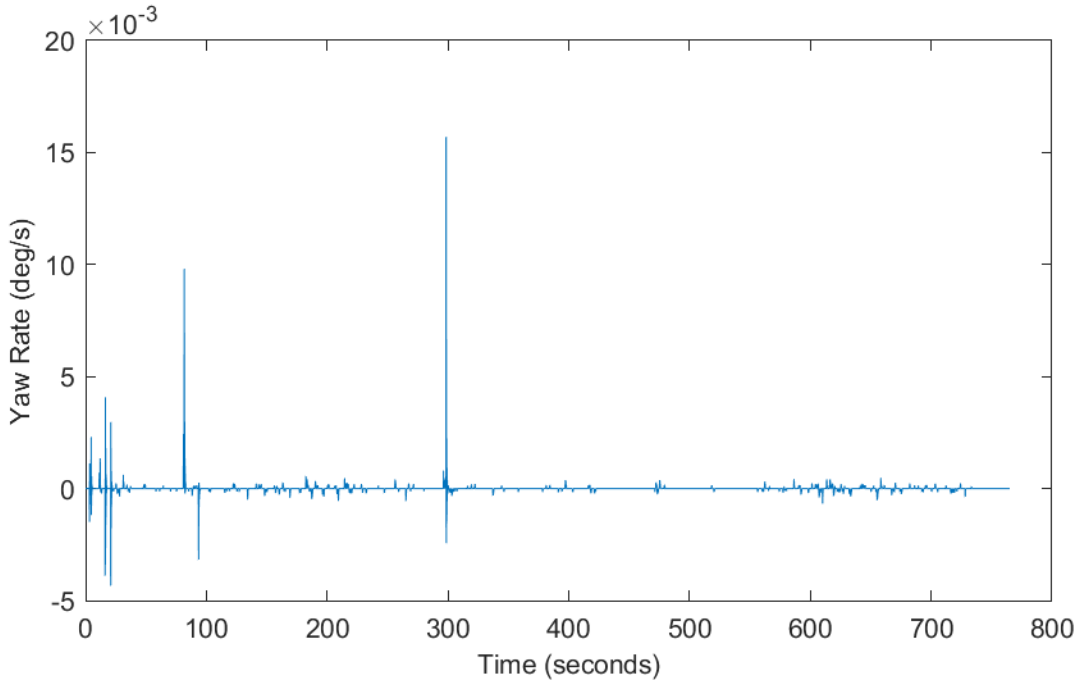

Figure 11.31 Dominant switching during HWFET: vehicle yaw rate.

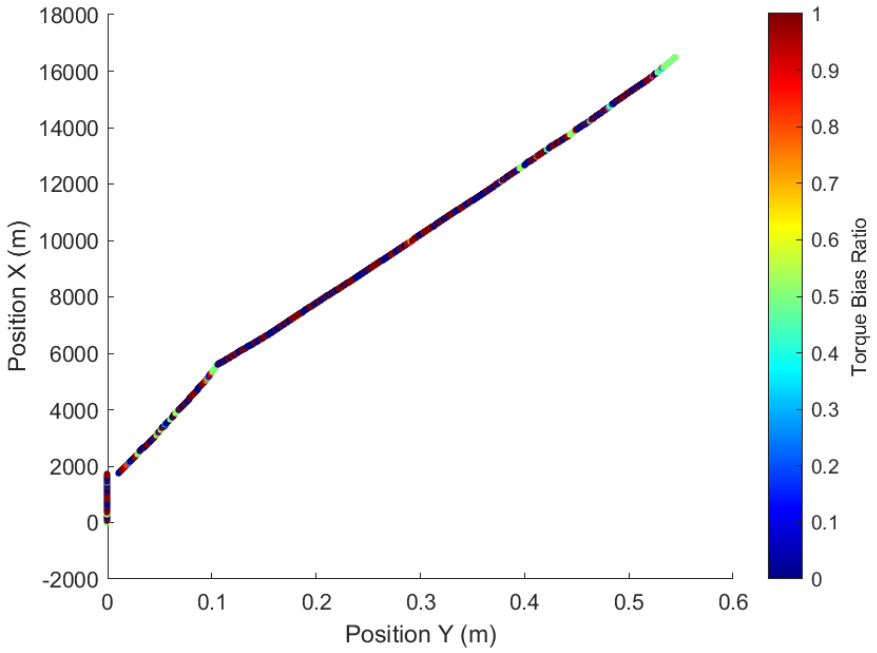

Figure 11.32 Dominant switching during HWFET: deviation form straight-line driving.

11.4 Efficiency tradeoff for stability strategy

11.4.1 UDDS

For the UDDS drive cycle while operating under the Efficiency Tradeoff for Stability Strategy, Figure 11.33 shows the E-Axle power required and power consumed. Figure 11.34 shows nearly equal torque being applied to the left and right motors. This is also demonstrated by the motor efficiency plot, Figure 11.35. This is because the maximum torque bias ratio being applied is 0.505, only 10% higher than the 50/50 split. A significant tradeoff in efficiency was needed to keep the vehicle from deviating off the straight-line driving.

Figure 11.36 shows this strategy produces vehicle yaw rates that are less than 0.05 deg/s which translates into some deviation from straight-line driving. Figure 11.37 shows the vehicle deviates 647.7 meters at the end of the drive cycle.

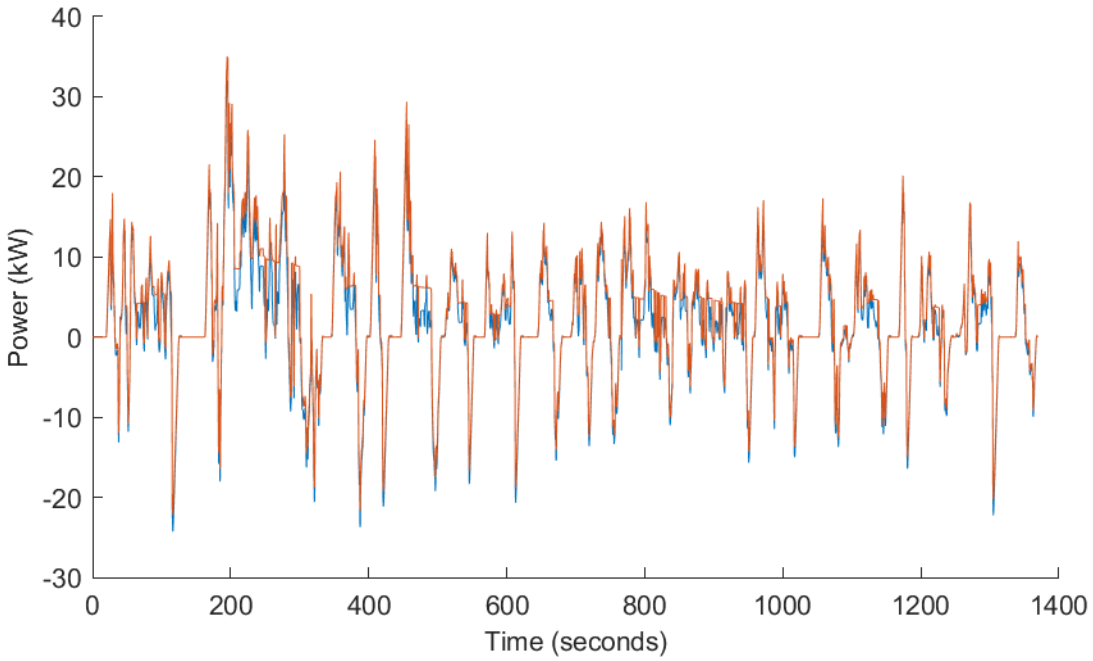

Figure 11.33 Efficiency tradeoff during UDDS power required (blue) and power consumed (orange).

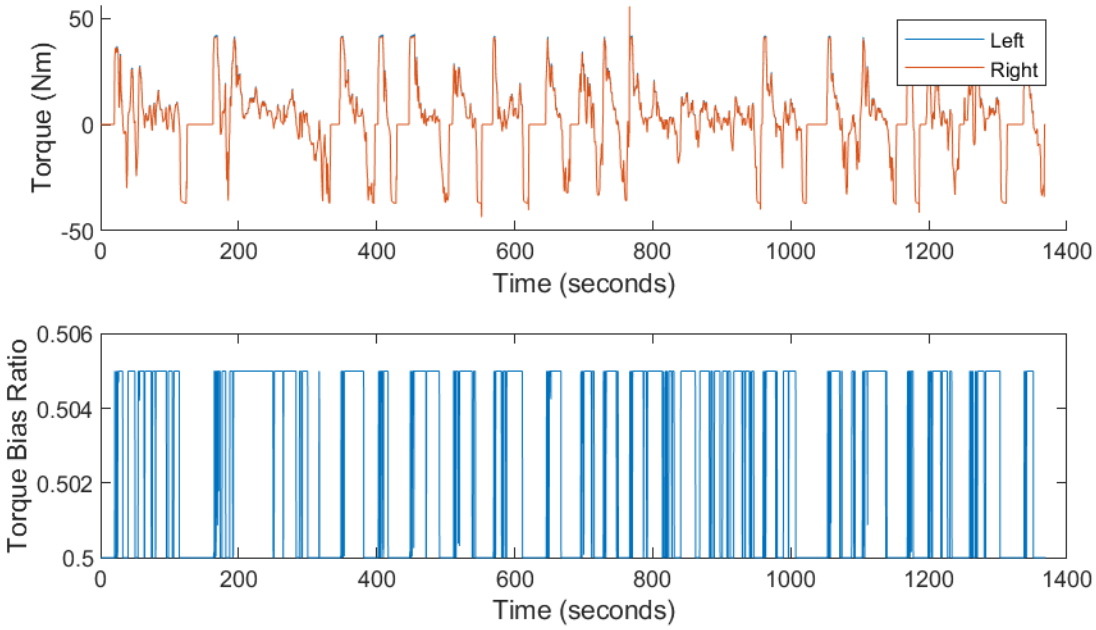

Figure 11.34 Efficiency tradeoff during UDDS: left and right motor torque (top) and torque bias ratio (bottom).

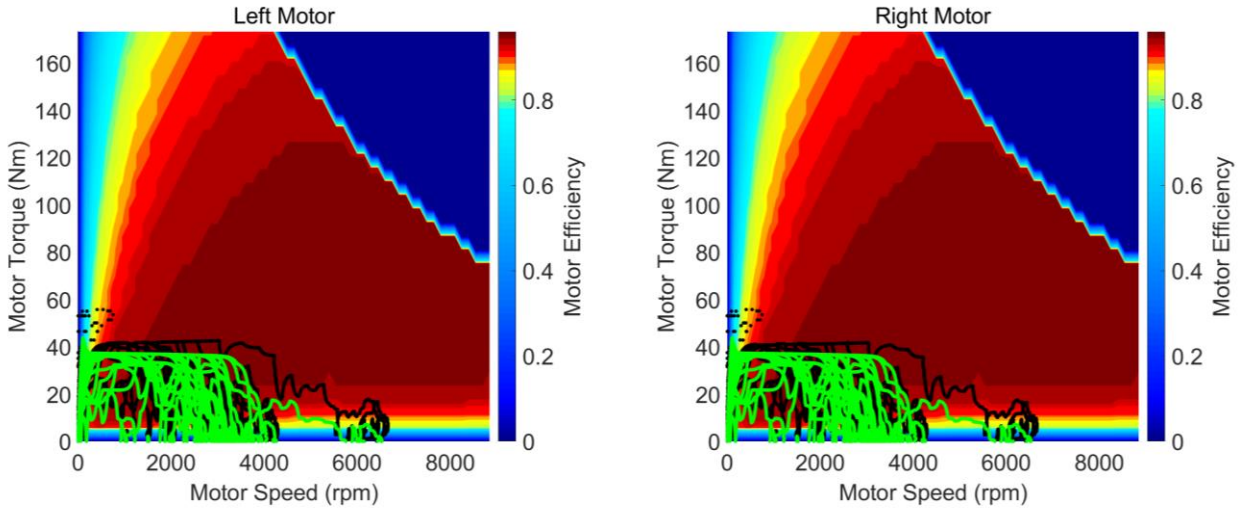

Figure 11.35 Efficiency tradeoff during UDDS: efficiency map with operating points for the left motor (left) and the right motor (right).

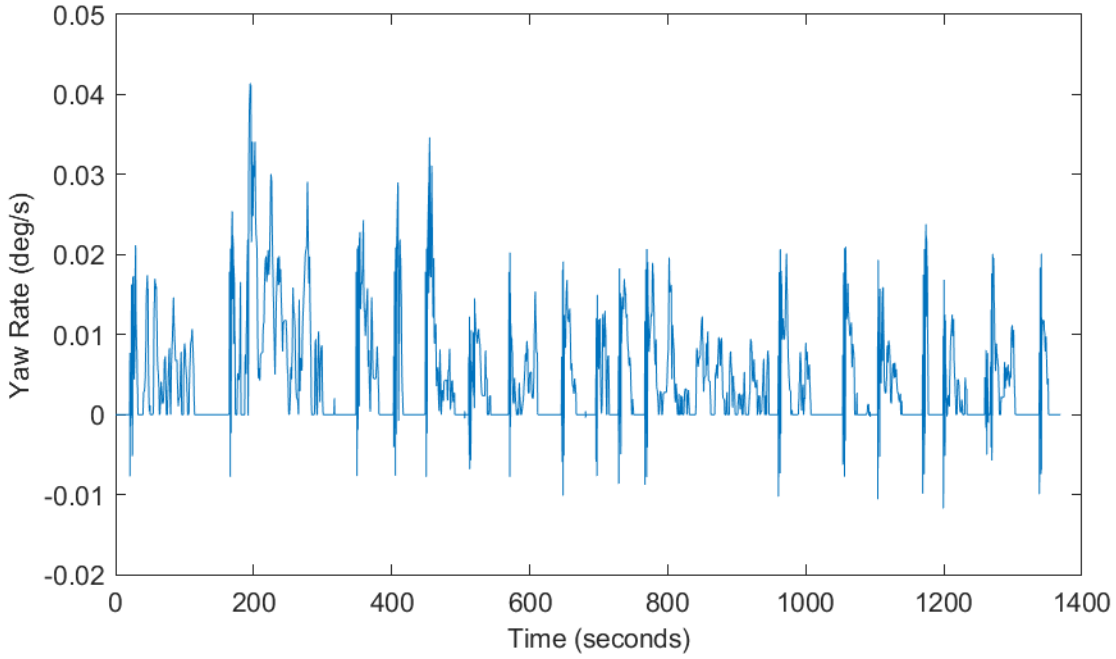

Figure 11.36 Efficiency tradeoff during UDDS: vehicle yaw rate.

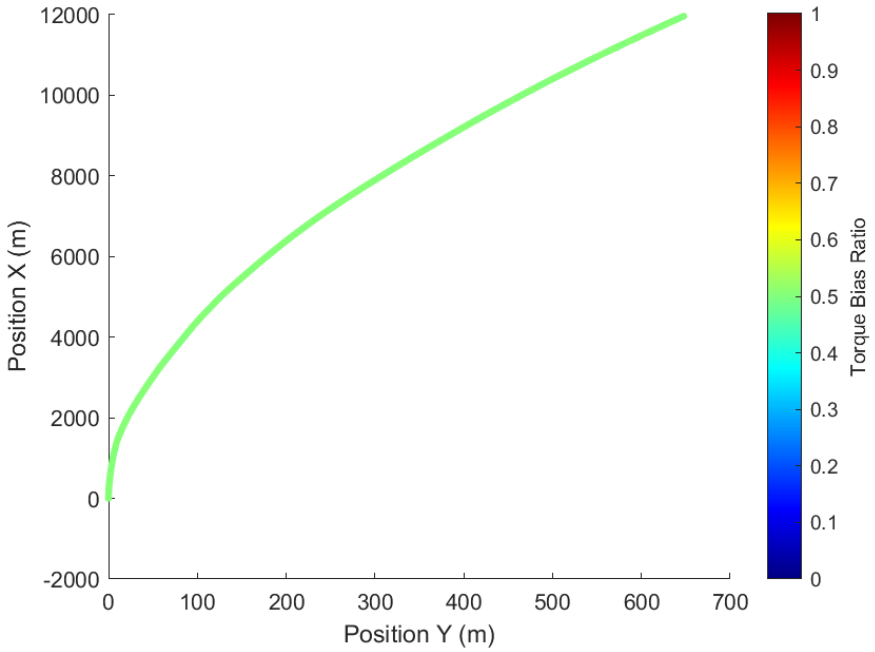

Figure 11.37 Efficiency tradeoff during UDDS: deviation form straight-line driving.

11.4.2 HWFET

For the HWFET drive cycle while operating under the Efficiency Tradeoff for Stability Strategy, Figure 11.38 shows the E-Axle power required and power consumed. Figure 11.39 shows nearly equal torque being applied to the left and right motors. This is also demonstrated by the motor efficiency plot, Figure 11.40. This is because the maximum torque bias ratio being applied is 0.505, only 10% higher than the 50/50 split. A significant tradeoff in efficiency was needed to keep the vehicle from deviating off the straight-line driving.

Figure 11.41 shows this strategy produces vehicle yaw rates that are less than 0.035 deg/s which translates into some deviation from straight-line driving. Figure 11.42 shows the vehicle deviates 1137 meters at the end of the drive cycle.

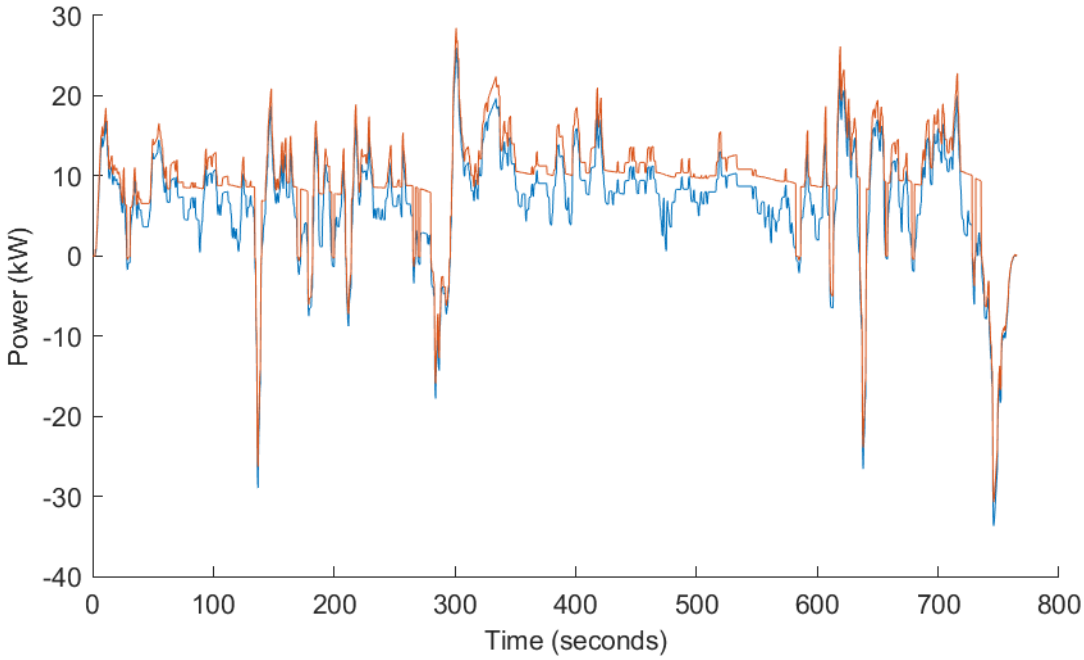

Figure 11.38 Efficiency tradeoff during HWFET: power required (blue) and power consumed (orange).

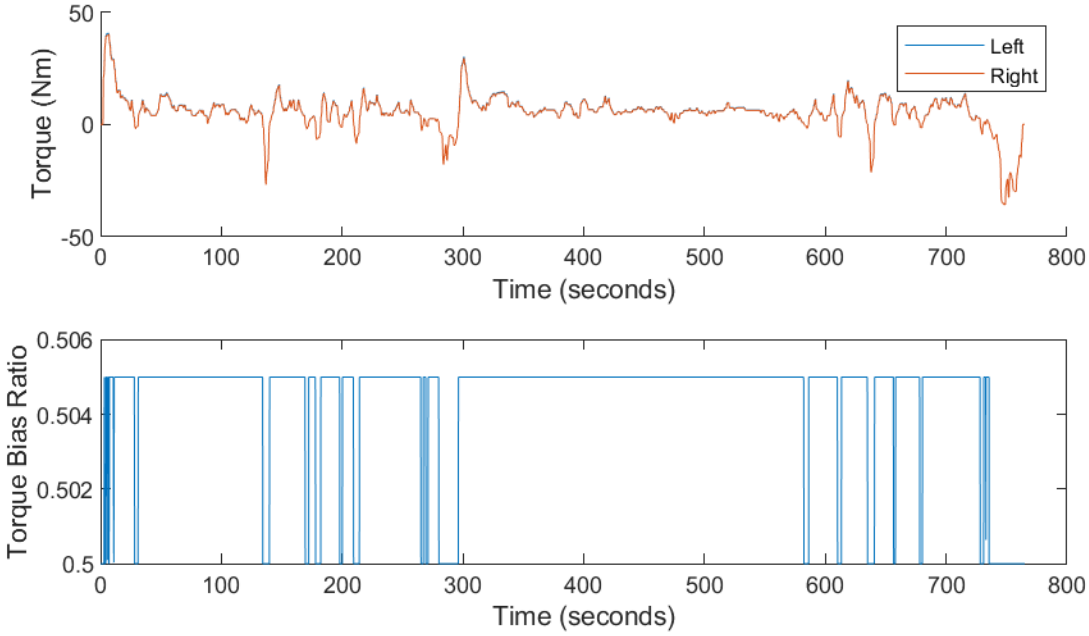

Figure 11.39 Efficiency tradeoff during HWFET: left and right motor torque (top) and torque bias ratio (bottom).

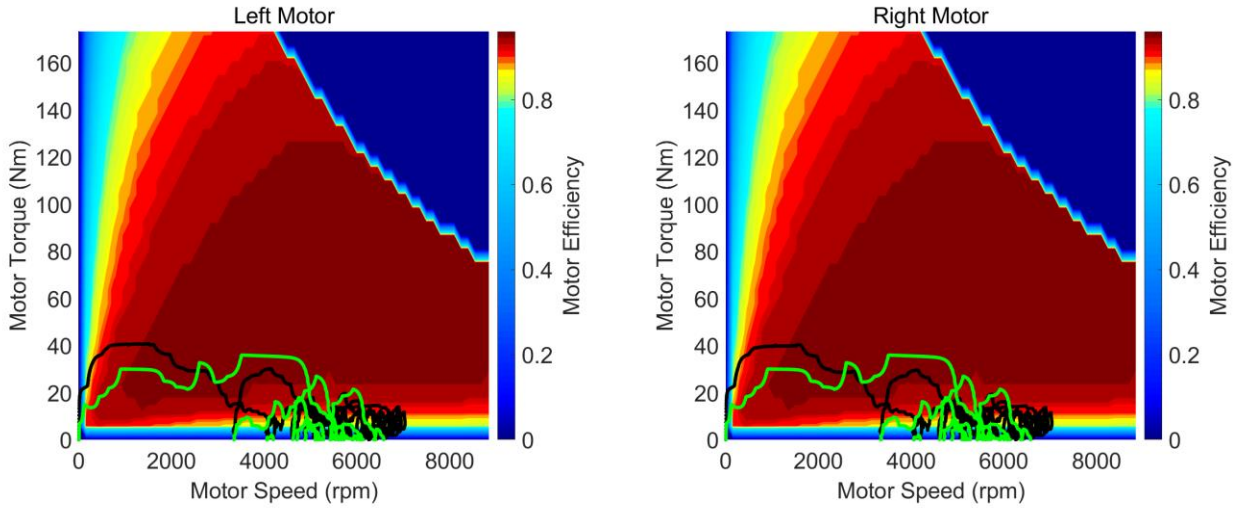

Figure 11.40 Efficiency tradeoff during HWFET: efficiency map with operating points for the left motor (left) and the right motor (right).

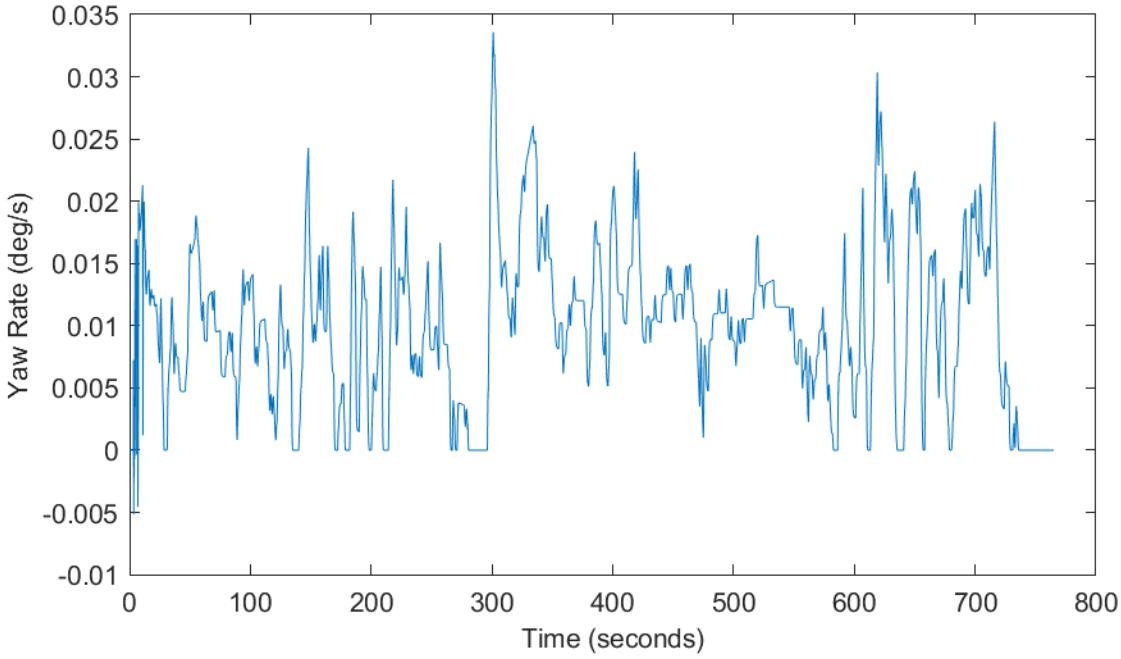

Figure 11.41 Efficiency tradeoff during HWFET: vehicle yaw rate.

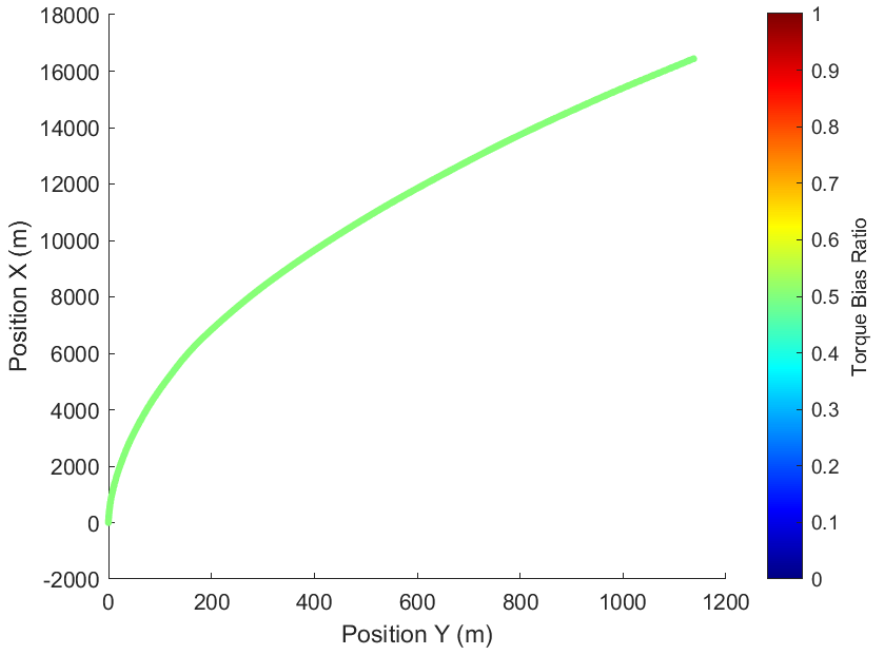

Figure 11.42 Efficiency tradeoff during HWFET: deviation form straight-line driving.

11.5 E-Axle motor coupling hardware change

11.5.1 UDDS

For the UDDS drive cycle when coupling the E-Axle motor outputs, Figure 11.43 shows the E-Axle power required and power consumed. Figure 11.44 shows the left motor supplies most of the torque, when torque is positive, and is supplemented by the right motor when additional torque is needed. The motor efficiency plot, Figure 11.45, shows for positive motor torque, the right motor is only used when the motor speed is less than about 4000 rpm.

Coupling the output of the left and right motors will allow equal distribution of torque between the left and right wheels independent of the two motor's torque outputs. Figure 11.46 confirms the resulting vehicle yaw rate is zero deg/s across the drive cycle. This translates into straight-line driving without any deviation, as shown in Figure 11.47.

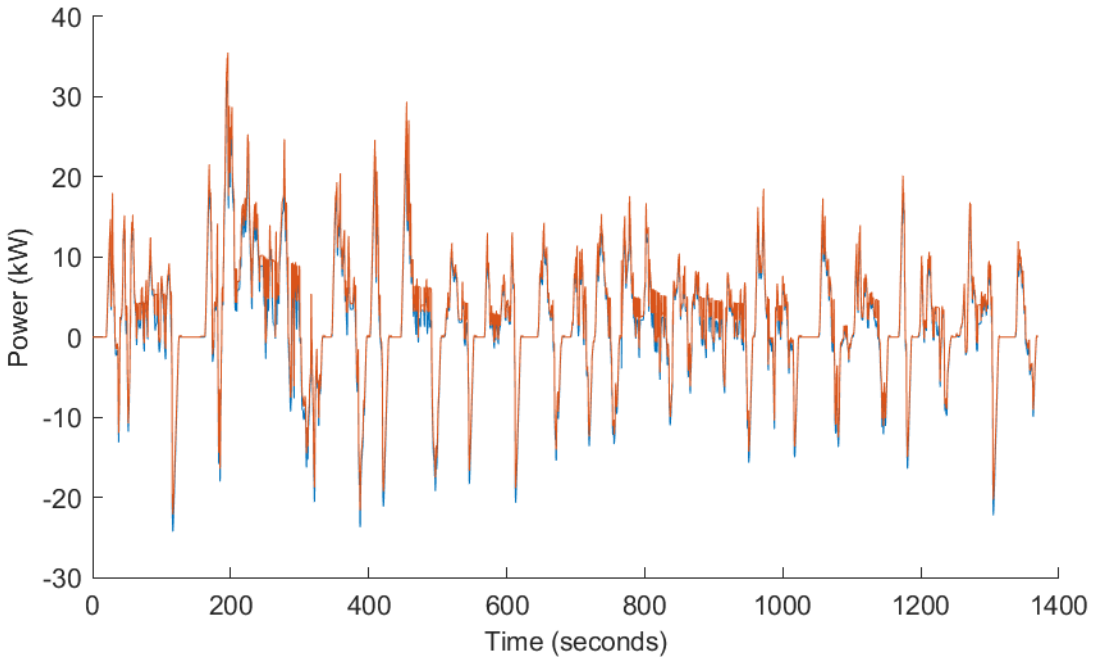

Figure 11.43 E-Axle motor coupling during UDDS: power required (blue) and power consumed (orange).

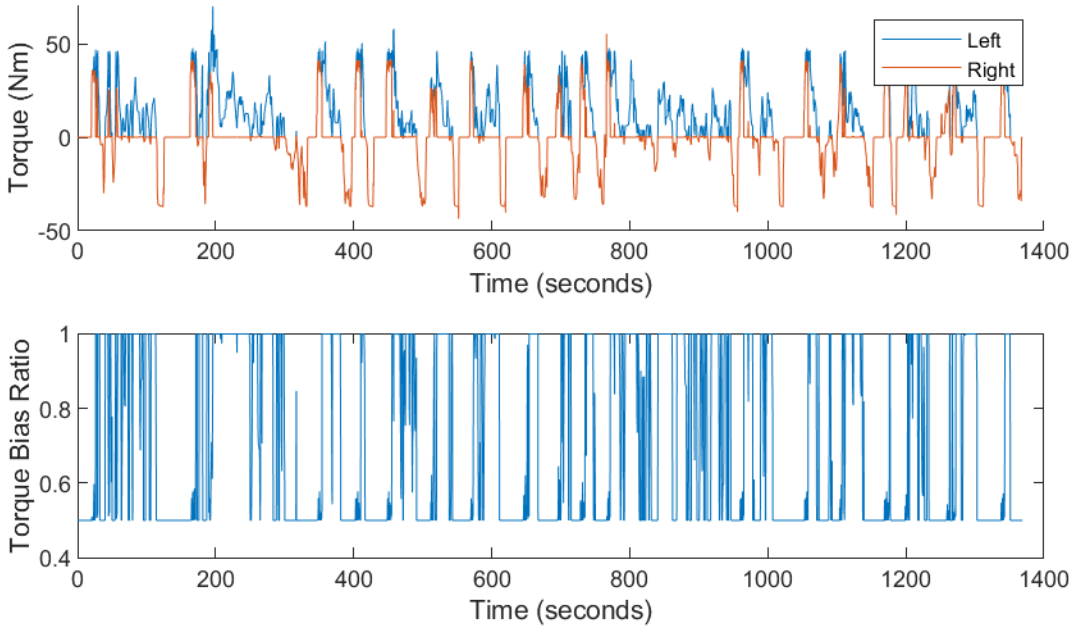

Figure 11.44 E-Axle motor coupling during UDDS: left and right motor torque (top) and torque bias ratio (bottom).

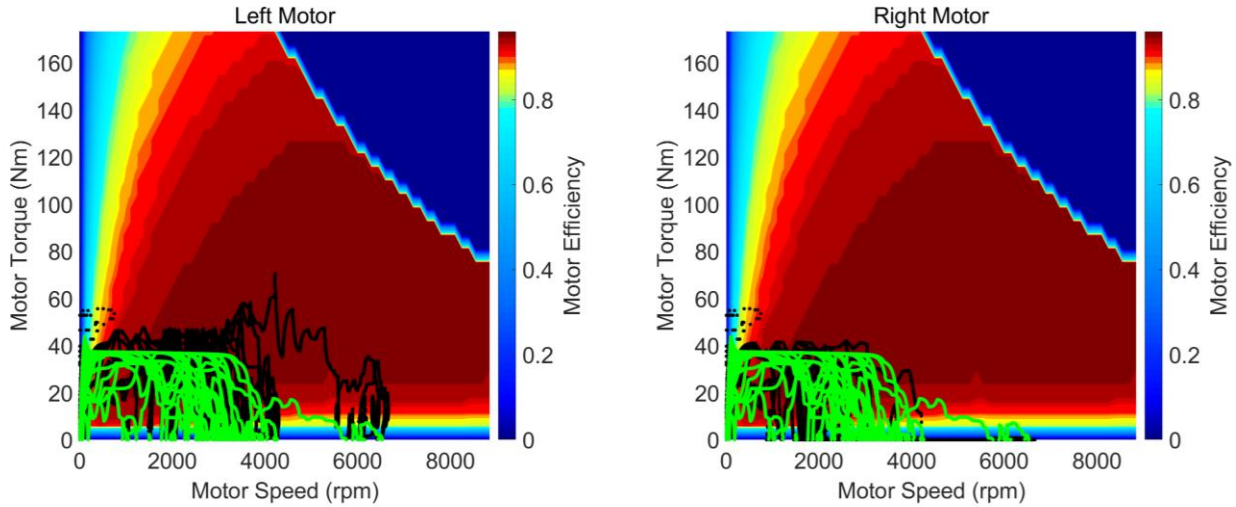

Figure 11.45 E-Axle motor coupling during UDDS: efficiency map with operating points for the left motor (left) and the right motor (right).

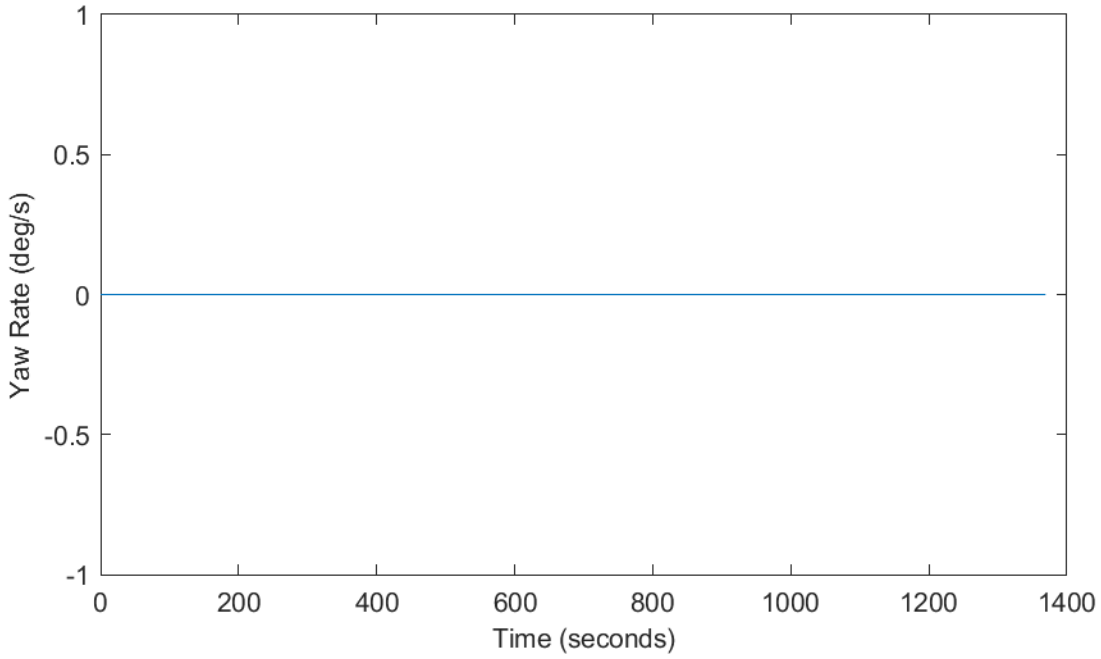

Figure 11.46 E-Axle motor coupling during UDDS: vehicle yaw rate.

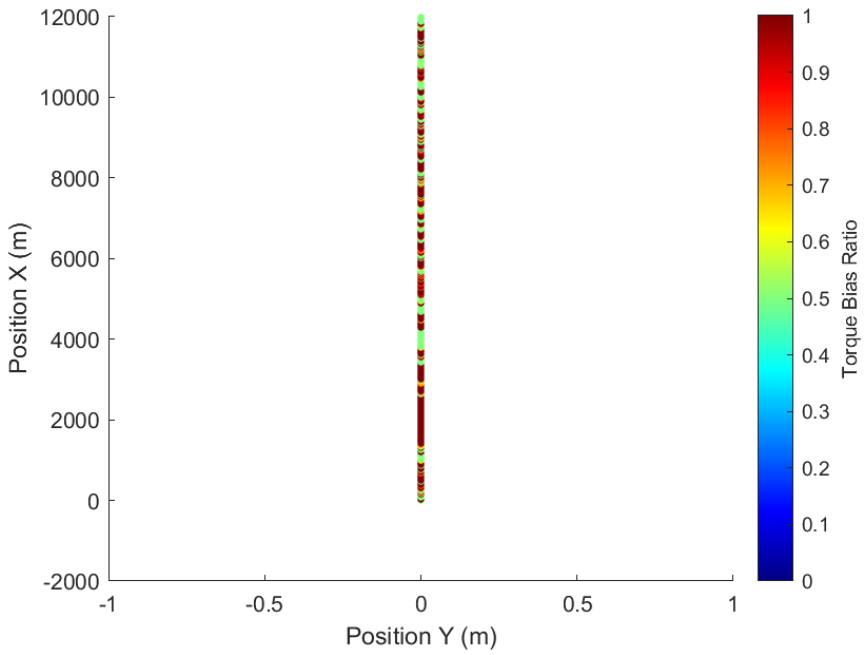

Figure 11.47 E-Axle motor coupling during UDDS: deviation form straight-line driving.

11.5.2 HWFET

For the HWFET drive cycle when coupling the E-Axle motor outputs, Figure 11.48 shows the E-Axle power required and power consumed. Figure 11.49 shows the left motor supplies most of the torque, when torque is positive, and is supplemented by the right motor when additional torque is needed. The motor efficiency plot, Figure 11.50, shows for positive motor torque, the right motor is only used when the motor speed is less than about 3000 rpm.

Coupling the output of the left and right motors will allow equal distribution of torque between the left and right wheels independent of the two motor's torque outputs. Figure 11.51 confirms the resulting vehicle yaw rate is zero deg/s across the drive cycle. This translates into straight-line driving without any deviation, as shown in Figure 11.52.

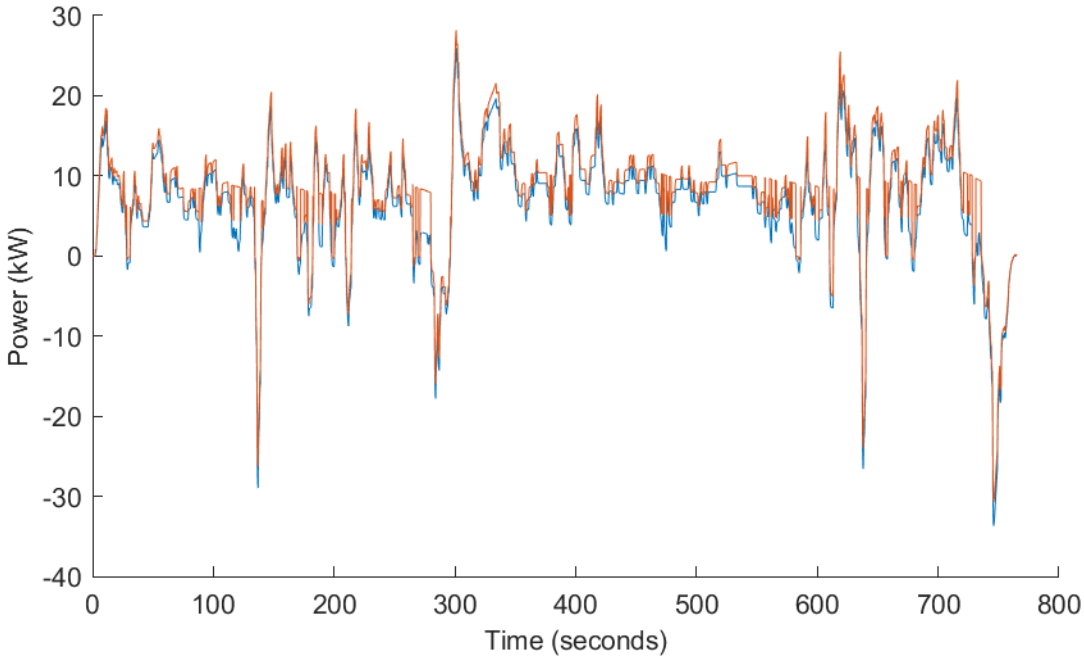

Figure 11.48 E-Axle motor coupling during HWFET: power required (blue) and power consumed (orange).

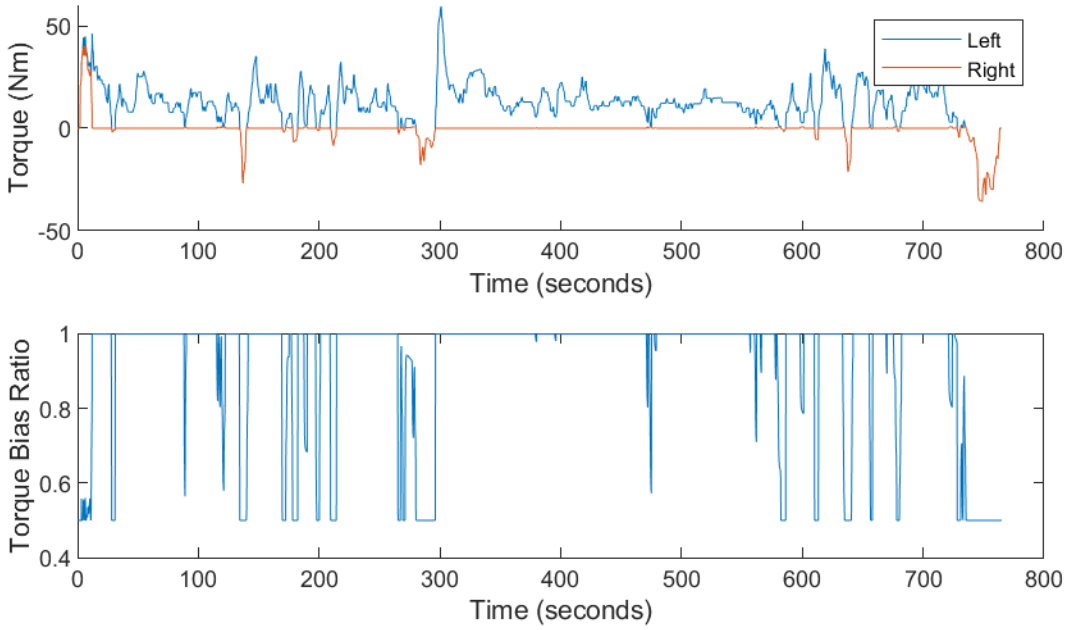

Figure 11.49 E-Axle motor coupling during HWFET: left and right motor torque (top) and torque bias ratio (bottom).

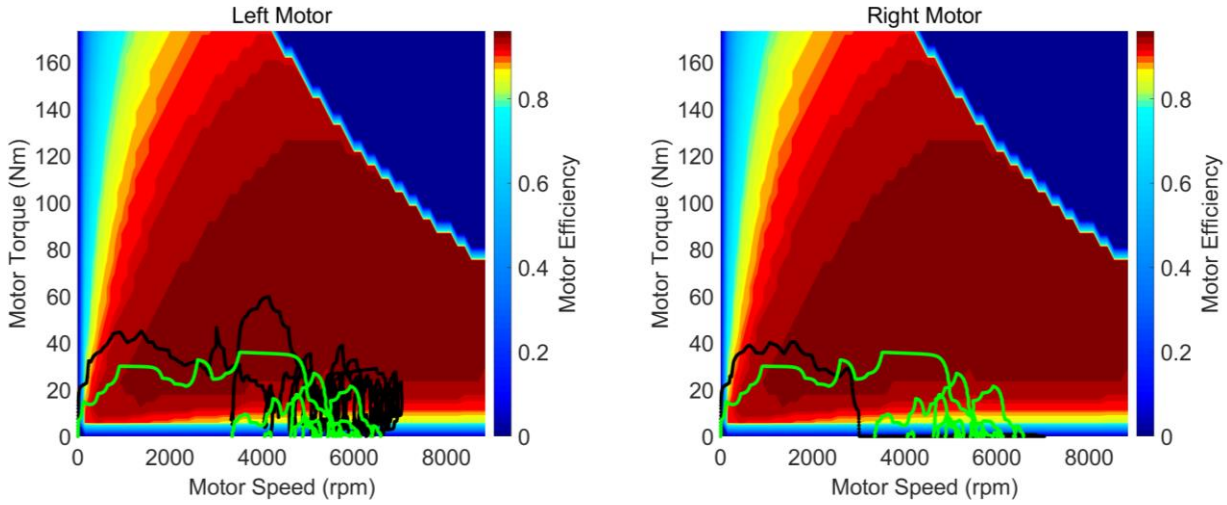

Figure 11.50 E-Axle motor coupling during HWFET: efficiency map with operating points for the left (left) and the right motor (right).

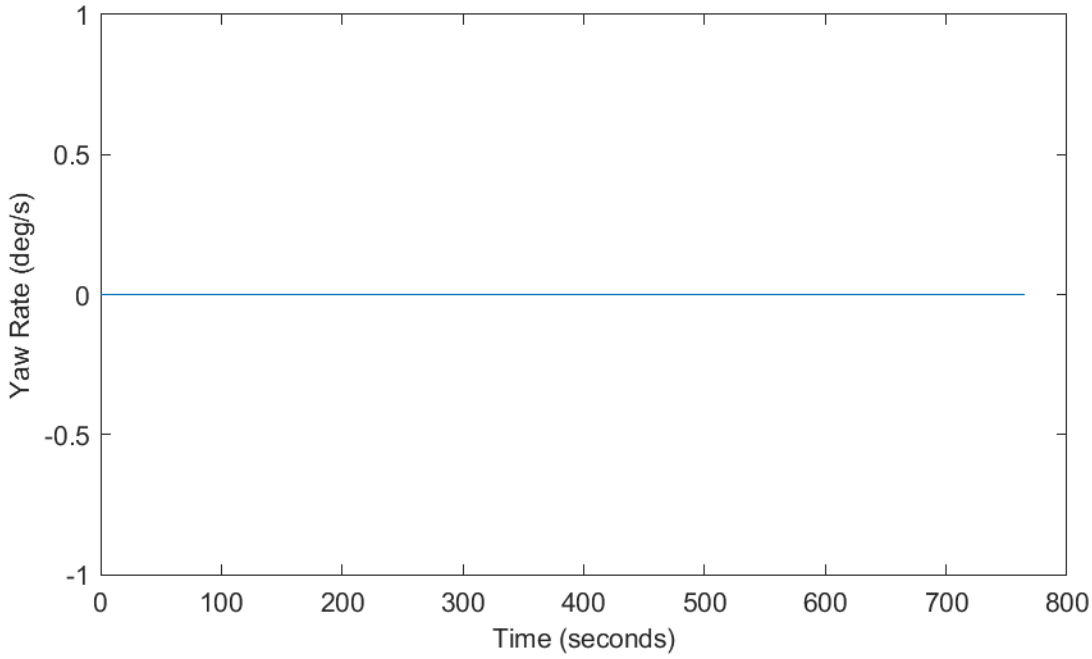

Figure 11.51 E-Axle motor coupling during HWFET: vehicle yaw rate.

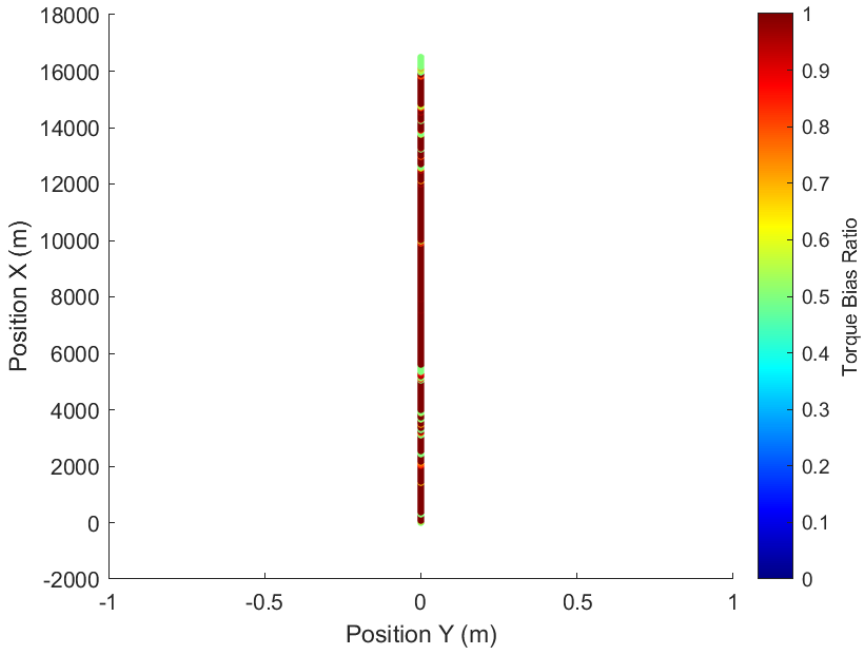

Figure 11.52 E-Axle motor coupling during HWFET: deviation form straight-line driving.

11.6 Strategy summary

11.6.1 UDDS

For all the yaw-mitigation strategies, Table 11.1 summaries the average absolute yaw rate, peak absolute yaw rate, and total off-axis deviation. The 50/50 baseline, driver steering, dominant switching, and output coupling are all able to maintain straight-line driving.

For all the yaw-mitigation strategies, Table 11.2 summarizes the energy and power consumed across the drive cycle. The output coupling, driver steering, and dominant switching perform the best as they are all able to operate using the efficiency-optimized torque vectoring look-up table. The efficiency tradeoff consumes the same amount of energy as the 50/50 baseline, proving to be a poor strategy to increase system efficiency.

Table 11.1 UDDS yaw-rate and off-axis deviation summary.

Metrics	50/50 (Baseline)	Driver Steering	Dominant Switching	Efficiency Tradeoff	Output Coupling
Average abs yaw rate (deg/s)	0	0	0	0.004	0
Peak abs yaw rate (deg/s)	0	1.004	0.029	0.041	0
Total off-axis deviation (m)	0	0.006	1.22	647.7	0

Table 11.2 UDDS energy and power summary.

Metrics	50/50 (Baseline)	Driver Steering	Dominant Switching	Efficiency Tradeoff	Output Coupling
Total positive (propulsion) energy consumed (kWh)	1.698	1.605	1.598	1.698	1.601
Total negative (regeneration) energy available (kWh)	0.521	0.520	0.520	0.521	0.521
Average propulsion power (kW)	7.927	7.263	7.580	7.838	7.370
Peak positive power (kW)	35.025	35.849	35.424	35.026	35.510
Peak negative power (kW)	22.123	22.122	22.103	22.123	22.123

11.6.2 HWFET

For all the yaw-mitigation strategies, Table 11.3 summaries the average absolute yaw rate, peak absolute yaw rate, and total off-axis deviation. The 50/50 baseline, driver steering, dominant switching, and output coupling are all able to maintain straight-line driving.

For all the yaw-mitigation strategies, Table 11.4 summarizes the energy and power consumed across the drive cycle. The output coupling, driver steering, and dominant switching perform the best as they are all able to operate using the efficiency-optimized torque vectoring look-up table. The efficiency tradeoff consumes the same amount of energy as the 50/50 baseline, proving to be a poor strategy to increase system efficiency.

Table 11.3 HWFET yaw-rate and off-axis deviation summary.

Metrics	50/50 (Baseline)	Driver Steering	Dominant Switching	Efficiency Tradeoff	Output Coupling
Average abs yaw rate (deg/s)	0	0	0	0.010	0
Peak abs yaw rate (deg/s)	0	0.369	0.016	0.034	0
Total off-axis deviation (m)	0	0.002	0.54	1137.4	0

Table 11.4 HWFET energy and power summary.

Metrics	50/50 (Baseline)	Driver Steering	Dominant Switching	Efficiency Tradeoff	Output Coupling
Total positive (propulsion) energy consumed (kWh)	2.156	1.961	1.951	2.156	1.955
Total negative (regeneration) energy available (kWh)	0.156	0.156	0.155	0.156	0.156
Average propulsion power (kW)	11.551	10.508	10.469	11.551	10.459
Peak positive power (kW)	28.452	28.539	28.105	28.452	28.159
Peak negative power (kW)	30.719	30.716	30.678	30.719	30.719

11.6.3 Fuel economy summary

Table 11.5 compares the UDDS, HWFET, and Combined fuel economy ratings across the yaw-mitigation strategies. Dominant switching and output coupling provides the highest increase in fuel economy over the 50/50 baseline, by about 10%. This is followed closely by the driver steering which increases fuel economy by 9.4%.

Table 11.5 Fuel economy ratings for the yaw mitigation strategies.

Fuel economy rating	**BEV MPGe**				
	50/50 (Baseline)	**Driver Steering**	**Dominant Switching**	**Efficiency Tradeoff**	**Output Coupling**
UDDS/City	64.6	70.1	70.6	64.6	70.4
HWFET/Highway	52.4	58.0	58.3	52.4	58.2
Combined fuel economy	59.1	64.7	65.1	59.1	64.9
Combined fuel economy – percent increase from 50/50	n/a	9.4%	10.1%	0.0%	9.8%

CHAPTER XII

CONCLUSION AND FUTURE WORK

12.1 Summary

The MSU COTF program converted a 2015 Subaru BRZ into a BEV. Before converting the conventional powertrain vehicle to a BEV, performance requirements equal to the original production vehicle were established for the selection of powertrain components. Among those performance requirements were straight-line acceleration from 0 kph to 96.5 kph (0 mph to 60 mph), acceleration time from 80.5 kph to 112.5 kph (50 mph to 70 mph), and gradeability. The minimum power required by the electric motor to meet the VTS requirements for the acceleration time and gradeability was determined to be 119.9 kW, which was driven by the 0 kph to 96.5 kph (0 mph to 60 mph) acceleration time. After reviewing and comparing available electric motors, a McLaren Engineering E-Axle with two independent 80 kW motors was chosen to build the BEV. The selected electric axle met the minimum power requirement of 119.9 kW and is equipped with an internal lube pump, heat exchangers, and motor controllers in an all-in-one package unit. Predicted performance of this E-Axle against the defined VTS parameters showed that the E-Axle met or exceeded all three VTS criteria.

A one-dimensional vehicle model based on the equation of linear motion was presented. Given the selected E-Axle and a 50/50 torque split, the vehicle performance and fuel economy of the BEV was determined using city and highway drive cycle analyses. The power required at the wheels, the efficiency of each motor, and the energy required at the E-Axle were determined. In

addition, the city, highway, and combined MPGe fuel economy were determined. The combined fuel economy of the BEV was determined to be 52.4 MPGe, representing a 118% increase over the production vehicle's fuel economy of 24 MPG. This highlights the efficiency advantage of BEVs over conventional vehicles.

To further increase the BEV fuel economy, an efficiency-optimized torque vectoring control strategy was developed. Instead of the 50/50, left/right torque split, an optimal split that maximizes E-Axle system efficiency was determined offline and then used in the simulation. Using the one-dimensional model, the optimized TV improved the combined fuel economy by 9.5% over the 50/50 split.

To characterize the yaw motion of the optimized TV, a dynamic 3DOF model was developed using Simulink's Vehicle Dynamic Blockset models and shown to be in good agreement with the one-dimensional model. For a 50/50 torque split using the 3DOF model, the combined fuel economy was 59.1 vs the 52.4 when using the 1DOF. For the optimized torque split using the 3DOF model, the combined fuel economy was 57.4 vs the 64.5 when using the one-dimensional model. Without any yaw mitigation, the vehicle significantly deviated from the intended straight-line driving path and traveled in a circle.

To mitigate the undesired yaw motion, four strategies were developed: allowing yaw corrections through driver steering, rapidly switching the dominant torque from side to side, limiting yaw motion by trading efficiency, and coupling the motor output shafts. Dominant switching and output coupling provided the highest increase in fuel economy over the 50/50 baseline, by about 10%. This is followed closely by the driver steering, which increased fuel economy by 9.4%. The driver steering, dominant switching, and output coupling were all able to

maintain straight-line driving. Trading efficiency did not yield any fuel economy improvements over the 50/50 baseline and deviated significantly from straight-line driving.

12.2 Conclusion and future work

Based on the vehicle's drive-cycle analysis, driver steering, dominant switching, and output coupling are valid strategies for efficiency-optimized torque vectoring that also mitigate the undesired effects of the yaw moment that results from unequal left/right torque distribution. From here the practicalities of the strategies would have to be evaluated. For example, in the driver steering strategy, is it acceptable for the driver to steer up to 8 deg to maintain the vehicle on its intended straight-line driving path. For the dominant switching, efficiencies in switching the motor on and off would need to be evaluated and accounted for. The output coupling strategy required a hardware change to couple the motor's output. The feasibility of the modification would have to be evaluated and may depend on the state of the design in its lifecycle (design, prototyping, post-production).

Trading efficiency for performance did not improve the vehicle's fuel economy over the 50/50 torque split baseline and it was also not able to fully mitigate off-axis deviations from straight-line driving. This is a result of the slightest amount of unequal torque being applied to the left/right wheels resulting in an undesired yaw-moment. Future work could consider a hybrid strategy that trades efficiency for performance but also has driver steering. This strategy would be more efficient than the current tradeoff strategy and reduce the required driver steering from the current driver steering strategy.

Another possibility for future work would be to investigate if there exists a relationship of vehicle yaw as a result of acceleration, vehicle speed, delta torque, etc. Finally, future work should include applying these methods on the COTF and validating the simulation results.

REFERENCES

[1] Z. Gao, T. LaClair, S. Ou, S. Huff, G. Wu, P. Hao, K. Boriboonsomsin and M. Barth, "Evaluation of electric vehicle component performance over eco-driving cycles", *Energy*, 172, 2019, 823-839.

[2] "Mississippi State University", 2014. Available: https://www.newsarchive.msstate.edu/newsroom/article/2014/09/msu-building-car-future. (Accessed November 2019).

[3] Y.-C. Liu, J. Batte, Z. Collins, J. Bateman, J. Atkins, M. Davis, D. Salley, C.L. Bethel, J. Ball, and C. Archibald, "Mechanical design, prototyping, and validation of a Martian robot mining system", *SAE International Journal of Passenger Cars - Mechanical Systems*, 10(1), 2017, 1289-1297.

[4] Y.-C. Liu, V. Meghat, and B. Machen, "Design and prototyping of a debris clean and collection system for a cylinder block assembly conveying line following an engineering systems design approach", *International Journal of Design Engineering*, 8(1), 2018, 1-18.

[5] Y.-C. Liu, V. Meghat, and B. Machen, "Design and prototyping of an *in situ* robot to clean a cylinder head conveying line following an engineering systems design approach", *International Journal of Design Engineering*, 7(2), 2017, 106-122.

[6] Y.-C. Liu, V. Meghat, B. Machen, and G. He, "Design and prototyping of cleaning systems for cylinder head and engine block conveying lines", SAE Technical Paper 2018-01-1387, Proceedings of SAE 2018 World Congress & Exhibition, Detroit, MI, USA, April 10-12, 2018.

[7] Y.-C. Liu, A. LeClair, M. Doude and R. F. Burch, "Development of a data acquisition system for autonomous vehicle systems", *International Journal of Vehicle Structures & Systems*, 10(4), 2018, 251-256.

[8] Y.-C. Liu, A. LeClair, M. Doude and R. F. Burch, "Design, installation, and validation of a data acquisition system", IMECE2018-87071, Proceedings of ASME 2018 International Mechanical Engineering Congress and Exposition, November 9-15, Pittsburgh, USA.

[9] Y.-C. Liu, A. J. Artigue, J. D. Sommers, and T. L. Chambers, "Theo Jansen project in engineering design course and a design example", *European Journal of Engineering Education*, 36(2), 2011, 187-198.

[10] K. L. Guiberteau, T. A. Kozman, J. Lee, and Y.-C. Liu, “Guidelines in wave energy conversion system design”, Proceedings of Industrial Energy Technology Conference (IETC 2014), New Orleans, LA, USA, May 20-23, 2014.

[11] Y.-C. Liu, G. Cavalier, J. Pastor, R. J. Viera, C. Guillory, K. Judice, K. Guiberteau, and T. A. Kozman, “Design and construction of a wave generation system to model ocean conditions in the Gulf of Mexico”, International Journal of Energy and Technology, 4(31), 2012, 1-7.

[12] Y.-C. Liu, S. Alidoust, and B. Qi, “Design, modeling, and evaluation of a cost effective particulate control system”, SAE International Journal of Aerospace, 5(1), 2012, 68-73.

[13] Y.-C. Liu, J. E. Ball, S. Abdelwahed, and G. He, “An automatic emergency braking system for collision avoidance assist of multi-trailer vehicle based on model prediction control”, SAE Technical Paper 2021-01-0117, Proceedings of SAE Digital Summit, online, June 16-18, 2021.

[14] Y. F. Peymani, S. A. Ghanbari, Y.-C. Liu, and A. Hayatdavoudi, “Design and validate a particulate matter management system computationally”, IMECE2011-64063, Proceedings of ASME 2011 International Mechanical Engineering Congress & Exposition, Denver, CO, USA, November 11-17, 2011.

[15] "Analysis Program: 2019 Annual Progress Report", Office of Energy Efficiency and Renewable Energy - Department of Energy, 2019. Available: https://www.energy.gov/sites/prod/files/2020/06/f76/VTO_2019_APR_ANALYSIS_compliant_052020.pdf. [Accessed 19 March 2021].

[16] "Fast Facts: U.S. Transportation Sector Greenhouse Gas Emissions 1990-2018", Office of Transportation and Air Quality - United States Environmental Protection Agency, 2019. Available: https://nepis.epa.gov/Exe/ZyPDF.cgi?Dockey=P100ZK4P.pdf. [Accessed 19 March 2021].

[17] M. A. Roscher, W. Leidholdt and J. Trepte, "High efficiency energy management in BEV applications", *International Journal of Electrical Power & Energy Systems*, 37(1), 2012, 126-130.

[18] *Automotive Handbook*, Robert Bosch, 2011.

[19] W. B. Brown and Y. Liu, "Electric axle sizing for the conversion of a conventional production vehicle to a prototype battery electric vehicle", SAE Technical Paper 2020-01-5093, 2020.

[20] A. O. Kiyakli and H. Solmaz, "Modeling of an electric vehicle with MATLAB/Simulink", *International Journal of Automotive Science and Technology*, 2(4), 2018, 9-15.

[21] J. P. Szybist, S. Busch, R. L. McCormick, J. A. Pihl, D. A. Splitter, M. Ratcliff, C. P. Kolodziej, J. M. Storey, M. Moses-DeBusk, D. Vuilleumier, M. Sjoberg, C. S. Sluder, T. Rockstroh and P. Miles, "What fuel properties enable higher thermal efficiency in spark-ignited engines?", *Progress in Energy and Combustion Science*, 82(1), 2021.

[22] L. Zhang and D. G. Dorrell, "Genetic Algorithm Based Optimal Component Sizing for an Electric Vehicle", 39th Annual Conference of the IEEE Industrial Electronics Society, Vienna, 2013.

[23] M. J. Akhtar, R. K. Behera and S. K. Parida, "Propulsion System Design of Electric Vehicle", 6th International Conference on Power Electronics Systems and Applications, Hong Kong, 2015.

[24] M. Ehsani, Y. Gao, S. E. Gay and A. Emandi, *Modern Electric, Hybrid Electric, and Fuel Cell Vehicles*, Second ed., CRC Press, 2009.

[25] B. Wang, D. L. Hung, J. Zhong and K. Teh, "Energy Consumption Analysis of Different Bev Powertrain Topologies by Design Optimization", *International Journal of Automotive Technology*, 19(5), 2018, 907-914.

[26] A. Emandi, "*Transportation 2.0*", 2011, 18-29.

[27] X. D. Xue, K. W. Cheng and N. C. Cheung, "Selection of Electric Motor Drives for Electric Vehicles", Australasian Universities Power Engineering Conference, Sydney, 2008.

[28] Q. Ren, D. A. Crolla and A. Morris, "Effect of transmission design on Electric Vehicle (EV) performance", IEEE Vehicle Power and Propulsion Conference, 2009.

[29] S. F. Tie and C. W. Tan, "A review of energy sources and energy management system in electric vehicles", *Renewable and Sustainable Energy Reviews*, 20(1), 2013, 82-102.

[30] S. Amjad, S. Neelakrishnan and R. Rudramoorthy, "Review of design considerations and technological challenges for successful development and deployment of plug-in hybrid electric vehicles", *Renewable and Sustainable Energy Reviews*, 14(3), 2010, 1104-1110.

[31] B. Propfe, M. Redelbach, D. J. Santini and H. Friedrich, "Cost analysis of Plug-in Hybrid Electric Vehicles including Maintenance & Repair Costs and Resale Values", *World Electric Vehicle Journal*, 5(4), 2012, 886-895.

[32] J. Hagman, S. Ritzen, J. J. Stier and Y. Susilo, "Total cost of ownership and its potential implications for battery electric vehicle diffusion", *Research in Transportation Business & Management*, 18(1), 2016, 11-17.

[33] N. Rezaei and K. Mehran, "Dynamic modelling and performance assessment of a single battery electric vehicle powertrain system employing an induction motor", 20th Workshop on Control and Modeling for Power Electronics (COMPEL), Toronto, 2019.

[34] M. A. Roscher, R. Michel and W. Leidholdt, "Improving Energy Conversion Efficiency by means of Power Splitting in Dual Drive Train EV Applications", *International Journal of Vehicular Technology*, 2013(2), 2013.

[35] M. Peng, L. Liu and C. Jiang, "A review on the economic dispatch and risk management of the large-scale plug-in electric vehicles (PHEVs)-penetrated power systems", *Renewable and Sustainable Energy Reviews*, 16(3), 2012, 1508-1515.

[36] J. A. Barlage, D. E. Bruder, V. P. Jones, E. Nielsen, T. L. Perttola and L. Pritchard, *All-Wheel Drive*, BorgWarner, 2009.

[37] G. Wu, X. Zhang and Z. Dong, "Powertrain architectures of electrified vehicles: Review, classification, and comparison", *Journal of The Franklin Institute*, 352(2), 2015, 425-448.

[38] R. A. Weinstock, P. T. Krein and R. A. White, "Optimal Sizing and Selection of Hybrid Electric Vehicle Components", IEEE Power Electronics Specialist Conference, Seattle, 1993.

[39] M. Ehsani, K. M. Rahman and H. A. Toliyat, "Propulsion System Design of Electric and Hybrid Vehicles", *IEEE Transactions on Industrial Electronics*, 44(1), 1997, 19-27.

[40] R. Sehab, B. Barbedette and M. Chauvin, "Electric Vehicle Drivetrain: Sizing and Validation Using General and Particular Mission Profiles", IEEE International Conference on Mechatronics, Istanbul, 2011.

[41] E. A. Grunditz and T. Thiringer, "Performance analysis of current BEVs based on a comprehensive review of specifications", *IEEE Transactions on Transportation Electrification*, 2(3), 2016, 270-289.

[42] "Engineering Design Process", Wikipedia, Available: https://en.wikipedia.org/wiki/Engineering_design_process. [Accessed 16 April 2021].

[43] D. W. Gao, C. Mi and A. Emandi, "Modeling and simulation of electric and hybrid vehicles", IEEE, 2007.

[44] K. L. Butler, M. Ehsani and P. Kamath, "A Matlab-based modeling and simulation package for electric and hybrid electric vehicle design", *IEEE Transactions on Vehicular Technology*, 48(6), 1999, 1770-1778.

[45] "Dynamometer Drive Schedules", U.S. Environmental Protection Agency, Available: https://www.epa.gov/vehicle-and-fuel-emissions-testing/dynamometer-drive-schedules. [Accessed 2 February 2020].

[46] A. Moawad, G. Singh, S. Hagspiel, M. Fellah and A. Rousseau, "Impact of real world drive cycles on PHEV fuel efficiency and cost for different powertrain and battery characteristics", *World Electric Vehicle Journal*, 3(1), 2009, 1-10.

[47] W. B. Brown and Y. Liu, "Modeling and Simulation of An Electric Vehicle with Independent Rear Motors to Estimate the Fuel Economy during EPA Drive Cycles", *International Journal of Vehicle Structures & Systems*, 12(5), 2020, 46-52.

[48] R. Milligan, T. Muneer and I. Smith, "A comparative range approach using the real world drive cycles and the battery electric vehicle", IEEE International Transportation Electrification Conference (ITEC), 2015.

[49] A. Panday and H. O. Bansal, "A Review of Optimal Energy Management Strategies for Hybrid Electric Vehicle", *International Journal of Vehicular Technology*, 2014(1), 2014.

[50] N. Sockeel, M. Shahverdi, M. Mazzola and W. Meadows, "High-Fidelity Battery Model for Model Predictive Control Implemented into a Plug-In Hybrid Electric Vehicle", *Batteries*, 3(2), 2017.

[51] E. Siampis, M. Massaro and E. Velenis, "Electric rear axle torque vectoring for combined yaw stability and velocity control near the limit of handling", 52nd IEEE Conference on Decision and Control, 2013.

[52] D. Piyabongkarn, J. Y. Lew, R. Rajamani, J. A. Grogg and Q. Yuan, "On the Use of Torque-Biasing Systems for Electronic Stability Control: Limitations and Possibilities", *IEEE Transactions on Control Systems Technology*, 15(3), 2007, 581-589.

[53] B. Jager, P. Neugebauer, R. Kriesten, N. Parspour and C. Gutenkunst, "Torque-vectoring stability control of a four wheel drive electric vehicle", 2015 IEEE Intelligent Vehicles Symposium (IV), 2015, 1018-1023.

[54] L. D. Novellis, A. Sorniotti, P. Gruber and A. Pennycott, "Comparison of Feedback Control Techniques for Torque-Vectoring Control of Fully Electric Vehicles", *IEEE Transactions on Vehicular Technology*, 63(8), 2014, 3612-3623.

[55] T. Goggia, A. Sorniotti, L. D. Novellis, A. Ferrara, P. Gruber, J. Theunissen, D. Steenbeke, B. Knauder and J. Zehetner, "Theoretical Design and Experimental Assessment", *IEEE Transactions on Vehicular Technology*, 64(5), 2015, 1701-1715.

[56] C. Geng, L. Mostefai, M. Denai and Y. Hori, "Direct Yaw-Moment Control of an In-Wheel-Motored Electric Vehicle Based on Body Slip Angle Fuzzy Observer", *IEEE Transactions on Industrial Electronics*, 56(5), 2009, 1411-1419.

[57] B. Tabbache, A. Kheloui and M. E. H. Benbouzid, "An Adaptive Electric Differential for Electric Vehicles Motion Stabilization", *IEEE Transactions on Vehicular Technology*, 60(1), 2011, 104-110.

[58] K. Jalali, T. Uchida, S. Lambert and J. McPhee, "Development of an Advanced Torque Vectoring Control System for an Electric Vehicle with In-Wheel Motors using Soft Computing Techniques", *SAE International Journal of Alternative Powertrains*, 2(2), 2013, 261-278.

[59] D. Kasinathan, A. Kassaiezadeh, A. Wong, A. Khajepour, S. Chen and B. Litkouhi, "An Optimal Torque Vectoring Control for Vehicle Applications via Real-Time Constraints", *IEEE Transactions on Vehicular Technology*, 65(6), 2016, 4368-4378.

[60] A. Parra, A. Zubizarreta and J. Perez, "A novel Torque Vectoring Algorithm with Regenerative Braking Capabilities", IECON 2019 - 45th Annual Conference of the IEEE Industrial Electronics Society, Lisbon, 2019.

[61] A. M. Dizqah, B. L. Ballard, M. V. Blundell, S. Kanarachos and M. S. Innocente, "A Non-Convex Control Allocation Strategy as Energy-Efficient Torque Distributors for On-Road and Off-Road Vehicles", *Control Engineering Practice*, 95(1), 2020.

[62] G. D. Filippis, B. Lenzo, A. Sorniotti, K. Sannen, J. D. Smet and P. Gruber, "On the Energy Efficiency of Electric Vehicles with Multiple Motors", IEEE Vehicle Power and Propulsion Conference (VPPC), 2016.

[63] L. D. Novellis, A. Sorniotti and P. Gruber, "Wheel Torque Distribution Criteria for Electric Vehicles With Torque-Vectoring Differentials", *IEEE Transactions on Vehicular Technology*, 63(4), 2014, 1593-1602.

[64] G. Liu and L. Jin, "A Study of Coordinated Vehicle Traction Control System Based on Optimal Slip Ratio Algorithm", *Mathematical Problems in Engineering*, 2016(1) 2016.

[65] J. Wang, S. Gao, G. Wang, Y. Wang and Q. Wang, "Wheel torque distribution optimization of four-wheel independent-drive electric vehicle for energy efficient driving", *Control Engineering Practice*, 110(1), 2021.

[66] A. Stoklosa, "2016 Subaru BRZ Review", Car and Driver, 2016 Available: https://www.caranddriver.com/reviews/a15100416/2016-subaru-brz-review/. [Accessed November 2019].

[67] Linamar. Available: https://www.linamar.com/products. [Accessed November 2019].

[68] Parker Hannifin Corporation.

[69] United States Environmental Protection Agency, "Light-duty automotive technology, carbon dioxide emissions, and fuel economy trends: 1975 through 2016", US EPA, 2016.

[70] "Gasoline Gallon Equivalent," Wikipedia, Available: https://en.wikipedia.org/wiki/Gasoline_gallon_equivalent. [Accessed 2 February 2020].

[71] Department of Energy, Office of Energy Efficiency and Renewable Energy, "Electric and Hybrid Vehicle Research, Development, and Demonstration Program; Petroleum-Equivalent Fuel Economy Calculation; Final Rule", *Federal Register*, 65(113), 2000, 36987-36989.

[72] "Fuel Economy of 2015 Subaru BRZ", fueleconomy.gov, Available: https://www.fueleconomy.gov/feg/PowerSearch.do?action=noform&path=1&year1=2015&year2=2015&make=Subaru&model=BRZ&srchtyp=ymm. [Accessed 10 June 2020].

[73] Mathworks, "Vehicle Dynamics Blockset", Available: https://www.mathworks.com/help/vdynblks/. [Accessed 12 June 2021].

[74] Mathworks, "Vehicle Body 3DOF", Available: https://www.mathworks.com/help/vdynblks/ref/vehiclebody3dof.html. [Accessed 12 June 2021].

[75] I. J. M. Besselink, A. J. C. Schmeitz and H. B. Pacejka, "An improved Magic Formula/Swift tyre model that can handle inflation pressure changes, Vehicle System Dynamics", *International Journal of Vehicle Mechanics and Mobility*, 48(1), 2010, 337-352.

[76] H. Pacejka, *Tire and Vehicle Dynamics*, Butterworth-Heinemann, 2012.

[77] Mathworks, "Combined Slip Wheel 2DOF", Available: https://www.mathworks.com/help/vdynblks/ref/combinedslipwheel2dof.html. [Accessed 12 June 2021].

[78] Global Center for Automotive Performance Simulation (GCAPS).

[79] Mathworks, "Predictive Driver", Available: https://www.mathworks.com/help/vdynblks/ref/predictivedriver.html. [Accessed 12 June 2021].